Quantitative Seismic Amplitude Analysis

Quantitative Seismic Amplitude Analysis

PROEFSCHRIFT

ter verkrijging van de graad van doctor

aan de Technische Universiteit Delft,

op gezag van de Rector Magnificus prof.ir. K.C.A.M. Luyben,

voorzitter van het College voor Promoties,

in het openbaar te verdedigen

op maandag 7 februari 2011 om 10:00 uur

door

Ayon Kumar DEY

Master of Science Geology and Geophysics,

The University of Calgary, Canada

geboren te St. John's, NL, Canada

Dit proefschrift is goedgekeurd door de promotoren:
Prof.dr.ir. A. Gisolf

Samenstelling promotiecommissie:

Rector Magnificus,	voorzitter
Prof.dr.ir. A. Gisolf,	Technische Universiteit Delft, promotor
Dr.ir. D. J. Verschuur,	Technische Universiteit Delft
Prof.dr. H. P. Urbach,	Technische Universiteit Delft
Prof.dr.ir. C. P. A. Wapenaar,	Technische Universiteit Delft
Prof.dr. M. D. Sacchi,	University of Alberta
Dr. P. Kelamis,	Saudi Arabian Oil Company (Saudi Aramco)
Ir. H. W. J. Debeye,	Fugro-Jason Netherlands BV

To my parents

Contents

1

Introduction

Global demand for energy resources, hydrocarbons in particular, continues to rise, Figure (1.1), while there is a decline in new reserve discovery and size. This poses a supply and demand problem that will only get worse as developing economies come online. Already, the world is beginning to see the development of this economic stress from the significant increase in the base cost of hydrocarbons, primarily driven by demand from China and India.
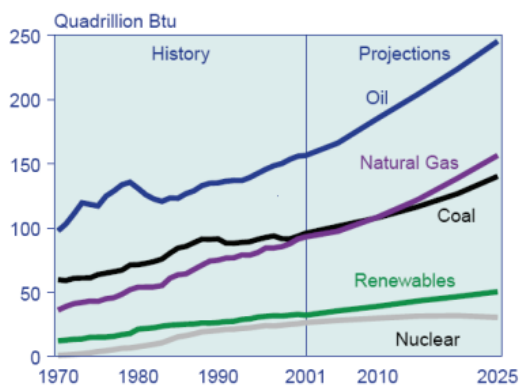
Figure 1.1: *Global energy consumption, from 1970 until 2001, and projected consumption from 2001 onward. (after U.S. Energy Information Administration, www.eia.doe.gov/oiaf/ieo/index.html)*

Figure (1.2) shows the net oil imports, as of 2006, for the various countries of the world. Notice that after the United States of America and Japan, it is China and India that are the largest importers of oil. Furthermore, the combined daily consumption of oil from 1980 until 2006 (Figure (1.3)) shows Asia and Oceania to be the largest daily consumers, as energy is needed to fuel the economic growth of the region.
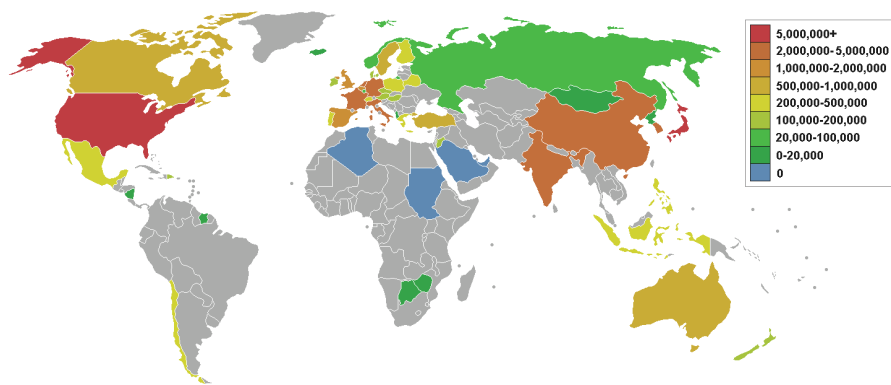
Figure 1.2: *Oil imports, as of 2006, by country (in barrels per day). (after CIA factbook, http://www.cia.gov/cia/pubications/factbook/rankorder/2175rank.html)*

While strongly contested, the Hubbert [1950] peak oil analysis is still supported and the petroleum industry is urged to prepare for the coming production decline. A modern version of this analysis, Figure (1.4), shows the hydrocarbon production curves using data up to and including 2004.

Berkhout [2007] discusses that it is expected that in 2025 the world will use 50% more energy than in 2005, while the contribution of nonfossil fuels will decline from 15% to 12%. Furthermore, Jack [1997] estimates global hydrocarbon recovery to be about 30-35% and that if this can be increased by a mere 1% then global supply is extended by 2 years. The implication is that the upstream oil and gas industry will face an enormous challenge to increase capacity and replace reserves. Hence, the current priorities are significantly improved technology portfolios and multi-disciplinary communication skills in the professional workforce. Enhanced reservoir knowledge is the primary avenue by which to address optimal production from existing fields. It the responsibility of science to enable technologies and workflows for this purpose.
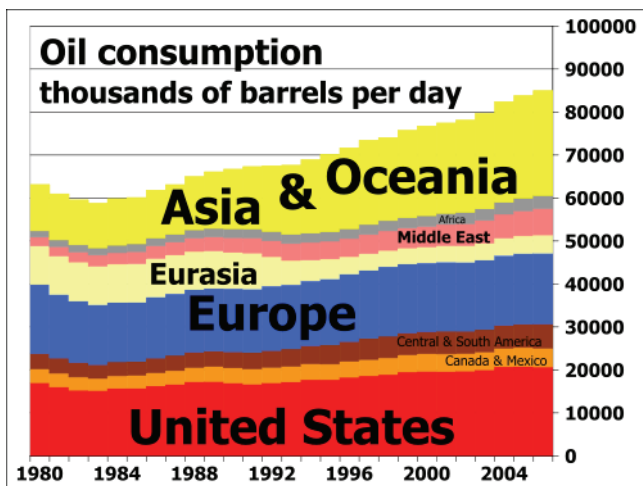
Figure 1.3: *Regional daily oil consumption from 1980 until 2006 (in thousands of barrels per day). (after U.S. Energy Information Administration, www.eia.doe.gov/emeu/international/RecentPetroleumConsumptionBarrelsperDay.xls)*

1.1   Enhanced reservoir knowledge

Whether or not there is an immediate crisis in the availability of hydrocarbon resources is up for debate, but it is clear that current global reserve recovery will not be able to sustain demand and carbon-energy replacements are not yet feasible. Leveraging applied science for enhanced reservoir exploitation, so as to allow for the discovery of fundamental advances in the transition to a reduced carbon based global economy, demands innovation. While a dedicated and focused effort is required by the applied geoscience community, this effort must recognise that the problems requiring attention cannot just be fractured into disciplinary subproblems, followed by an independent solution process for each of these subproblems. Modular/segmented problem solving easily leads to less-than-optimal formulations of the component elements and the sum of suboptimal solutions is rarely an optimal total end result.

Berkhout [2005] discusses the so-called Seismic Value Chain (Figure (1.5)). It visualizes the cyclic interaction between seismic acquisition, imaging and reservoir characterization. In this double feed-forward and double feed-back value chain, seismic reservoir characterization goals drive structural imaging and structural imaging drives seismic acquisition (double feed-back). Moreover, new capabilities in acquisition initiate new developments in imaging and these new imaging technologies inspire new interpretation concepts that steer developments in characterization (double
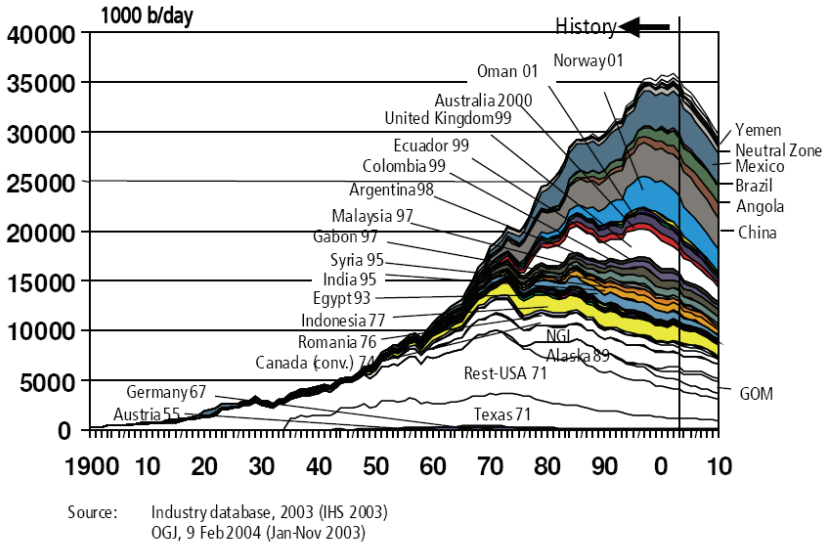
Figure 1.4: *Hubbert-style graph, using 2004 data, showing the world's oil production peak/plateau (in thousands of barrels per day). Note that the curves do not take into account the Organisation of Petroleum Exporting Countries (OPEC) nor the nations of the former Soviet Union. (after U.S. government document, www.fossil.energy.gov/programs/reserves/npr/publications/npr_strategic_significancev1.pdf)*

feed-forward). Hence, modern seismic innovation to address the global imbalance in hydrocarbon supply and demand requires both feed-forward and feed-back processes.

Maximum added-value requires that targets be set at the end of the value chain. With realisation that each end-goal is a many-to-one process, these final targets need to be road mapped back all the way to acquisition (Figure (1.6)). Innovational added-value of Seismic Value Chain depends on the quality of the involved technological and human capital, as well as the capability of organisations to remove barriers and allow for the integration of these abilities for maximum economic value at the end of the chain.

1.2 Statement of the problem

Currently, the seismic value chain paradigm is in a feed-forward mode of cyclic interaction. Large investments over the last 10-15 years in the data acquisition have produced a dramatic increase in the understanding of designing economical acqui-

THE SEISMIC VALUE CHAIN
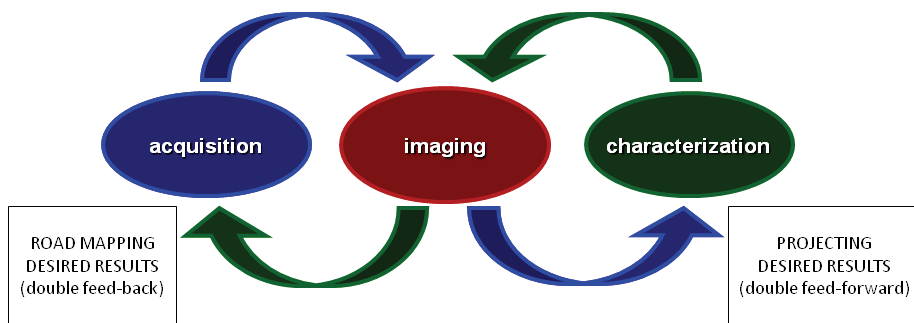
Figure 1.5: *The Seismic Value Chain (after Berkhout [2005]).*

sition geometries. Modern seismic data now have the potential to yield the best images in terms of spatial resolution, amplitude accuracy, and increased illumination in terms of offset and azimuth. In turn, the imaging community as a whole has introduced new algorithms that exploit the richness of these new data sets so as to deliver a fundamentally improved image of the subsurface to be used for quantitative seismic reservoir characterisation. Today's challenge lies with the reservoir characterisation node of the value chain. An immediate requirement is extracting quantitative rock properties information from these improved data-sets and images, to move from a geophysically based elastic characterisation of reservoirs towards a more effective, geologically accessible, parameterization. This leads to the following fundamental question:

> How can quantitative information about a subsurface hy-
> drocarbon reservoir be gained using modern surface seismic
> data measurements?

That is to say, a knowledge gap exists between common current reservoir analysis methods that are fundamentally qualitative in nature and the quantitative information required to enhance reservoir production. In the time-lapse (i.e. repeated seismic) sense, we may ask: how can the change in hydrocarbon saturation be estimated away from the well? At the most general level, estimating the reservoir density and its changes are the most direct way to quantify this desired information. As is the case in many interdisciplinary questions, the answer is complex and detailed. Two key questions explored in seeking a solution are as follows.
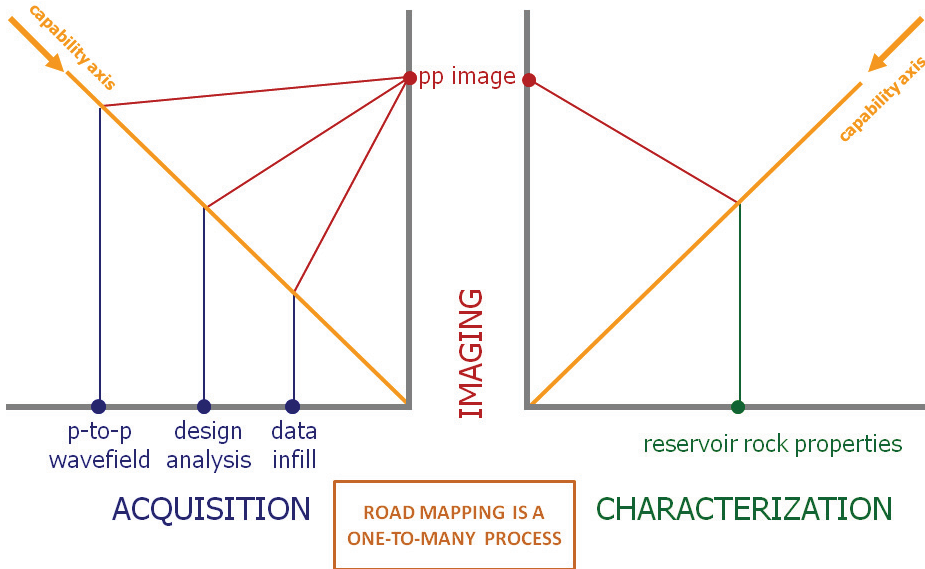
Figure 1.6: *Illustrative road mapping of a seismic reservoir characterisation goal (after personal communication about Berkhout [2005]).*

THE FORWARD QUESTION: How can the seismic amplitude response of key reservoir properties be quantitatively simulated for a layered earth?

THE INVERSE QUESTION: How can key reservoir properties be quantitatively estimated from the seismic amplitude data of a layered earth?

1.3   Proposed solution

The current state of affairs in reservoir characterization does not fully exploit the wide-angle information present in seismic data. This is partially due to the fact that the current paradigm for analyzing reflectivities is at odds with the assumptions made for standard seismic data processing. This work reconciles these differences by resolving the issue of scale dependency in forward modeling of wide-angle seismic data from well logs. Subsequent to this, a framework is created which furthers the

use of pre-critical seismic data in quantitative hydrocarbon reservoir characterization and management. The estimation of high-resolution reservoir rock properties is cast as a linear-in-the-parameters optimization problem where all the primary information carried in the pre-critical seismic amplitudes can be exploited. Further improvement to the reservoir property estimates is achieved through the simultaneous consideration of compressional and converted wave pre-stack seismic amplitudes. In turn, these broadband reservoir properties are converted to parameters that can be used in quantitative fluid detection. Figure (1.7) visualizes the flow and relationship between the answers to the key questions that will address the knowledge gap outlined in the problem statement.
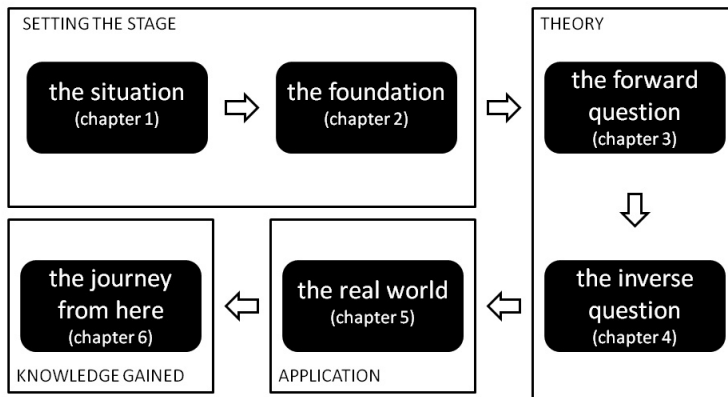
Figure 1.7: *Schematic outline of thesis.*

1.4   Thesis deliverables

Integrated hydrocarbon reservoir management is proving to be ideal for optimal production and development of a reservoir via enhanced production. An accurate and reliable seismically estimated map of hydrocarbon saturation, or the change in hydrocarbon saturation, is vital to this process. This is because seismic is the only measurement that commonly exists between wells that can guide the reservoir simulator. Given recent advances in seismic data processing and in the acquisition of

seismic data, quantitatively estimating maps of the change in reservoir hydrocarbon saturation is now viable. Quantitative seismic amplitude analysis, that can be applied to the detection of the change in hydrocarbon saturation, is the primary goal of this research and is realized through the deliverables listed below.

■ 1.4.1 Linear long-offset forward modeling

This research shows that the use of current single interface models to calculate reflectivities, in a layered earth at long offset, is inconsistent with the assumed convolutional earth model. Chapter 3 derives a model that is almost fully scale independent in the earth input and can naturally account for thin-bed effects. The only limitation in angle-of-incidence is the critical angle at the reservoir top. This is particularly important if long offset seismic is to be exploited in order to extract information about reservoir fluid saturation and effective stress, because it is in the long offset domain that the customary ways to calculate reflectivity violate the linear convolution data model that underlies the seismic data processing. Also at long offsets, there are genuine internal multiples being created but it is assumed that these are removed/handled during imaging or, possibly, calibrated out.

■ 1.4.2 Sparse linear pre-stack waveform inversion

This research also develops a method by which accurate broadband estimates of reservoir properties are estimated from multi-component seismic data. Chapter 4 shows that the key features of the parameter estimation method (i.e. inversion) are: simultaneous use of all the pre-critical amplitude information available, accounting for the data's band-limitation and the ray-parameter dependence of this band-limitation, and the imposition of a minimum structure condition on the parameter estimates. Starting with fully linearized P-P and P-S reflectivity equations, forward model operators are constructed. Ray-parameter dependent band-limitation is introduced via the matrix representation of convolutional filtering. Then a simultaneous inversion operator is formed that is used to build the system of normal equations with adaptive diagonal regularization which, in turn, are used to estimate high-resolution (i.e. broadband) reservoir rock properties.

2

A review of the single interface earth

2.1 Theoretical basis

Quantitative seismic amplitude analysis is concerned with relating observed changes in seismic amplitudes to corresponding changes in elastic/reservoir properties. Hence, the basis of all seismic amplitude analysis is the elastic vector wave equation, as it is our best current description of observed seismic data. In the frequency domain, this is expressed as

$$\rho\omega^2\mathbf{U} + (\lambda + \mu)\nabla(\nabla \cdot \mathbf{U}) + \mu\nabla^2\mathbf{U} = \mathbf{0}, \tag{2.1.1}$$

where ρ is the mass density, ω is angular frequency, λ and μ are Lamé parameters. Note that $\mathbf{U}$ is the sum of two fields, relating to the scalar (Φ) potential function and the vector ($\boldsymbol{\Psi}$) potential function. These potential functions have the same dimension as Fourier transformed pressure and the displacement field $\mathbf{U}$ can be written as:

$$\mathbf{U} = \mathbf{U}_\Phi + \mathbf{U}_{\boldsymbol{\Psi}} = \frac{1}{\rho\omega^2}(\nabla\Phi + \nabla \times \boldsymbol{\Psi}) \text{ with } \nabla \cdot \boldsymbol{\Psi} = 0. \tag{2.1.2}$$

The seismic amplitude problem of plane wave reflection and transmission at a plane interface is a 2D problem. This is because only a single plane of propagation is considered, that being the plane spanned by the incident wave's slowness vector and the normal to the interface on which the wave is incident. The incident P-wave's energy is partially reflected, partially transmitted, and partially converted to other modes, as illustrated in Figure (2.1).
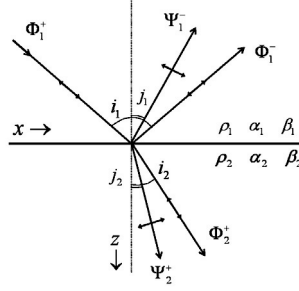
Figure 2.1: *Energy/ray partitioning of a plane P-wave incident on the boundary between two horizontal half-spaces. The incident P-wave's (Φ_1^+) energy is partially reflected(Φ_1^- and Ψ_1^-) and partially transmitted (Φ_2^+ and Ψ_2^+). Conversion of P-energy to S-energy gives rise to the Ψ terms. The half-space properties are density (ρ), P-wave velocity (α), and S-wave velocity (β). Note that horizontal slowness = $p = \frac{\sin i_1}{\alpha_1} = \frac{\sin i_2}{\alpha_2} = \frac{\sin j_1}{\beta_1} = \frac{\sin j_2}{\beta_2}$*

Taking the z-axis normal to the interface and the x-axis to be the slowness vector direction in the plane of propagation, the situation is described by a wave field with three independent modes of propagation, each with a scalar wave equation. These are the scalar longitudinal (or P-wave) equation $\nabla^2\Phi + (\omega/\alpha)^2\Phi = 0$, the scalar parallel polarised transverse (or S_V-wave) equation $\nabla^2\Psi_y + (\omega/\beta)^2\Psi_y = 0$, and the scalar perpendicular polarised transverse (or S_H-wave) equation $\nabla^2\mathbf{U}_y + (\omega/\beta)^2\mathbf{U}_y = 0$. The S_V-wave is a shear-wave vibrating in the plane of propagation and is fully determined by the y-component of the vector potential $\mathbf{\Psi}$. As the S_H-mode (a shear-wave vibrating perpendicular to the plane of propagation) is fully decoupled, it is not of interest in this analysis.

These scalar wave equations allow the five waves schematically outlined in Figure (2.1) to be written as

$$
\begin{aligned}
\Phi_1^+ &= & \exp[-\tfrac{i\omega}{\alpha_1}(x\sin i_1 + z\cos i_1)], \\
\Phi_1^- &= R_{PP} & \exp[-\tfrac{i\omega}{\alpha_1}(x\sin i_1 - z\cos i_1)], \\
\Psi_1^- &= R_{PS} & \exp[-\tfrac{i\omega}{\beta_1}(x\sin j_1 - z\cos j_1)], \\
\Phi_2^+ &= T_{PP} & \exp[-\tfrac{i\omega}{\alpha_2}(x\sin i_2 + z\cos i_2)], \text{ and} \\
\Psi_2^+ &= T_{PS} & \exp[-\tfrac{i\omega}{\beta_2}(x\sin j_2 + z\cos j_2)].
\end{aligned}
\tag{2.1.3}
$$

Equation (2.1.3) is solved for R_{PP}, R_{PS}, T_{PP}, and T_{PS} by applying continuity of displacement and continuity of stress as boundary conditions on the systems. The solution is in terms of media parameters on either side of the interface and the angles

incidence, reflection, and transmission. In the same manner as Aki and Richards [2002], the following variables are defined

$$a = \rho_2(1 - 2\beta_2^2 p^2) - \rho_1(1 - 2\beta_1^2 p^2), \quad b = \rho_2(1 - 2\beta_2^2 p^2) + 2\rho_1\beta_1^2 p^2,$$

$$c = \rho_1(1 - 2\beta_1^2 p^2) + 2\rho_2\beta_2^2 p^2, \qquad d = 2(\rho_2\beta_2^2 - \rho_1\beta_1^2),$$

$$E = b\frac{\cos i_1}{\alpha_1} + c\frac{\cos i_2}{\alpha_2}, \qquad\qquad F = b\frac{\cos j_1}{\beta_1} + c\frac{\cos j_2}{\beta_2},$$

$$G = a - d\frac{\cos i_1}{\alpha_1}\frac{\cos j_2}{\beta_2}, \qquad\qquad H = a - d\frac{\cos i_2}{\alpha_2}\frac{\cos j_1}{\beta_1}, \text{ and}$$

$$D = EF + GHp^2.$$

And the Knott-Zoeppritz equations, Knott [1899] and Zoeppritz [1919], for the reflectivities and transmitivities (based on scalar potentials) are

$$
\begin{aligned}
R_{PP} &= \left[\left(b\frac{\cos i_1}{\alpha_1} - c\frac{\cos i_2}{\alpha_2}\right)F - \left(a + d\frac{\cos i_1}{\alpha_1}\frac{\cos j_2}{\beta_2}\right)Hp^2\right]/D \\
R_{PS} &= -2\frac{\cos i_1}{\alpha_1}\left(ab + cd\frac{\cos i_2}{\alpha_2}\frac{\cos j_2}{\beta_2}\right)p\alpha_1/(\beta_1 D)\cdot\left(\frac{\beta_1}{\alpha_1}\right) \\
T_{PP} &= 2\rho_1\frac{\cos i_1}{\alpha_1}F\alpha_1(\alpha_2 D)\cdot\left(\frac{\rho_2\alpha_2}{\rho_1\alpha_1}\right) \\
T_{PS} &= -2\rho_1\frac{\cos i_1}{\alpha_1}Hp\alpha_1(\beta_2 D)\cdot\left(\frac{\rho_2\beta_2}{\rho_1\alpha_1}\right)
\end{aligned}
\tag{2.1.4}
$$

2.2 Application to amplitude interpretation

Although Equation (2.1.4) relates reflection, transmission, and mode-conversion amplitudes to media properties, the complexity of the relationships prevents any real insight. That is to say, these expressions offer little in terms of an amplitude interpretation tool that is of practical use. Gassman [1951] improved the situation by theoretically developing how systematic changes in reservoir lithology, porosity, and pore-fill will affect the elastic properties. Thereby providing the petro-physical link to seismic by showing how changes in reservoir properties will change the elastic properties and seismic amplitude response. However, as thoroughly reviewed in Hilterman [2001], the era of practical amplitude interpretation is marked by the seminal paper by Koefoed [1955]. This work relates the angle/offset/ray-parameter dependance of the compressional-to-compressional mode reflection coefficient at a boundary to the change in Poisson's ratio across that boundary. The general conclusion is that the shape of the reflection coefficient curve enables making inferences about the lithological nature of rock strata.

Specifically, Koefoed [1955] makes fundamental observations observations that form the basis of modern, quantitative, seismic amplitude analysis. These observations are paraphrased below.

[1] If the lower medium experiences an increase in P-wave velocity and an increase in Poisson's ratio, with other relevant properties of both strata held constant and equal to each other, then the reflection coefficient increases with angle of incidence. This effect becomes more pronounced as the velocity contrast decreases.

[2] If the lower medium experiences an increase in P-wave velocity and the upper medium an increase in Poisson's ratio, with other relevant properties of both strata held constant and equal to each other, then the reflection coefficient decreases with angle of incidence.

[3] If the lower medium experiences an increase in P-wave velocity while Poisson's ratios for both are increased and kept equal to each other, with other relevant properties of both strata held constant and equal to each other, then the reflection coefficient increases with angle of incidence.

[4] The interchange of the *lower* medium and the *upper* medium only minimally changes the shape of the reflection coefficient curve for angles of incidence that are less than 30°.

This conceptual basis for seismic amplitude analysis received strong forward progress in the work of Bortfeld [1961], as a tool was provided to explore Koefoed's observations and conclusions. Assuming that the media properties did not change greatly across an interface, the so-called small contrast approximation, Bortfeld [1961] presents a two-term simplification of the Zoeppritz [1919]. The Bortfeld approximation is written as

$$R_{\mathrm{PP}}\left(i_1\right) = \underbrace{\frac{1}{2}\ln\left(\frac{\alpha_2\rho_2\cos i_1}{\alpha_1\rho_1\cos i_2}\right)}_{\text{fluid term}} + \underbrace{\left(\frac{\sin i_1}{\alpha_1}\right)^2\left(\beta_1^2 - \beta_2^2\right)\left[2 + \frac{\ln\left(\rho_2/\rho_1\right)}{\ln\left(\beta_2/\beta_1\right)}\right]}_{\text{rigidity term}} \quad (2.2.5)$$

In this simplification, Equation (2.2.5), the first term is the *fluid* term and responds to pore-fill, while the second term is the *rigidity* term and responds to lithology. The work retained the essence of the complex, full equations but is simple enough to reveal the quantitative relationship between the elastic properties of the rock and the reflection amplitude response of the seismic. It shows that the fluid term (i.e. the normal incident, or acoustic impedance, reflectivity) can differentiate pore-fluid content. In fact, the maximum pore fluid discrimination from Equation (2.2.5) is what

would eventually be called the *fluid factor* stack by the amplitude analysis community. Furthermore, through Gassman [1951], it offers insight into fluid substitution problems.

The understanding that the acoustic impedance reflectivity has the potential to discriminate pore fluid gives rise to post-stack seismic amplitude anomaly interpretation. The fluid term of the Bortfeld [1961] equation allows interpreters to identify three types of post-stack amplitude behaviour related to hydrocarbon detection. A *bright spot* anomaly occurs when the seismic amplitudes on the stack brighten with respect to the background amplitudes. This occurs when a wet reservoir that is overlain by a layer with higher acoustic impedance becomes hydrocarbon charged. The migration of hydrocarbons into the reservoir lowers its acoustic impedance, increases the contrast with the cap rock and causes a corresponding increase in the reflection coefficient. If the overlying layer has a lower acoustic impedance, then the introduction of hydrocarbon into the reservoir will cause the stack amplitudes to experience a phase reversal. This is due to the fact that the hydrocarbons now reduce the reservoir's acoustic impedance to a level lower than the overlying layer. As such, the sign of the reflection coefficient changes and a *phase reversal* amplitude anomaly occurs. The *dim-out* anomaly is a third type of seismic amplitude anomaly that appears on the stack section. This situation is similar to that for the phase reversal anomaly except that the hydrocarbon charging of the reservoir does not decrease the acoustic impedance response enough to cause a phase change. Instead, the acoustic impedance contrast is decreased and the reflection amplitudes become weaker or dim.

Paige [1973], as discussed in Hilterman [2001], starts to bring the focus back to pre-stack amplitude behaviour. The emphasis of this work is that hydrocarbon related amplitude anomalies can be hidden or obscured on the full stack. It goes on to illustrate that, quite often, hydrocarbon related amplitude changes are more clearly revealed by analysing partial-offset stacks. That is to say, this work shows that limited range stacks can highlight anomalous amplitude behaviour that varies as a function of the range of data being stacked. These can serve as a better direct hydrocarbon indicator than the full-stack amplitudes alone and is the basis of the now standard near-mid-far partial-offset stack analysis. This emphasis back to pre-stack data is highlighted further with the work of Aki and Richards [2002], 1st edition published in 1980, where the Bortfeld [1961] work is further simplified as:

$$R_{\text{PP}}\left(\theta\right) = \frac{1}{2}\frac{\Delta\rho}{\rho}\left(1 - 4\frac{\beta^2}{\alpha^2}\sin^2\theta\right) + \frac{1}{2}\frac{\Delta\alpha}{\alpha}\sec^2\theta - \frac{1}{2}\frac{\Delta\beta}{\beta}\left(8\frac{\beta_2}{\alpha^2}\sin^2\theta\right), \quad (2.2.6)$$

where $\theta = (i_1 + i_2)/2$, $\alpha = (\alpha_1 + \alpha_2)/2$, $\beta = (\beta_1 + \beta_2)/2$, $\rho = (\rho_1 + \rho_2)/2$, and $\Delta(\cdot)$ is the difference between the upper and lower medium properties. This simplification of the Knott-Zoeppritz equation clearly brings to light how variations in the reservoir's rock properties will affect the pre-stack seismic amplitudes at the boundary between

the two layers.

Ostrander [1982, 1984] subsequently demonstrates that the direct detection of hydro-carbon charged reservoirs is possible from actual field acquired data. It was the first widely disseminated work to confirm the relationship between pre-stack amplitude variations and reservoir rock properties with successful wells. The observations of Koefoed [1955] were finally verified with this field experiment. Shuey [1985], armed with the observations of Koefoed and their verification by Ostrander, provides the quantitative tool to transform these observations into an amplitude interpretation theory. By reformulating Equation (2.2.6), Shuey [1985] presents a model for seis-mic amplitudes that is interpreted in terms of various rock property contributions at different angle ranges. It relates rock property variations to the near-mid-far stacks of Paige [1973] and shows which rock property combinations are important at successive offset/angle ranges. Further rearrangement of the Shuey [1985] model, by Verm and Hilterman [1995], shows each angle range to have a response from a single rock-property contribution and is written as

$$
R_{\text{PP}}\left(i_1\right) = \overbrace{\underbrace{\frac{1}{2}\left(\frac{\Delta\alpha}{\alpha}+\frac{\Delta\rho}{\rho}\right)\left(1-4\frac{\beta^2}{\alpha^2}\sin^2 i_1\right)}_{\text{acoustic impedance}}}^{\text{near, } 0°-15°} + \overbrace{\underbrace{\frac{\Delta\nu}{(1-\nu)^2}}_{\text{Poisson's ratio}}\sin^2 i_1}^{\text{mid, } 15°-30°}
$$
$$
+ \overbrace{\underbrace{\frac{1}{2}\frac{\Delta\alpha}{\alpha}}_{\text{P-wave velocity}}\left(\tan^2 i_1-4\frac{\beta^2}{\alpha^2}\sin^2 i_1\right)}^{\text{far, } \geq 30°}.
$$

(2.2.7)

Only the first two terms of Equation (2.2.7) are required to verify the observations of Koefoed. Furthermore, Shuey [1985] shows how to extract the acoustic impedance and Poisson's ratio contrasts directly from the amplitudes of a common depth point gather. After fitting a line to the amplitudes associated with a reflector of interest, the intersection of this line with the vertical axis is the estimated normal incidence reflectivity (also called the intercept) and the slope of this line is the estimated Poisson's ratio contrast (also called the gradient).

An often overlooked aspect of the Shuey [1985] work is its suggestion of the first practical method to seismically infer lithology. The proposed workflow is to extract the rock property contrasts from seismic, cross-plot them, and compare them to cross-plots of the same properties that have been measured in the well. Rutherford and Williams [1989] capitalise on this cross-plotting suggestion, combined with the previous post-stack amplitude anomaly classifications, and propose a qualitative classification methodology based on the amplitudes from reflections from suspected hydrocarbon saturated formations. The modern version of this scheme [Asveth et

al., 2005], based on the North American polarity standard, defines the following classes of pre-stack amplitude anomalies.

Class I - Dim Out Anomaly The gather amplitudes dim as the angle of incidence increases, with potential phase reversal at incidence angles larger than $30°$. The full stack amplitudes are dimmer over the hydrocarbon saturated zone than over the water saturated zone. The near stack/traces (i.e. $\theta_i \in [0°, 15°]$) display a peak-trough wavelet character over the reservoir.

Class II - Natural/Brightening Anomaly The gather amplitudes are weak troughs or absent at near normal incidence and amplitudes brighten (i.e. troughs become stronger) as the incidence angle increases. The amplitude variation of this anomaly carries lithological information, not fluid information, and is highlighted well with partial stacks, as the reservoir amplitudes will be very dim troughs on the full stack. The far stack/traces (i.e. $\theta_i \in [30°, \theta_{max}]$) display a trough-peak wavelet character over the reservoir.

Class IIp - Phase Reversal Anomaly The gather amplitudes are weakly positive near normal incidence and experience a phase reversal then trough/peak brightening as the incidence angle increases. The amplitude variation of this anomaly also carries lithological information, not fluid information, and is highlighted well with partial stacks, as the anomaly will disappear on the full stack. The far stack/traces (i.e. $\theta_i \in [30°, \theta_{max}]$) display a trough-peak wavelet character over the reservoir.

Class III - Bright Spot Anomaly The gather amplitudes are constant or experience a very slight increase as the angle of incidence increases. Full and all partial stacks display bright amplitudes and hydrocarbon prediction is possible from the full stack alone. The entire angle range displays a trough-peak wavelet character. These are associated with hydrocarbon charged soft sand reservoirs.

Class IV The gather amplitudes are constant or experience a very slight decrease as the angle of incidence increases with phase reversal possible at extremely large angles of incidence. These are fairly rare and tend to be associated with soft sand reservoirs that are gas charged and overlain by compacted/silty shales.

When the intercept (I) and gradient (G) are used to define a cross-plot space composed of four quadrants, these classes can be categorised as in Table (2.1).

Class	Impedance	Quadrant	I	G
I	high	4	$+$	$-$
II	low/none	3	$-$	$-$
IIp	low/none	4	$+$	$-$
III	low	3	$-$	$-$
IV	low	2	$-$	$+$

Table 2.1: *Intercept-Gradient cross-plot analysis table for the various pre-stack amplitude anomaly classes, after Asveth et al. [2005]*

.

3

Layered earth amplitude modeling

3.1 Introduction

The first step in any quantitative seismic amplitude interpretation study is to assess the availability and the quality of well data. Well-log information is needed to assess the validity of the seismic data and for quantitative calibration. This step is absolutely essential. If no correspondence between seismic data and well data can be established, either the seismic data or the well data, or both data sets, are in serious error and there is no point in continuing the study until the discrepancy is resolved. Acceptance of a certain degree of mismatch between seismic and well data depends on the amount of noise in either data set. Furthermore, the acceptance of the match would be strongly guided by the plausibility of the matching filter needed to achieve correlation between the measured seismic and the forward modelled response from the well. Once this correlation is accepted, the exercise yields an estimate of the seismic source wavelet $w(t)$ including quantitative calibration, an estimate of the noise in the seismic and an estimate of the absorption parameter Q.

The current state of affairs in seismic amplitude interpretation does not fully exploit the long offset information present in seismic data. A primary reason for this is the fact that the current paradigm for analyzing amplitudes is at odds with the assumptions made for standard seismic data processing. Chapter 3 addresses this issue by addressing linearity and accuracy in forward modelling of seismic data from well-logs, for large ray-parameters, wide-angles, or large offsets. Presented is a layered-earth forward model that is linearized in the elastic properties of the earth. This model preserves linearity at large ray-parameter and can naturally handle fine-layering induced anisotropy. A low-contrast small ray-parameter model is extended to a large ray-parameter model by fully linearising the elastic property contrasts. Overall lin-

earity of the forward model is extended to the layered-earth situation by partitioning the compressional wave and shear wave velocity fields into two fundamental scales. A kinematic scale that governs wave-field propagation effects and a dynamic scale that governs wave-field scattering effects. This partitioning of the velocity fields also leads naturally to forward modelling with full accounting for stretch effects, to resolving the angle-of-incidence versus ray-parameter dichotomy in seismic amplitude analysis, and to the full accounting of induced anisotropy effects due to fine-layering of isotropic media.

With the onset of routine long offset acquisition, this forward model recognizes the physics of seismic wave propagation and allows for a more complete exploitation of the amplitude information available in pre-critical seismic data. This is particularly important if long offset seismic is to be exploited in order to extract direct information about reservoir fluid saturation; because it is in the long offset domain that the customary ways to calculate amplitudes violate the linear data model that underlies the seismic data processing.

3.2   Compressional-to-compressional mode modelling

The basic data set available in a well consists of sonic logs for compressional (P) and shear (S) waves and a density log, which after editing, depth-matching and processing, will result in continuous density ρ, compressional-wave velocity α and shear-wave velocity β curves, usually at a sampling of $0.1524m$ (i.e. standard $0.5ft$ sampling). The link to the seismic data is through the reflectivities R_i, which are a function of the ρ, α and β values at either side of the interface at depth z_i. Reflectivities and transmitivities at a single plane interface between two half spaces are given by the Zoeppritz [1919] equations. Figure 3.1 illustrates the application of the Zoeppritz [1919] P-P equation to a standard set of α, β, and ρ logs. This represents using the P-P Zoeppritz equation to model primaries-only seismic amplitudes in a layered earth situation.

On the left-hand side is the result of applying the Zoeppritz P-P reflectivity operator to unfiltered logs followed by the application of the depth equivalent of a 0-0-80-$120Hz$ high-cut filter, propagating the response to the top of the log, imaging in pseudo-time (i.e. depth converted time), and, finally, applying a zero-phase 5-10-50-$75Hz$ band-pass seismic wavelet. On the right-hand side is the result of first high-cut depth filtering the logs, followed by application of the operator. The propagation, imaging, and wavelet of this response is as in the previous panel. For the (time-invariant) convolutional seismic data model these results should be identical. This image demonstrates that for the long offsets, large ray-parameters, or wide angles, the result depends on the choice of band-width for the input data. That is to say, filtering and reflectivity computation are not commutable operations once the ray-parameter being considered is greater than half the critical ray-parameter.
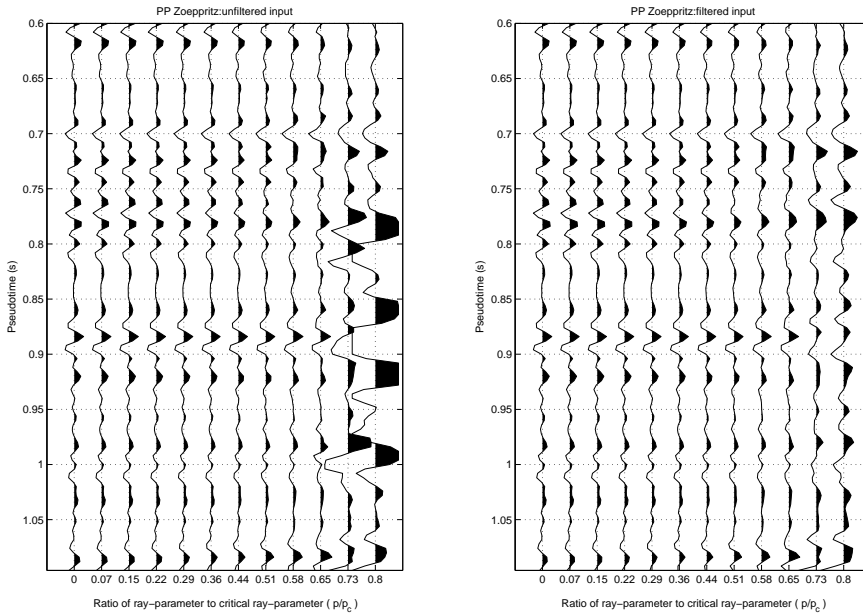
Figure 3.1: *An illustration of how the P-P Zoeppritz equation violates the assumed time-invariant convolutional model for seismic data. The left panel shows the result of computing primaries-only P-P Zoeppritz reflectivities from input logs and then applying a high-cut filter. The right panel shows the result of applying the same high-cut filter to the input logs and then computing the primaries-only P-P Zoeppritz reflectivities. Note that the x-axis scale represents the ray-parameter being considered as a fraction of the minimum critical ray-parameter. This allows a clearer picture of how the model breaks down at "long"-offsets. Also not that filtering and reflectivity calculation are not commutable.*

Therefore, the Zoeppritz equation violates the underlying seismic data model in a long offset layered earth situation. Furthermore, Figure 3.2 illustrates the inaccuracy of the Zoeppritz operator for long offset layered earth modelling. The primaries-only Zoeppritz response (left) is compared to the invariant embedding [Ken] full-waveform response (right), which is also based on the Zoeppritz equations. Both responses have been imaged to zero-offset time. Notice the breakdown in the accuracy of the primaries-only Zoeppritz response at long offset.

Bortfeld [1961] simplifies the Zoeppritz [1919] P-P equation by assuming that successive rock properties of the earth do not vary greatly. This so-called small contrast approximation to Zoeppritz' equation is:
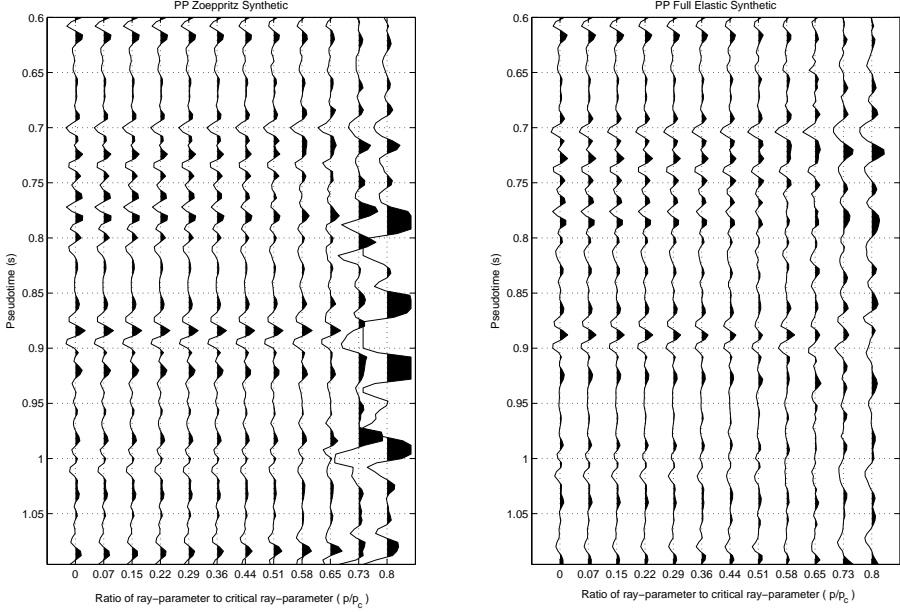
Figure 3.2: *A comparison of a primaries-only P-P Zoeppritz response (left) and its corre-sponding total elastic P-P response (right). As the critical ray-parameter is approached (i.e. at the long-offsets), the primaries-only amplitudes are inaccurate.*

$$R_{\mathrm{PP}}(\theta_1) = \frac{1}{2}\ln\left(\frac{\rho_2}{\rho_1}\right) + \frac{1}{2}\ln\left(\frac{\alpha_2}{\alpha_1}\right) - \frac{1}{2}\ln\left(\frac{\cos\theta_2}{\cos\theta_1}\right) -$$
$$\frac{\sin^2\theta_1}{\alpha_1}(\beta_2+\beta_1)^2\left[\ln\left(\frac{\beta_2{}^2}{\beta_1{}^2}\right) + \frac{1}{2}\ln\left(\frac{\rho_2}{\rho_1}\right)\right]. \tag{3.2.1}$$

with

$$p = \frac{\sin\theta_1}{\alpha_1} = \frac{\sin\theta_2}{\alpha_2} = \frac{\sin\phi_2}{\beta_2} = \frac{\sin\phi_1}{\beta_1} \text{ (Snell's Law)}.$$

Notice, however, that the Bortfeld equation is not fully linearised in the compres-sional wave velocity contrast. To resolve this problem and discover an accurate long-offset linear forward model, Equation (3.2.1) is revisited. Expanding as a Tay-lor series in powers of p^2 gives:

$$R_{\mathrm{PP}}\left(p\right) = \Omega_0 + \Omega_1 p^2 + \Omega_2 p^3 + \cdots$$

with

$$
\begin{aligned}
\Omega_0 &= \frac{1}{2}\ln\left(\frac{\alpha_2\rho_2}{\alpha_1\rho_1}\right), \\
\Omega_1 &= -\left(\beta_1+\beta_2\right)^2\left[2\ln\left(\frac{\beta_2}{\beta_1}\right)+\ln\left(\frac{\rho_2}{\rho_1}\right)\right]+\frac{1}{8}\left(\alpha_1+\alpha_2\right)^2\ln\left(\frac{\alpha_2}{\alpha_1}\right), \text{ and} \\
\Omega_2 &= \frac{1}{16}\left(\alpha_2+\alpha_1\right)^2\left(\alpha_2^2+\alpha_1^2\right)\ln\left(\frac{\alpha_2}{\alpha_1}\right).
\end{aligned}
$$

From Ω_2 onward, the coefficients do not contribute new information as they depend on α_1 and α_2 only but they do serve to widen the range for which the pre-critical reflections, $R_{\mathrm{PP}}\left(p\right)$, can be accurately calculated. After further linearisation and application of Snell's Law, the series converges to:

$$
\begin{aligned}
R_{\mathrm{PP}}\left(\bar{\theta}\right) &= A' - 4B'\left(\frac{\bar{\beta}^2}{\bar{\alpha}^2}\right)\sin^2\bar{\theta}+\frac{C'}{1-\sin^2\bar{\theta}} \\
A' &= \frac{1}{2}\Delta\ln(\rho) \\
B' &= 2\Delta\ln(\beta)+\Delta\ln(\rho) \\
C' &= \frac{1}{2}\Delta\ln(\alpha) \\
\bar{\alpha} &= \left(\alpha_1+\alpha_2\right)/2 \\
\bar{\beta} &= \left(\beta_1+\beta_2\right)/2 \\
\bar{\theta} &= \left(\theta_1+\theta_2\right)/2.
\end{aligned}
\tag{3.2.2}
$$

In a slightly different form this equation was reported in Aki and Richards [2002] as their Eq.(5.46). The difference lies in the way the contrasts are represented. Aki and Richards [2002] represent the contrasts as $\frac{1}{2}\Delta\rho/\bar{\rho}$, $\frac{1}{2}\Delta\alpha/\bar{\alpha}$, and $\frac{1}{2}\Delta\beta/\bar{\beta}$, whereas in Equation (3.2.2) the contrasts are in the $\frac{1}{2}\Delta\ln(\cdot)$ notation. While for truly small contrasts this does not make a difference, for not so small contrasts the $\frac{1}{2}\Delta\ln(\cdot)$ representation is much more accurate. The elastic parameter contrasts described in this manner are identical to the linear perturbation coefficients $\delta\mathcal{T}$ applied to the first-order Taylor expansion of the asymptotic ray series described in Chapman [2004].

Figure 3.3 illustrates that also Equation (3.2.2) is a reflectivity operator that violates the assumed convolutional/linear seismic data model in a layered earth. Again it is seen that this operator does not preserve commutability with filtering. Furthermore, Figure 3.4 shows that Equation (3.2.2) is also inaccurate at long offsets.
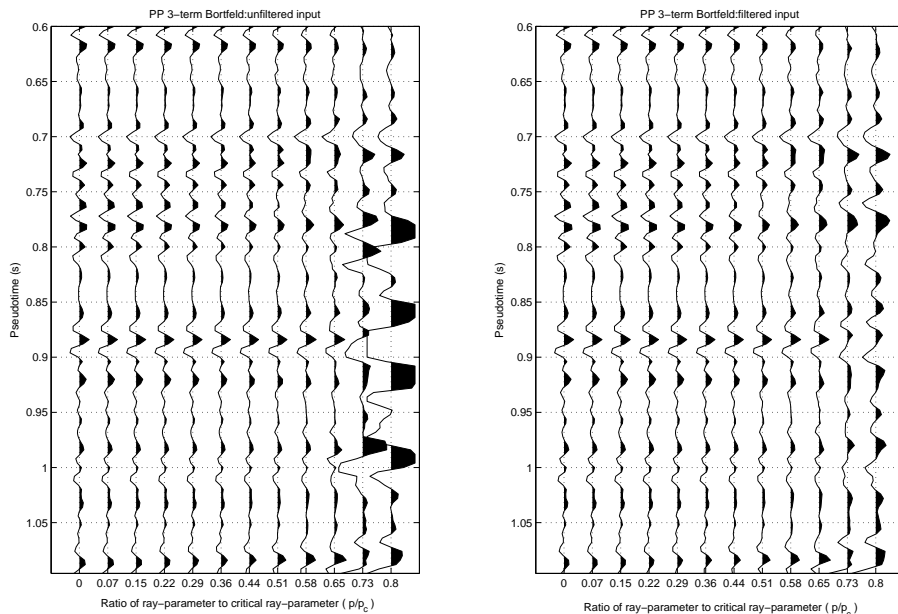
Figure 3.3: *An illustration of how the three-term P-P Bortfeld equation violates the assumed time-invariant convolutional model for seismic data. The left panel shows the result of computing primaries-only three-term P-P Bortfeld reflectivities from input logs and then applying a high-cut filter. The right panel shows the result of applying the same high-cut filter to the input logs and then computing the primaries-only three-term P-P Bortfeld reflectivities. Filtering is still not a commutable operation.*

■ 3.2.1   Explicit background velocities

Equation (3.2.2) is not completely linear and some non-linearity remains due to the $\left(\bar{\beta}/\bar{\alpha}\right)^2$ factor. This may look somewhat puzzling, because Equation (3.2.2) seems to be a strict linearisation of the P-P Zoeppritz equation in the material property contrasts, which, for a single interface, indeed it is. Non-linearity has crept in when the small contrast approximation is applied to a sequence of contrasts (i.e. applied to a well-log/layer-earth situation), thereby making $\bar{\alpha}$ and $\bar{\beta}$ functions of depth. To avoid this non-linearity, we do not linearise in terms of contrasts across interfaces. Instead, we linearise in terms of contrasts of material properties, at any depth, to a background medium. On the one hand this background medium should be sufficiently smooth for waves to propagate in it without being scattered by its inhomogeneity, and on the other hand it should be sufficiently close to the real
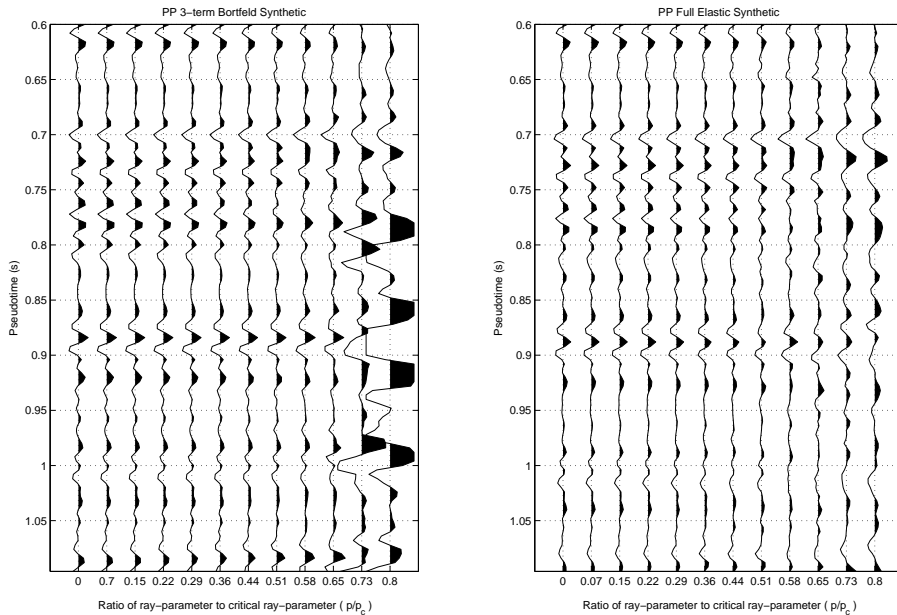
Figure 3.4: *A comparison of a primaries-only three-term P-P Bortfeld response (left) and its corresponding total elastic P-P response (right). As the critical ray-parameter is approached (i.e. at the long-offsets), the primaries-only amplitudes are still inaccurate.*

medium to allow linearisation in the contrasts. Whether or not such a background medium can be defined, depends on the type of experiment being conducted and the regional earth properties themselves.

At this stage we should realize the nature of the experiment we are trying to simulate. A seismic experiment is being forward modelled, the result of which is assumed to be described by a time-invariant convolution data model (i.e. a linear, primary reflections only, model) and which should, therefore, have the property that filtering is a commutable operation. In addition, we realize that for seismic wave propagation in a fine scale inhomogeneous medium, the notions angle of incidence and ray-parameter are defined in terms of wave-fronts, rather than in terms of a high frequency ray approximation at the detail-level of the medium. The amplitudes of these wave-fronts carry quantitative information on the reflectivities of the interfaces encountered, at a resolution set by the bandwidth of the seismic wavelet. The curvatures and slopes of the wave-fronts carry kinematic information on the propagation of the waves, and it is this information that defines propagation angles and ray-parameters. This kinematic information contained in the wave-front pertains to

a background medium governing the wave propagation. To calculate a linear seismic response to a layered medium, let the waves propagate in a smooth background medium and be scattered by the contrasts against this background. Inspecting the amplitude spectrum of two-way-time converted P-wave and S-wave velocity well-logs allow for an understanding of the kinematic information band-width contained in seismic data. What the spectra shown in Figure 3.5 say is that the velocity field is completely dominated by the low frequency band from $0Hz$ up to about $2.5 - 3Hz$. This is consistent with the observation that it is roughly this spectral band that can be retrieved from kinematic seismic velocity measurements.
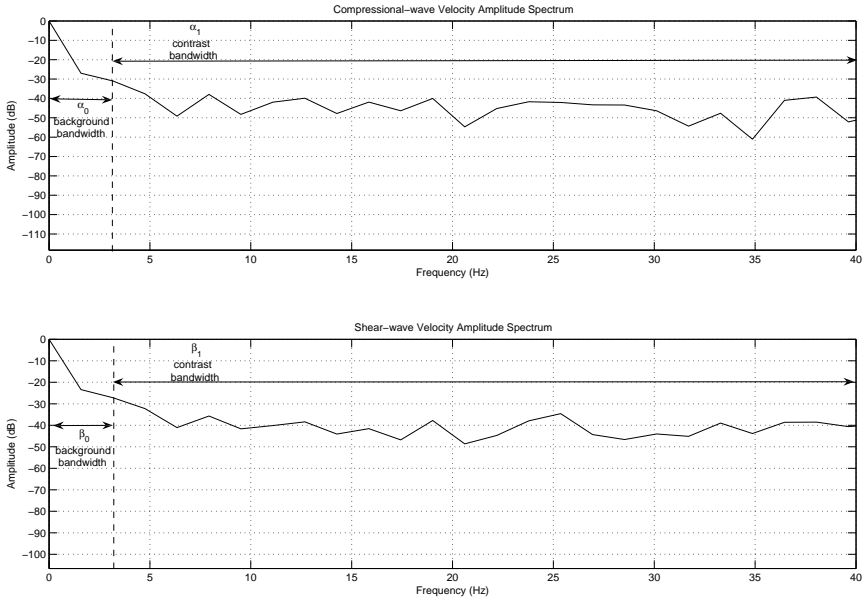
Figure 3.5: *Amplitude spectra of a compressional-wave velocity log (top) and a shear-wave velocity log (bottom).*

With the above in mind, reconsider Equation (3.2.2) when applied to forward modelling of the seismic response to a finely layered medium. The amplitude information related to the contrasts in the media properties across interfaces is contained in the A', B' and C' coefficients. The kinematic information contained in the seismic data, pertaining to the background medium, is represented by $\sin^2 \bar{\theta}$ and $(\bar{\beta}/\bar{\alpha})^2 \sin^2 \bar{\theta}$ in Equation (3.2.2). However, $\bar{\beta}/\bar{\alpha}$ is still given by the full velocities in the real medium and, therefore, also carries the contrast information. Mathematically, we separate

the two sets of information as:

$$\alpha = \alpha_0 + \alpha_1$$
$$\beta = \beta_0 + \beta_1$$

(3.2.3)

where α_0 and β_0 represent the background velocities defined by the 0-3Hz spectral bands that dominate the kinematic behavior of the seismic wave-field. If this claim of wave-field propagation being governed by a kinematic region of the velocity field is true, then a wavefront propagating in a medium with a detailed velocity structure will be smooth. Figure 3.6 shows a snapshot of a wavefront that has been propagated in such a medium via a finite-difference solution to the wave equation.

Wavefield at 1.350 s
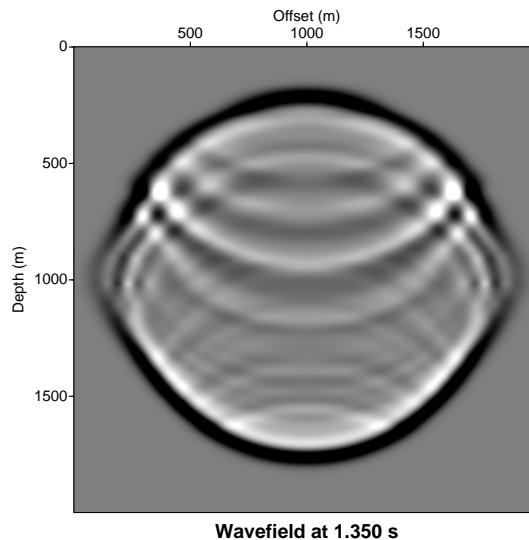
Figure 3.6: *A seismic wavefront propagated in a detailed velocity model.*

Notice the smooth nature of the wavefront. Hence, wave-fronts propagate according to the trend of the velocity structure and not the detail. This also establishes α_0 and β_0 as the velocity functions required to map from the angle (θ) domain to the ray-parameter (p) domain.

In a linear forward modelling procedure, it must hold that $\alpha_1 \ll \alpha_0$ and $\beta_1 \ll \beta_0$. Figure 3.7 illustrates this concept of separated velocity fields.
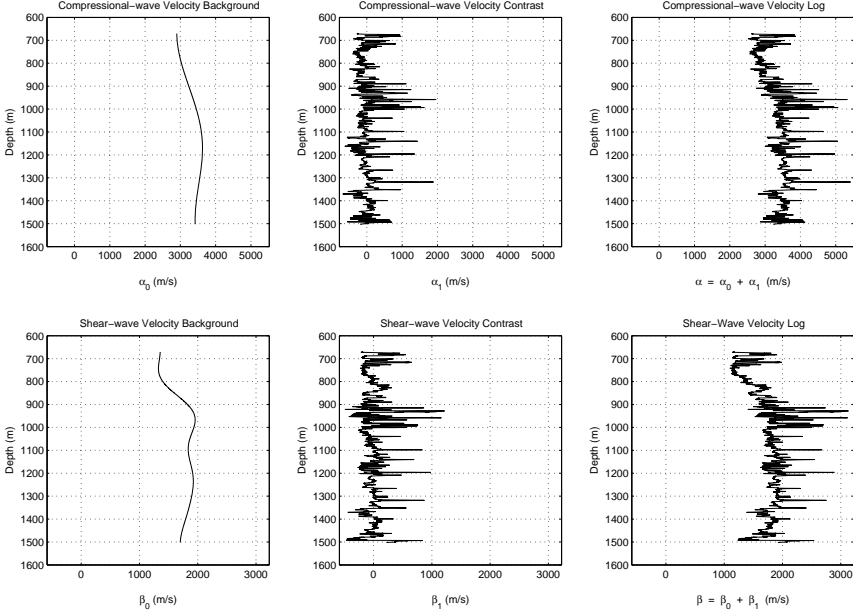
Figure 3.7: *The compressional-wave (top panel) and shear-wave (bottom panel) velocities decomposed into a background and contrasts against this background (i.e. kinematic and dynamic parts).*

Note that α_1 and β_1 represent the contrasts of the true medium against the background medium, whereas A', B' and C' represent contrasts across interfaces. If the problem is linearizable, these two types of contrasts should be of the same order of magnitude.

■ 3.2.2   A linear P-P velocity-separated forward model

Using Equation (3.2.3), instead of $\bar{\alpha}$ and $\bar{\beta}$, in Equation (3.2.2) and noting that $\alpha_1 B'$ and $\beta_1 B'$ are now second order quantities, the first order linearisation in terms of contrasts against a background is:

$$R_{\mathrm{PP}}\left(\theta\right) = A' - 4B'\left(\frac{\beta_0^2}{\alpha_0^2}\right)\sin^2\theta + \frac{C'}{1-\sin^2\theta}. \qquad (3.2.4)$$

In terms of scattering theory, the α_0 and β_0 are the zero-order velocity fields representing a medium that does not scatter the incident wave-field, but describes the

travel times (i.e. the kinematics) of the waves in the true medium accurately. The contrasts against these backgrounds are α_1 and β_1 and these velocity fields drive the scattering of the wave-field. In the first-order Born approximation, the scattered field is linear in the contrasts. From a perturbation theory point of view, Equation (3.2.4) is seen as small perturbations, or weak contrasts, against a null interface reference model [Chapman, 2004].

The linearity offered by the reflectivity operator Equation (3.2.4) is shown in Figure 3.8. The data set available for this modelling, shown in Figure 3.9, consists of sonic logs for compressional (P) wave velocity, α and shear (S) wave velocity, β, and a density, ρ, log from an AVO dataset. These α, β and ρ curves are sampled at a rate of $0.1524m$ and are the same logs used for the Zoeppritz and three-term Bortfeld modelling.
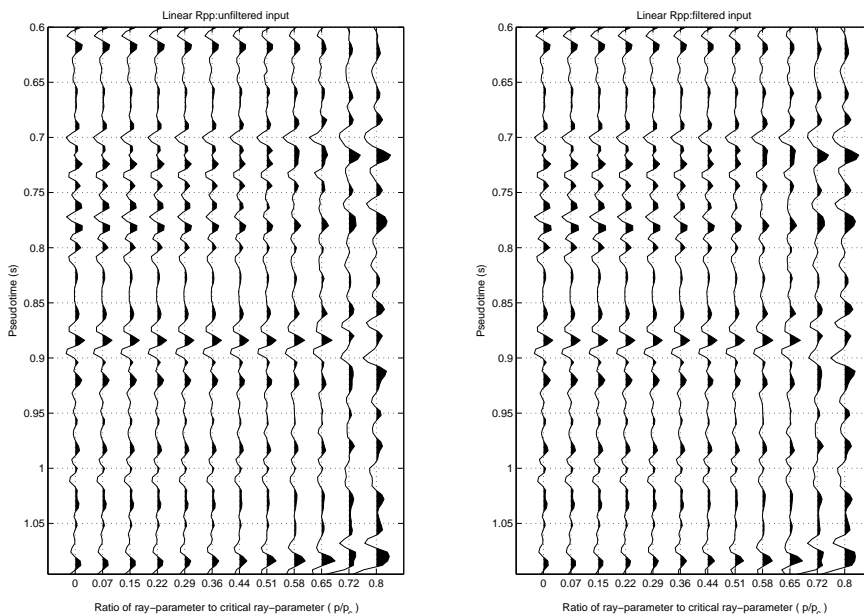
Figure 3.8: *An illustration of how the three-term P-P velocity-separated equation agrees with the assumed time-invariant convolutional model for seismic data. The left panel shows the result of computing primaries-only three-term P-P velocity-separated reflectivities from input logs and then applying a high-cut filter. The right panel shows the result of applying the same high-cut filter to the input logs and then computing the primaries-only three-term P-P velocity-separated reflectivities. Filtering is now a commutable operation.*
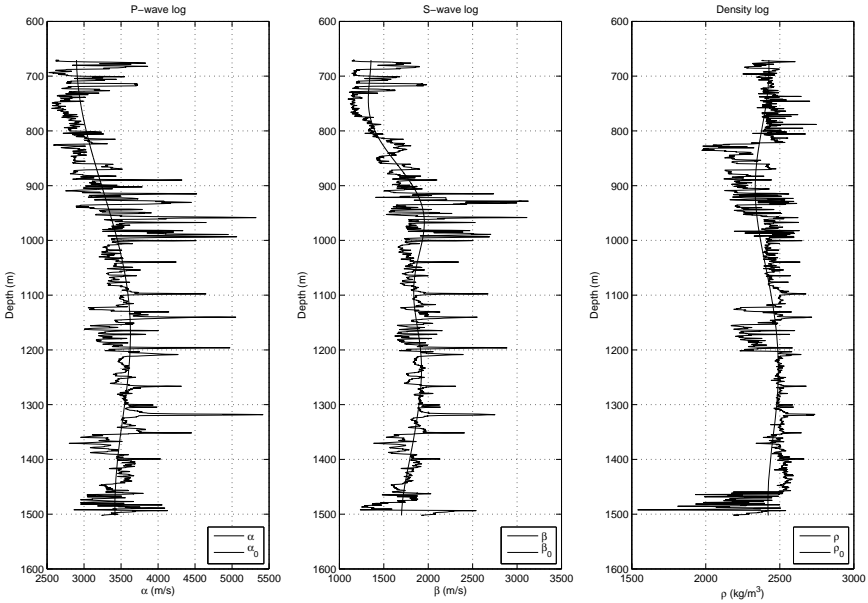
Figure 3.9: *The input α, β, and ρ well logs from the MOBIL AVO data set. Note the overlying (i.e. kinematic/macro scale) α_0, β_0, and ρ_0 backgrounds.*

Linearity is still not exact. This is because, although only slowly varying, α_0 and β_0 are functions of depth or pseudo-time. However, remembering that the background medium is sufficiently smooth not to scatter propagating waves in the seismic bandwidth, this non-linearity is by definition negligible.

The validity of the proposed forward model can only be proved, of course, by a comparison with real measurements. In this case that would mean that a synthetic seismogram, linearly modelled from well-log data, would be compared with a real imaged seismic data trace. Unfortunately, a fully imaged 3-D seismic data trace over the well-location, still has an uncertainty attached to it with respect to its positioning accuracy. The best thing, therefore, is creating a full elastic synthetic from the log data. As far as issues of linearity are concerned, this will really tell how accurate the linear modelling is. The comparison between the linearly modelled gather based on Equation (3.2.4) and full elastic modelling is shown in Figure 3.10. Since the ray-parameter range used for the comparison leads to fairly large incidence angles over the time gate shown, the start of amplitude blow-up is seen on the outer most traces of the linear gather. The limit of the validity of linearisation has been reached. Note, however, that the amplitudes are still better controlled than in either version

of the Zoeppritz or Bortfeld result. Overall, the linear modelling tracks the full elastic modelling amplitude-wise and character-wise, very well. When the reflection angle gets wider and wider, eventually the reflectivities will become too large for linearisation and the convolution model breaks down.
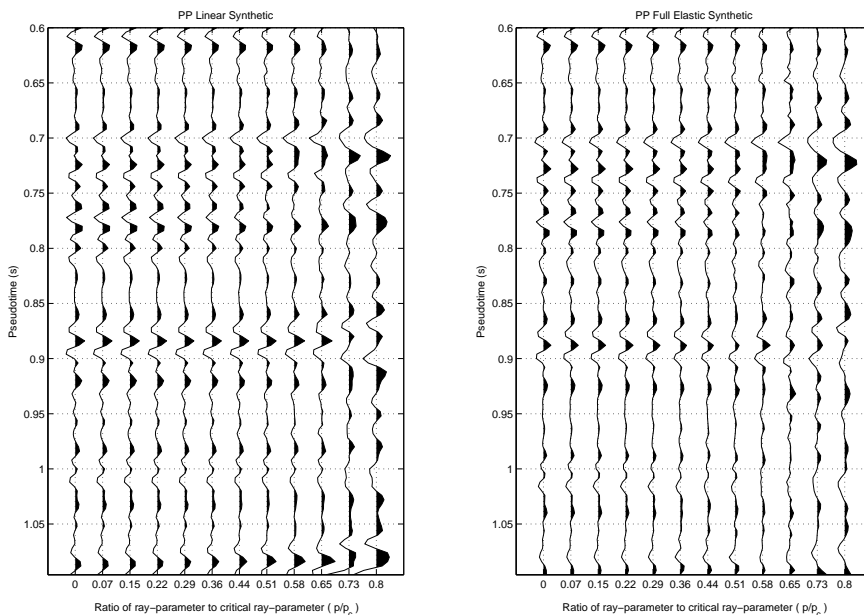
Figure 3.10: *A comparison of a primaries-only three-term P-P velocity-separated response (left) and its corresponding total elastic P-P response (right). As the critical ray-parameter is approached (i.e. at the long-offsets), the primaries-only amplitudes are now much more accurate.*

■ 3.2.3   Layering induced anisotropy

In any finely layered medium there is velocity dispersion and anisotropy. This is not due to intrinsic anisotropy in the individual layers, but to multiple scattering at the layer interfaces. Recall, however, that in order to linearise the modelling algorithm for a layered earth situation, the contrasts of the local medium parameters are defined against a background medium, rather than across interfaces, as the parameters to be linearized. This background medium, which only describes the propagation of the waves that are scattered by the contrasts, can be, and often

should be, anisotropic and dispersive.

It may look contradictory that a smoothly varying medium, specifically defined as non-reflective for the frequencies in the seismic wavelet, would show dispersion which is based on multiple scattering. This paradox is explained by considering the following argument. Given the highest frequency in the wavelet, the smoothly varying velocity profile of the background medium can be represented as a staircase of very small steps, none of which would give a measurable reflection at any frequency in the wavelet. For a wave propagating in such a medium there is a gradual, but very systematic, accumulation of peg-leg multiples leading to a phase-shifted and broadened 'pseudo primary' arrival, as described by O'Doherty and Anstey [1971]. This effect is all the more observable because of the systematic change in the smoothly varying media properties. The energy that is scattered back to the surface, on the other hand, is very small at any one time and is spread out over the full two-way propagation time of the 'pseudo-primary', and beyond.

In theoretical work by Shapiro et al. [1994] and Shapiro and Hubral [1995], reviewed in Mavko et al. [1998], on horizontally layered random media, it is derived that dispersion is driven by the auto-correlations and cross-correlations of the medium properties α, β, and ρ. The correlation functions of the contrasts are small compared to the correlation functions of the background functions themselves. In other words, the smoothly varying background model by itself already explains most of the dispersion.

Anisotropy induced by fine layering is another manifestation of the dispersion effect described above. Having established that this anisotropy can be accounted for in the background medium, it is now of interest to investigate how the background anisotropy affects the reflection coefficients. Of particular concern is investigating the similarity between accounting for background anisotropy and the more traditional approach of defining an anisotropy contrast across a single interface as shown in Thomsen [1993], Rüger [1996], and Tsvankin [2001].

Following the above authors, the case of weak anisotropy is written as:

$$
\begin{aligned}
\alpha_0\left(\theta\right) &= \alpha_0^i\left[1 + \delta_0 \sin^2\theta \cos^2\theta + \epsilon_0 \sin^4\theta\right] \\
\beta_0\left(\theta\right) &= \beta_0^i\left[1 + \frac{\alpha_0^{i^2}}{\beta_0^{i^2}}\left(\epsilon_0 - \delta_0\right)\sin^2\theta \cos^2\theta\right]
\end{aligned}
\tag{3.2.5}
$$

where ϵ_0 and δ_0 are the well known Thomsen [1986] parameters, describing a vertically transverse isotropic (V.T.I.) background model. The isotropic part of the velocities is denoted by α_0^i and β^i. Substituting the anisotropic velocity expressions in the equation for the reflectivity (Equation (3.2.4)) and linearising in the coefficients ϵ_0 and δ_0 gives:

$$R_{\mathrm{PP}}(\theta) = R_{\mathrm{PP}}^{i}(\theta) + R_{\mathrm{PP}}^{a}(\theta) \tag{3.2.6}$$

with

$$R_{\mathrm{PP}}^{i}(\theta) = A' - 4B'\left(\frac{\beta_0^{i^2}}{\alpha_0^{i^2}}\right)\sin^2\theta + \frac{C'}{1 - \sin^2\theta}$$

and

$$R_{\mathrm{PP}}^{a}(\theta) = -8B'\sin^4\theta\left[\epsilon_0 - \delta_0\left(1 - \frac{\beta_0^{i^2}}{\alpha_0^{i^2}}\right)\cos^2\theta\right].$$

$R_{\mathrm{PP}}^{a}(\theta)$ is that part of the reflectivity that is caused by the anisotropy in the background medium. Note that $R_{\mathrm{PP}}^{a}(\theta)$ contains all the fine detail present in B', which represents the contrasts between the fine scale layers that are isotropic themselves. Reconciling fine layering effects on seismic amplitudes in the manner described above allows for the proper use of seismically estimated (i.e. data driven) Thomsen's parameters. This is because the anisotropy parameters are estimated and used at the background scale. In forward modelling of a synthetic seismic response from well-logs, the background anisotropy constants ϵ_0 and δ_0 could be estimated from the logs, using Backus averaging (Backus [1962]) or an algorithm like the one presented by Shapiro and Hubral [1995]. Anisotropy estimates at the appropriate scale can also be taken from seismic in the way described by Hilterman [2001].

Let us compare this result directly to the result obtained by Rüger [1996] for a single interface between two anisotropic layers with anisotropy contrasts $\Delta\epsilon$ and $\Delta\delta$:

$$R_{\mathrm{PP}_{\mathrm{Rüger}}}^{a}(\theta) = \frac{1}{2}\Delta\delta\sin^2\theta + \frac{1}{2}\Delta\epsilon\sin^2\theta\tan^2\theta.$$

The anisotropy contrasts $\Delta\epsilon$ and $\Delta\delta$ for the single interface can be translated to equivalent background anisotropy constants ϵ_0 and δ_0 that drive the isotropic contrast B' to produce the same anisotropy contribution to the reflectivity. Should the situation arise where both intrinsic and layering-induced anisotropy are present (i.e. a thick shale cap overlying a reservoir of stacked thin sandstones), then a proper accounting of the effects on the reflection coefficients involves combining the Rüger [1996] result with Equation (3.2.6). This case is written as:

$$R_{\mathrm{PP}}(\theta) = R_{\mathrm{PP}}^{i}(\theta) + R_{\mathrm{PP}}^{a}(\theta) + R_{\mathrm{PP}_{\mathrm{Rüger}}}^{a}(\theta) \tag{3.2.7}$$

where all terms are defined as before.

Alternatively, Equation (3.2.4) could be written in terms of the ray-parameter p :

$$R_{\text{PP}}(p) = A' - 4B'\beta_0^2 p^2 + \frac{C'}{1 - \alpha_0^2 p^2}. \tag{3.2.8}$$

Realize, however, that when calculated for a stack of thin isotropic layers, $R_{\text{PP}}(p, z)$ and $R_{\text{PP}}(\theta, z)$ do not refer to the same physical experiments. Whereas $R_{\text{PP}}(p, z)$ is the result of a single experiment with an incident plane wave with horizontal slowness p, $R_{\text{PP}}(\theta, z)$ can only be constructed from many different experiments with plane waves selected to give the same angle of incidence at all depths z . For this reason $R_{\text{PP}}(p, z)$ is preferred for the purpose of seismic-to-well matching.

Under the same weak anisotropy assumption, the anisotropy equations for α_0 and β_0 in terms of the same ϵ_0 and δ_0 coefficients, can be re-written as a function of p:

$$\alpha_0(p) = \alpha_0^i \left[1 + \delta_0 \alpha_0^{i^2} p^2 \left(1 - \alpha_0^{i^2} p^2 \right) + \epsilon_0 \alpha_0^{i^4} p^4 \right]$$
$$\beta_0(p) = \beta_0^i \left[1 + \frac{\alpha_0^{i^2}}{\beta_0^{i^2}} (\epsilon_0 - \delta_0) \alpha_0^{i^2} p^2 \left(1 - \alpha_0^{i^2} p^2 \right) \right] \tag{3.2.9}$$

When substituting these expressions in Equation (3.2.8), the result for $R_{\text{PP}}^a(p)$ is different because α_0 now appears in the C' term, rather than in the B' term. This should not be surprising because, as pointed out above, $R_{\text{PP}}(\theta, z)$ and $R_{\text{PP}}(p, z)$ refer to different experiments. $R_{\text{PP}}(p, z)$ is the more physically meaningful quantity. The contribution to $R_{\text{PP}}(p)$, stemming from the anisotropy in the background, to first order in ϵ_0 and δ_0 is:

$$R_{\text{PP}}^a(p) = -8B' \alpha_0^{i^4} p^4 \left(1 - \alpha_0^{i^2} p^2 \right) (\epsilon_0 - \delta_0)$$
$$+ \frac{2C' \alpha_0^{i^4} p^4}{\left(1 - \alpha_0^{i^2} p^2 \right)^2} \left[\delta_0 \left(1 - \alpha_0^{i^2} p^2 \right) + \epsilon_0 \alpha_0^{i^2} p^2 \right].$$

When applied to a stack of thin layers, α_0^i, δ_0 and ϵ_0 are slowly varying with depth while B' and C' are functions of depth at the fine scale.

The full elastic gather in Figure 3.10, computed from the logs shown in Figure 3.9, shows no indication of thin layering induced velocity anisotropy. Both the linearly modelled gather and the full elastic gather have been imaged with an anisotropy-free (i.e. isotropic) background velocity field. If the full elastic modelling at the fine log scale had introduced anisotropy, then the imaged gather would display anisotropic *pull-up*, at the scale at which propagation effects can be observed. No such pull-up

is observed. Figure 3.11 shows that the Thomsen parameters ϵ and δ for weak elastic anisotropy, computed following Backus [1962], are quite small. This implies that the reflectivity response must be dominated by the isotropic contribution.
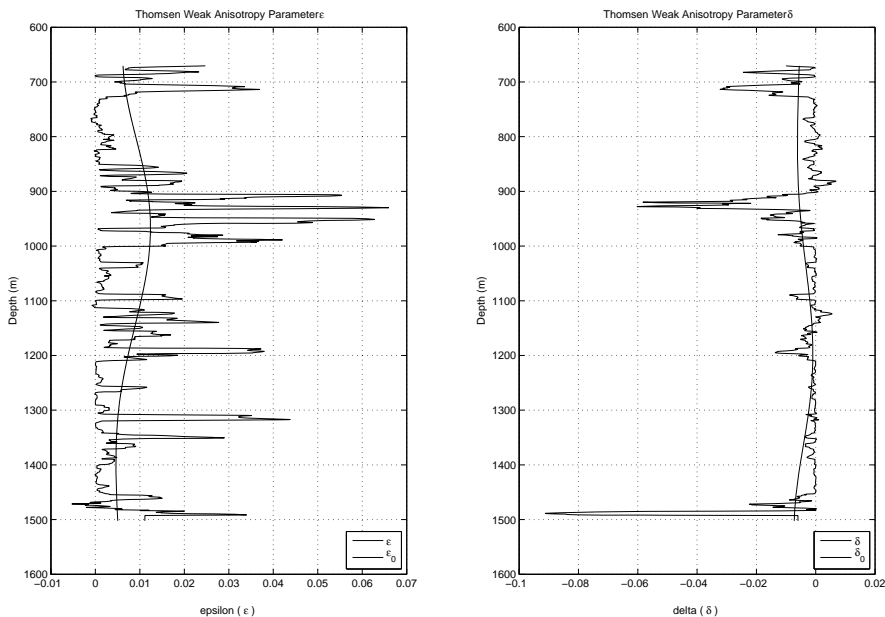
Figure 3.11: *Backus average computed effective weak elastic anisotropy (Thomsen) parameters for the logs shown in Figure 3.9.*

Further investigation shows that this minimal induced anisotropic effect is not surprising since Figure 3.12 shows that, on the basis of Backus averaging, the expected maximum P-wave anisotropy of about 6.5 % and the expected maximum S-wave anisotropy of around 18 % are not sustained over time durations long enough (or thicknesses large enough, rather) to produce an observable pull-up.

As an illustrative example of how velocity anisotropy due to multiple scattering from thin layering can be handled using the ray-parameter formulation of Equation (3.2.6) is shown in Figure 3.13. The choice of values for ϵ_0 and δ_0 are made based on those reported in Thomsen [1986], Alkhalifah et al. [1996], and Berryman et al. [1999]. Note the strong anisotropic pull-up, observed at the scale of the background.
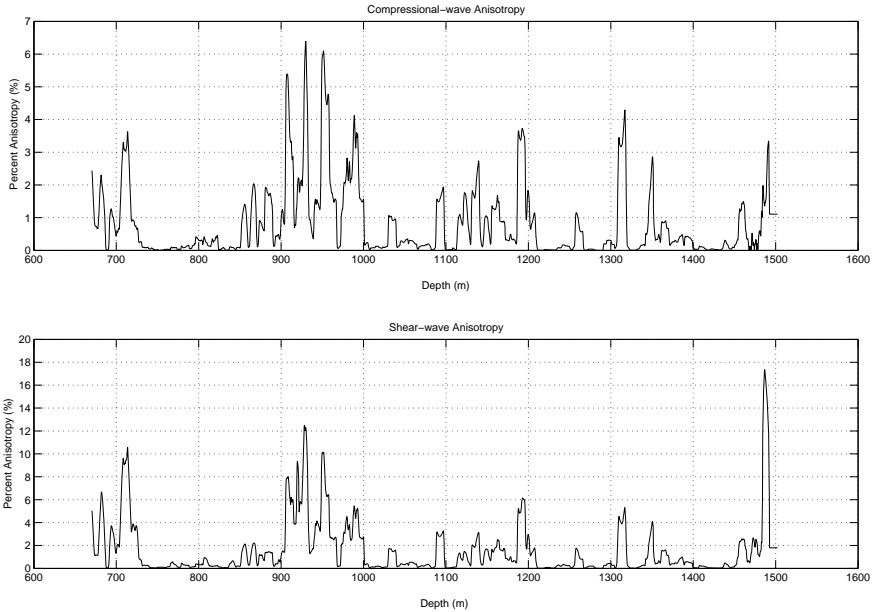
Figure 3.12: *Backus average computed amounts of induced compressional-wave and shear-wave anisotropy for the logs shown in Figure 3.9.*

■ 3.2.4   Analytic seismic amplitude forward modelling

Now consider, analytically, the seismic response to the subsurface seen in the well, in terms of amplitude versus ray-parameter (AVP) amplitudes, imaged at the well location. This is basically the imaging step, referred to in the previous section, that extracts in-situ AVP amplitudes from surface recorded or forward modelled data. The reason this analysis is relevant to wide-angle linear forward modelling, is that non-linearities may be introduced when one picks the wrong scale for the velocity field used in imaging and in the description of the stretch involved when imaging wide-angle data.

In the data-driven approach taken within the DELPHI consortium, the seismic AVP amplitudes are treated as being the result of successive shot-receiver re-focusing (back-propagation). The one-way-travel-time re-focusing (back-propagation) operators required for this are obtained from the seismic data explicitly by use of the Common Focal Point (CFP) technology [Thorbecke, 1997; Berkhout, 1997a,b].

In Figure 3.14 the well stick is shown at the location of the well $\underline{x}_w$. In the well, there
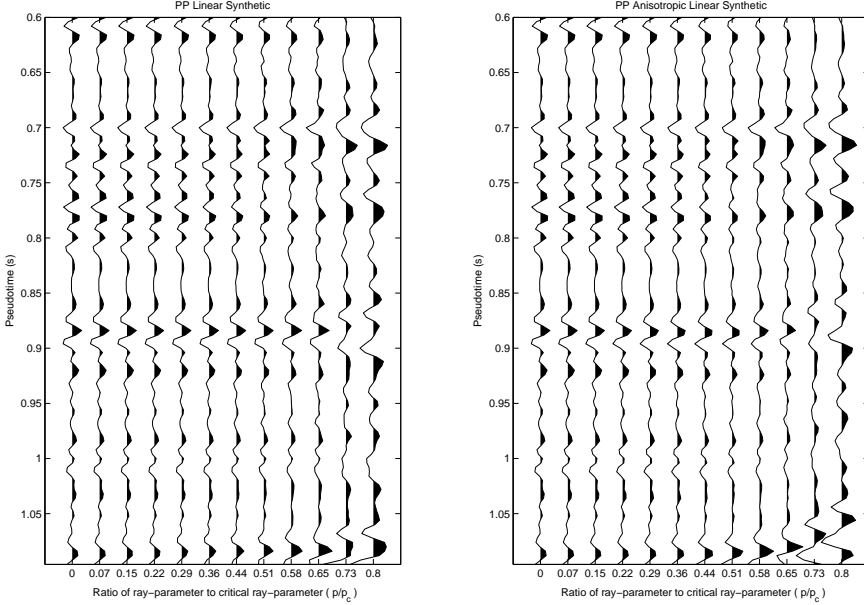
Figure 3.13: *An illustration of handling induced anisotropy with $\epsilon_0 = 0.1$ and $\delta_0 = -0.005$. The left panel shows the isotropic linear response and the right panel shows the anisotropic linear response.*

are interfaces at depths z_j with reflectivities R_j, calculated using Equation (3.2.4). This is done at the original $0.1524m$ sampling of the logs, but having established the linearity of the reflectivity operator, the reflectivities can be filtered and re-sampled to the seismic sampling rate. The analysis begins at the point where there is a re-focused receiver, positioned at depth z_j in the well, recording data from a source located at the surface at position $\underline{x}_s$. The re-focusing of the receivers to the location $(\underline{x}_w, z_j)$ is performed using the one-way-travel-time re-focusing operator $T_j(\underline{x}_w, \underline{x}_s)$.

For the signal recorded by the receiver at position $(\underline{x}_w, z_j)$ we write:

$$s(\underline{x}_s, 0; \underline{x}_w, z_j; t) = \sum_i R_i(p_{ij}) \frac{w(t - T_{ij})}{T_{ij}} \qquad (3.2.10)$$

where $w(t)$ is the seismic source wavelet and where $p_{ij} = \sin(\theta_{ij})/v_i$ is is the slowness of the wave reflected at the ith interface. T_{ij} and θ_{ij} are generally unknown, but for $i = j$ the relation $T_{jj} = T_j$ holds, which is the re-focusing operator that is known, and therefore $\theta_{jj} = \theta_j$. In Figure 3.14 an example position $i > j$ is shown. The
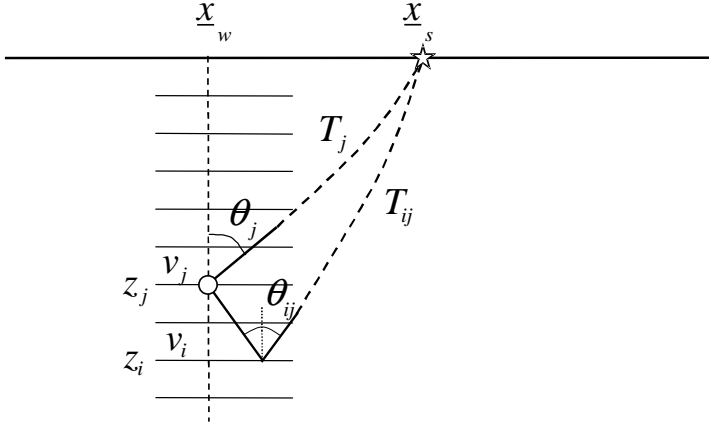
Figure 3.14: *Diagram showing a set of horizontal reflectors at the well location. There is a re-focused receiver location at depth z_j, shot into from the surface source location $\underline{x}_s$. The travel-time T_j is part of the one-way-travel-time re-focusing operator for depth z_j. Arrivals at the receiver location at z_j from other reflectors have arrival times T_{ij}.*

geometrical meaning of T_{ij} is then immediately clear. Bear in mind, however, that Equation (3.2.10) describes a re-focused record and that T_j is not the first arrival time, but is preceded by reflections related to the interfaces for which $i < j$. T_{ij} for $i < j$ is perfectly well defined, but there is no simple geometrical interpretation of it, like for the case where $i > j$. Subsequent re-focusing of the sources to the location $(\underline{x}_w, z_j)$ would create a full stack image there. For the extraction of AVP amplitudes, however, we do not integrate over all source positions, but only over those from which the rays arrive at the reflection point $(\underline{x}_w, z_j)$ with slowness $p_j = \sin(\theta_j)/v_j$. In the Common Focal Point (CFP) technology developed at Delft University of Technology [van de Rijzen, 2007] this information is explicitly available, but there are other imaging techniques where the image gathers in offset can be translated to ray-parameter, or incident angle, at the reflection point (i.e. ray-parameter or angle gathers).

Analytic extraction of AVP amplitudes from the record described by Equation (3.2.10) now simply means filling in T_j for t in Equation (3.2.10) and correcting the amplitudes for propagation effects by multiplying by T_j , resulting in:

$$a(z_j, p_j) = \sum_i R_i(p_{ij}) \frac{T_j}{T_{ij}} w(T_j - T_{ij}). \qquad (3.2.11)$$

In the summation over i in Equation (3.2.11), the jth term $w(0)R_j(p_j)$ contains the desired information on the reflector at z_j, whereas the remainder of the summation:

$$\sum_{i\neq j} R_i(p_{ij}) \frac{T_j}{T_{ij}} w(T_j - T_{ij})$$

describes the interference effects from surrounding reflectors, due to the non-zero length of the seismic source wavelet. For a delta-pulse wavelet the interference contribution to Equation (3.2.11) would disappear.

In the following analysis, assume that the seismic wavelet $w(t)$ is short compared to the one-way-travel-times T_j. This means that in the summation in Equation (3.2.11) only a relatively small number of neighboring interfering reflectors need to be considered. Also assume that in the small neighborhood around the jth reflector the following approximations hold:

$$\frac{T_j}{T_{ij}} \approx 1$$

$$\sin(\theta_{ij}) \approx \sin(\theta_j)$$

$$p_{ij} \approx p_j \tag{3.2.12}$$

$$T_{ij} - T_j \approx 2\cos(\theta_{ij}) \sum_{k=j+1}^{i} \frac{d}{v_k}$$

where d is the layer thickness. Introducing the pseudo-two-way-travel-times:

$$\tau_i = 2\sum_{k=1}^{i} \frac{d}{v_k} \text{ and } \tau_j = 2\sum_{k=1}^{j} \frac{d}{v_k} \tag{3.2.13}$$

and using the above approximations, Equation (3.2.12) can be written as:

$$T_j - T_{ij} = (\tau_j - \tau_i)\sqrt{1 - p_j^2 v_j^2}.$$

Equation (3.2.11) then reads:

$$a(\tau, p) = \sum_i R_i(p) w\left[(\tau - \tau_i)\sqrt{1 - p^2 v^2}\right]. \tag{3.2.14}$$

where we dropped all subscripts j because τ now becomes the running variable for all depth points for which AVP amplitudes are extracted. From the discussion on the band-width of the geometrical velocity information in seismic data, it should

now be clear that for the velocity function v in Equation (3.2.11) one should use the narrow band low frequency velocity function α_0. The approximations made in Equation (3.2.12) are consistent with this.

The trace $a(\tau, p)$ in Equation (3.2.14) looks like a simple convolution of the primary reflection series $R(\tau, p)$ with a stretched seismic wavelet $w(\tau/\zeta)$, where

$$\zeta = \frac{1}{\sqrt{1 - p^2 \alpha_0^2}}$$

is the well known stretch factor. Note that Equation (3.2.14) is not an exact convolution because α_0 in the stretch factor ζ depends on the pseudo-time τ. Given the length of the seismic wavelet and the slowly varying character of α_0, this non-linearity is negligible.

Equation (3.2.14) illustrates the fundamental problem of reduced resolution for illumination with oblique incidence and is generally valid, independent of the imaging algorithm used. Equation (3.2.14) is derived here because stretch is an inevitable consequence of using wide angle seismic. With the help of the background velocity function, which has such a scale that it can be derived from seismic, one can calculate the stretch as a function of slowness and account for it in the seismic-to-well match. It is interesting to note that the non-linearity that would be introduced when using a fine scale velocity model in Equation (3.2.14) is of the same nature as the non-linearity observed if using Equation (3.2.2) instead of Equation (3.2.4) for the modelling of the reflectivities.

Although stretch cannot be avoided as far as resolving the subsurface in depth or pseudo-time is concerned, it can be avoided in a comparison of seismic and well-derived amplitudes for the purpose of extracting the seismic source wavelet. Rather than comparing the imaged data, analytically represented by Equation (3.2.14), with the well reflectivities and obtain a stretched wavelet, we can propagate the well data and the imaged seismic data back to the surface, as plane waves, and perform the comparison in the linear Radon domain, which is a proper time domain where the wavelet should be undistorted, as demonstrated below.

Under the same approximations as made before ($\theta_{ij} \approx \theta_j$ and $p_{ij} \approx p_j$) and using Equation (3.2.13), Equation (3.2.14) can be re-written as:

$$a\left(\tau_j, p\right) = \sum_i R_i\left(p\right) w \left(\sum_{k=1}^{j} \frac{2d}{v_k} \sqrt{1 - p^2 v_k^2} - \sum_{k=1}^{i} \frac{2d}{v_k} \sqrt{1 - p^2 v_k^2} \right). \qquad (3.2.15)$$

Propagating this amplitude as a plane wave to the surface through a stack of horizontal plane layers with velocities $\frac{1}{2} v_j$, means assigning the sample $a\left(\tau_j, p\right)$ to time t of the time-trace $s\left(\underline{x}_w, t, p\right)$ at the surface, where:

$$t = \sum_{k=1}^{j} \frac{2d}{v_k} \sqrt{1 - p^2 v_k^2}$$

is the propagation time of a slanting plane wave from depth z_j to the well-head. This then gives:

$$s\left(\underline{x}_w, t, p\right) = \sum_i R_i\left(p\right) w\left(t - \sum_{k=1}^{i} \frac{2d}{v_k}\sqrt{1 - p^2 v_k^2}\right), \qquad (3.2.16)$$

which indeed shows the undistorted wavelet $w(t)$. Note that Equation (3.2.16) is just a trick to avoid stretch in the seismic-to-well comparison. Since both the well data and the imaged seismic are propagated to the surface using a well-derived horizontally layered velocity model, Equation (3.2.16) will never represent the true linear Radon transform of a surface seismic record. If we do not use imaged data as a starting point for our quantitative analysis, the stretch can simply be avoided by considering fully redatumed seismic data at the top of the logged interval. This data can directly be compared to the synthetic data modelled from the logs.

3.3 Compressional-to-shear mode modelling

P-S converted wave amplitude modelling is beset with many of the same problems as P-P modelling. Figure 3.15 illustrates the application of the Zoeppritz [1919] P-S equation to a standard set of α, β, and ρ logs. This represents using the P-S Zoeppritz equation to model primaries-only seismic amplitudes in a layered earth situation.

On the left-hand side is the result of applying the Zoeppritz P-S reflectivity operator to unfiltered logs followed by the application of high-cut filtering. On the right-hand side is the result of first high-cut filtering the logs and then applying the P-S operator. As in the P-P case, these results should be identical. This image demonstrates that for the long offsets, large ray-parameters, or wide angles, filtering and reflectivity computation are also not commutable operations in the P-S case. This is particularly noticeable once the ray-parameter being considered is greater than half the critical ray-parameter. Therefore, the P-S Zoeppritz equation is not consistent with the underlying seismic data model in a long offset layered earth situation. Furthermore, in the same manner as the P-P case, Figure 3.16 illustrates the inaccuracy of the operator for long offset layered earth modelling. The P-S Zoeppritz response (left) is compared to the full-waveform response (right). Notice the progressive breakdown in the accuracy of the Zoeppritz response at longer and longer offsets.

Aki and Richards [2002] simplifies the non-linear P-S equation in the same way as the P-P equation and this linearised approximation, with respect to potentials instead of particle displacement, is:
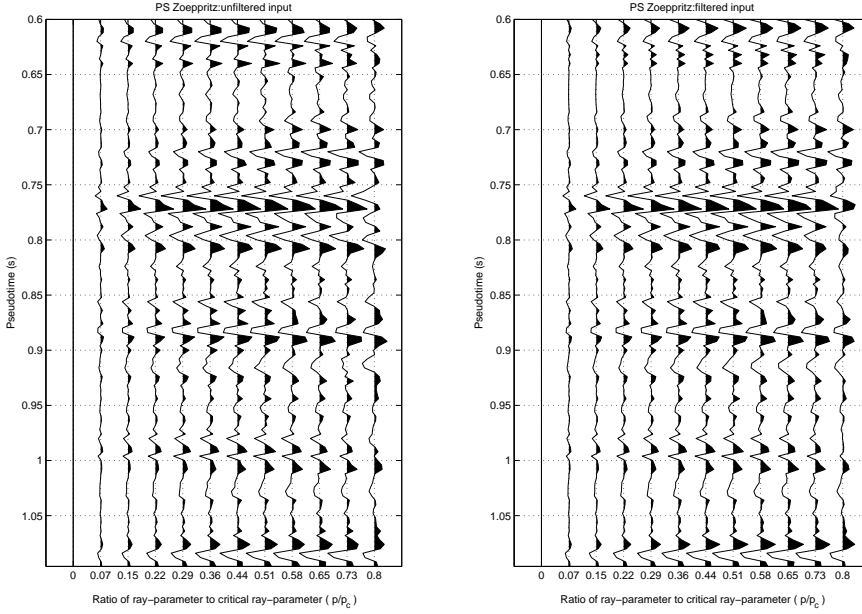
Figure 3.15: *An example of how the P-S Zoeppritz equation is inconsistent with the assumed time-invariant convolutional model for seismic data. The left panel shows the P-S Zoeppritz reflectivities computed from input logs and then filtered. The right panel shows the result of first filtering the logs and then computing the reflectivities.*

$$R_{\text{PS}}\left(\bar{\theta}\right) = -\frac{1}{2}\frac{p\bar{\beta}}{\cos\bar{\phi}}\left(\xi_0\Delta\ln\rho - \xi_1\Delta\ln\beta\right)$$

$$\xi_0 = 1 - 2\bar{\beta}^2 p^2 + 2\bar{\beta}^2\frac{\cos\bar{\theta}}{\bar{\alpha}}\frac{\cos\bar{\phi}}{\bar{\beta}}$$

$$\xi_1 = 4\bar{\beta}^2 p^2 - 4\bar{\beta}^2\frac{\cos\bar{\theta}}{\bar{\alpha}}\frac{\cos\bar{\phi}}{\bar{\beta}} \tag{3.3.17}$$

$$\bar{\alpha} = \left(\alpha_1 + \alpha_2\right)/2$$

$$\bar{\beta} = \left(\beta_1 + \beta_2\right)/2$$

$$\bar{\phi} = \left(\phi_1 + \phi_2\right)/2$$

$$\bar{\theta} = \left(\theta_1 + \theta_2\right)/2$$

with
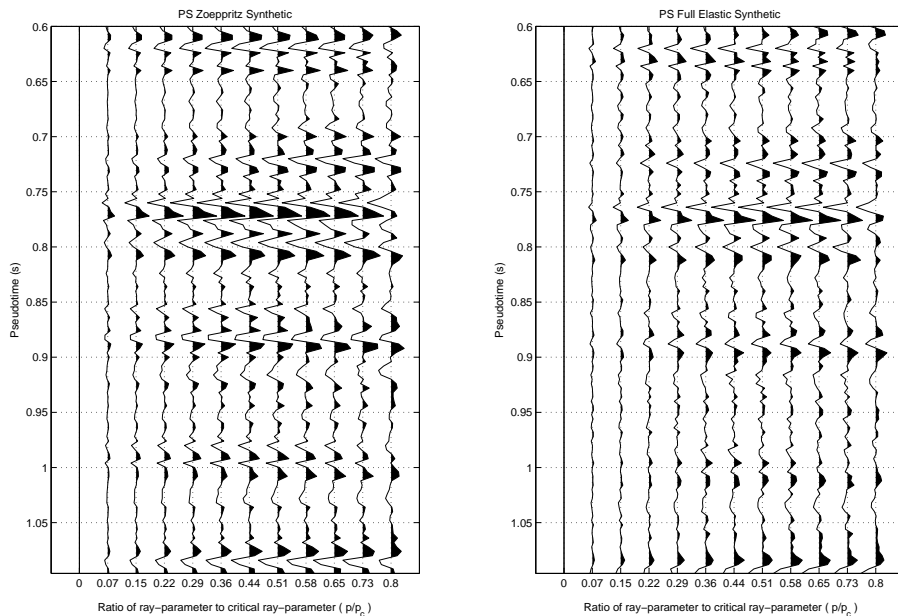
Figure 3.16: *Comparing the primaries-only P-S Zoeppritz response (left) and its corresponding total elastic response (right). As the critical ray-parameter is approached, the primaries-only amplitudes becomes inaccurate.*

$$p = \frac{\sin\theta_1}{\alpha_1} = \frac{\sin\theta_2}{\alpha_2} = \frac{\sin\phi_2}{\beta_2} = \frac{\sin\phi_1}{\beta_1} \text{ (Snell's Law)}.$$

Figure 3.17 illustrates that Equation (3.3.17) is also a reflectivity operator that violates the assumed convolutional/linear seismic data model in a layered earth. Again it is seen that this operator does not preserve commutability with filtering. Furthermore, Figure 3.18 shows that Equation (3.3.17) is also inaccurate at long offsets.

■ 3.3.1   A linear P-S velocity-separated forward model

As in the P-P case, using Equation (3.2.3), instead of $\bar{\alpha}$ and $\bar{\beta}$, in Equation (3.3.17) and noting that $\alpha_1 B'$ and $\beta_1 B'$ are now second order quantities, the first order linearisation in terms of contrasts against a background is:
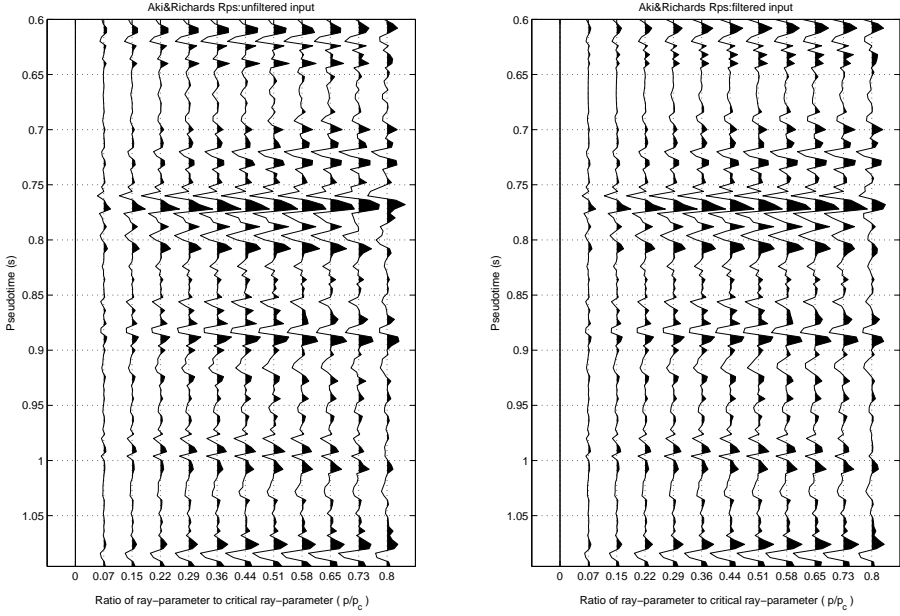
Figure 3.17: *The linearised P-S Aki and Richards equation also violates the assumed data model for seismic measurements. The left panel shows the result of computing linearise P-S reflectivities and then filtering. The right panel shows the result of first filtering the input wire-line logs and then computing the reflectivities.*

$$R_{\text{PS}}(\theta) = -\frac{1}{2}\frac{p\beta_0}{\cos\phi}\left(\xi_0 \Delta \ln \rho - \xi_1 \Delta \ln \beta\right)$$

$$\xi_0 = 1 - 2\beta_0^2 p^2 + 2\beta_0^2 \frac{\cos\theta}{\alpha_0}\frac{\cos\phi}{\beta_0} \qquad\qquad (3.3.18)$$

$$\xi_1 = 4\beta_0^2 p^2 - 4\beta_0^2 \frac{\cos\theta}{\alpha_0}\frac{\cos\phi}{\beta_0}.$$

Using Snell's law to rewrite Equation (3.3.18) in terms of p gives:
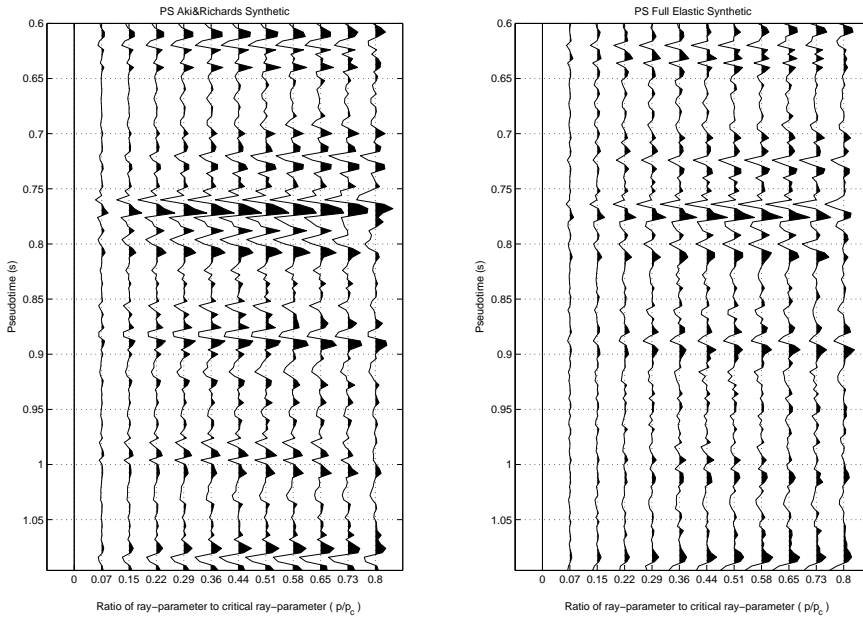
Figure 3.18: *Comparing the linearised P-S response (left) and the full elastic P-S response (right) shows that, at the long-offsets, the primaries-only amplitudes are still inaccurate.*

$$R_{PS}(p) = -\frac{1}{2}\frac{p\beta_0}{\sqrt{1-\beta_0^2 p^2}}\left(\xi_0 \Delta \ln \rho - \xi_1 \Delta \ln \beta\right)$$

$$\xi_0 = 1 - 2\beta_0^2 p^2 + 2\beta_0^2 \frac{\sqrt{1-\alpha_0^2 p^2}}{\alpha_0}\frac{\sqrt{1-\beta_0^2 p^2}}{\beta_0} \qquad (3.3.19)$$

$$\xi_1 = 4\beta_0^2 p^2 - 4\beta_0^2 \frac{\sqrt{1-\alpha_0^2 p^2}}{\alpha_0}\frac{\sqrt{1-\beta_0^2 p^2}}{\beta_0}.$$

The linearity offered by the reflectivity operator Equation (3.3.18) is shown in Figure 3.19 and its comparison to the P-S full elastic response is shown in Figure 3.20.
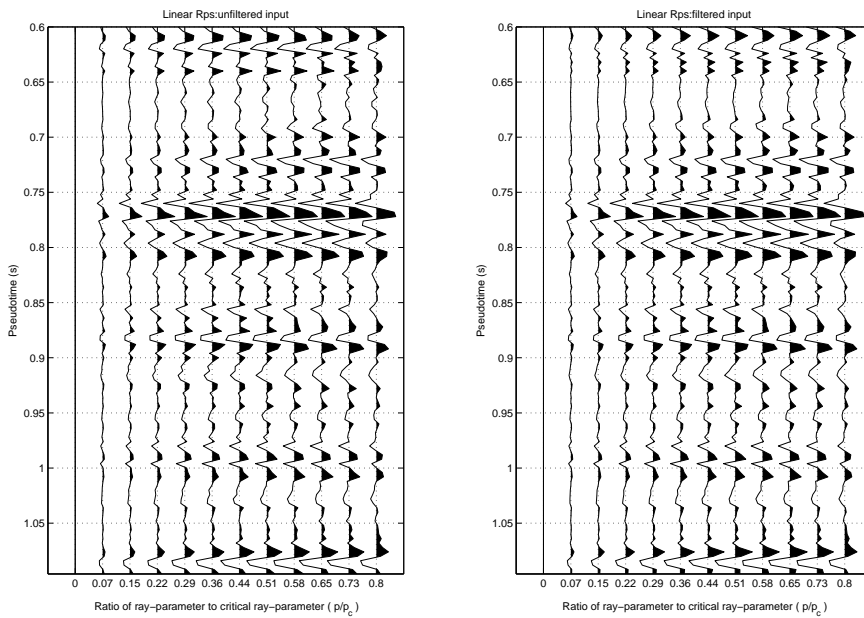
Figure 3.19: *The left panel shows the result of computing reflectivities and then filtering using the P-S velocity-separated equation, while the right panel shows the result of first filtering and then computing reflectivities.*
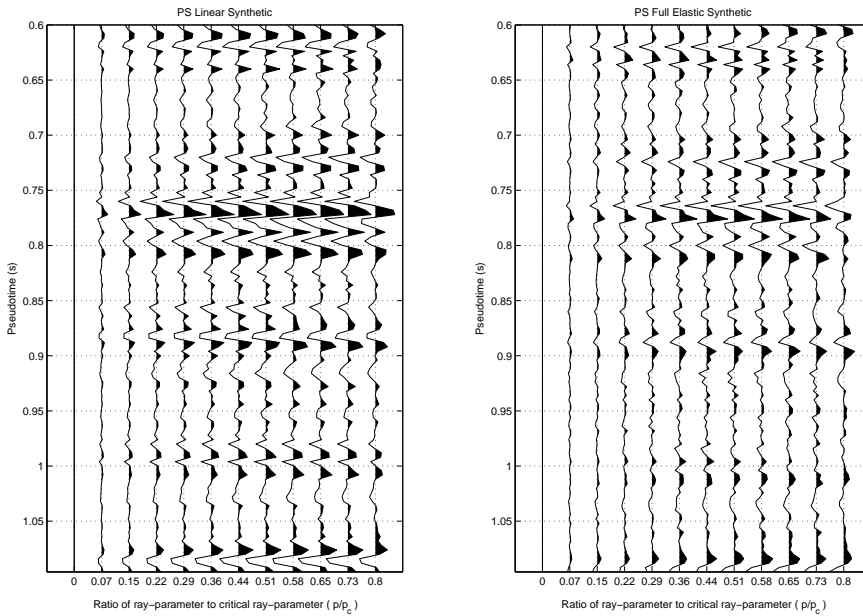
Figure 3.20: *Comparing the P-S velocity-separated response (left) and the full elastic P-S response (right) shows that the primaries-only amplitudes are now more accurate at long offset.*

■ 3.3.2 Layering induced anisotropy

Following from the case of P-P anisotropy [Thomsen, 1993; Rüger, 1996; Tsvankin, 2001] and linearising in accordance with weak elastic anisotropy gives:

$$R_{\mathrm{PS}}(p) = R_{\mathrm{PS}}^{i}(p) + R_{\mathrm{PS}}^{a}(p) \tag{3.3.20}$$

with $R_{\mathrm{PS}}^{i}(p)$ defined by Equation (3.3.19) and

$$
\begin{aligned}
R_{\mathrm{PS}}^{a}(p) =& \frac{1}{2}\left(\xi_2 \Delta \ln \rho - \xi_3 \Delta \ln \beta\right) \\
\xi_2 =& \frac{c}{d} + \frac{g}{h} + \frac{k}{l} \\
\xi_3 =& 2\left(\frac{g}{h} + \frac{k}{l}\right) \\
c =& \frac{\beta_0 p}{\sqrt{1-\beta_0^2 p^2}} \sqrt{1 - 2\left(\alpha_0 p\right)^4 \left(\frac{1-\alpha_0^2 p^2}{1-\beta_0^2 p^2}\right)(\epsilon_0 - \delta_0)} \\
& - \frac{\beta_0 p}{\sqrt{1-\beta_0^2 p^2}} \left[1 + 2\frac{\alpha_0^4 p^2}{\beta_0^2}\left(1 - \alpha_0^2 p^2\right)(\epsilon_0 - \delta_0)\right] \\
d =& \sqrt{1 - 2\left(\alpha_0 p\right)^4 \left(\frac{1-\alpha_0^2 p^2}{1-\beta_0^2 p^2}\right)(\epsilon_0 - \delta_0)} \\
g =& \frac{2\beta_0^3 p^3}{\sqrt{1-\alpha_0^2 p^2}} \left[1 - 3\left(\frac{\alpha_0}{\beta_0}\right)^2 p^2\left(1 - \alpha_0^2 p^2\right)(\epsilon_0 - \delta_0)\right] \\
& - \frac{2\beta_0^3 p^3}{\sqrt{1-\alpha_0^2 p^2}} \sqrt{1 - 2\alpha_0^4 p^4 \frac{1-\alpha_0^2 p^2}{1-\beta_0^2 p^2}(\epsilon_0 - \delta_0)} \\
h =& \sqrt{1 - 2\alpha_0^4 p^4 \frac{1-\alpha_0^2 p^2}{1-\beta_0^2 p^2}(\epsilon_0 - \delta_0)} \\
k =& \frac{1}{\alpha_0}\left[1 + 2\frac{\alpha_0^4}{\beta_0^2}p^2\left(1 - \alpha_0^2 p^2\right)(\epsilon_0 - \delta_0)\right] \sqrt{1 - 2\alpha_0^4 p^4\left(\delta_0 + \frac{\alpha_0^2 p^2}{1-\alpha_0^2 p^2}\epsilon_0\right)} \\
l =& -\frac{1}{\alpha_0}\left[1 + 2\alpha_0^2 p^2\left(1 - \alpha_0^2 p^2\right)\delta_0 + \alpha_0^4 p^4 \epsilon_0\right].
\end{aligned}
$$

As an illustrative example of how velocity anisotropy due to multiple scattering from thin layering can be handled using the ray-parameter formulation of Equation (3.3.20) is shown in Figure 3.21. The choice of values for ϵ_0 and δ_0 are made

based on those reported in Thomsen [1986], Alkhalifah et al. [1996], and Berryman et al. [1999]. Note the strong anisotropic pull-up, implying that induced anisotropy has a very pronounced effect on P-S converted wave seismic and should not be neglected.
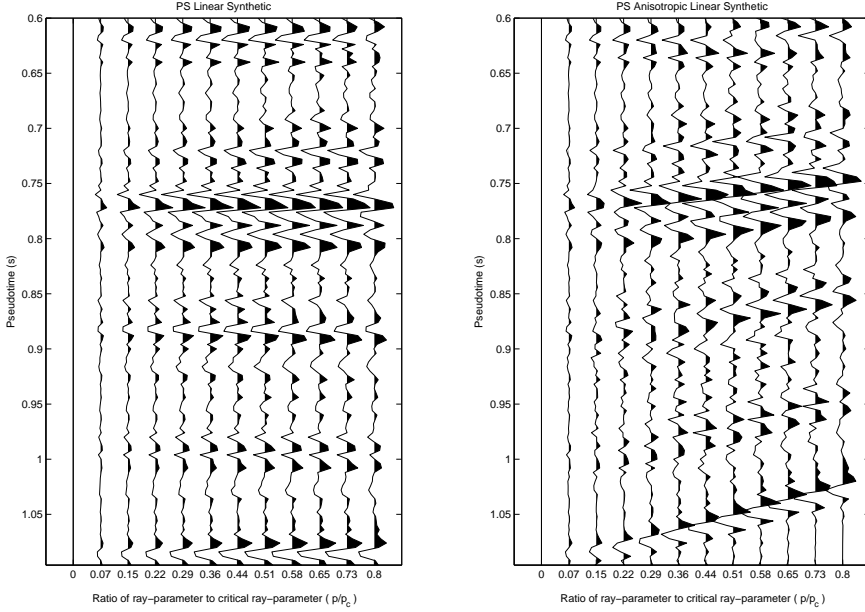
Figure 3.21: *An illustration of handling induced anisotropy with $\epsilon_0 = 0.1$ and $\delta_0 = -0.005$. The left panel shows the isotropic linear P-S response and the right panel shows the anisotropic linear P-S response.*

3.4   Conclusions

Advances in seismic acquisition has created a need for innovation in seismic imaging and characterisation. The fact that very long offset data maintains amplitude fidelity, and its acquisition has now become routine, demands new methods to analyse these long offset amplitudes. This chapter has developed an accurate method to simulate long offset amplitudes that is in agreement with the assumed convolutional model of seismic data.

The essence of the approach has been to achieve consistency between the assumptions underlying the seismic signal processing and imaging on the one hand, and the

reflectivity model to be used for forward modelling and inversion, on the other. This is particularly important if long offset seismic is to be exploited to extract information about reservoir fluid saturation and effective stress, because it is in the long offset domain that the customary ways to calculate reflectivity violate the linear convolution data model that underlies the seismic data processing. Scale dependency in the forward modelling is introduced when applying a non-linear method to calculate reflectivities to match seismic data processed on the basis of a linear data model. This chapter resolves this inconsistency by introducing a forward modelling operator that is linearised in the earth input as far as physically meaningful.

For clarity it is good to review once more what is meant by linearity. The forward system being considered is the whole seismic set-up, including sources, recording and some data processing. The input to this system is the earth or a model of it, the output is a seismic data set. The inverse system creates a quantitative image of the earth from the seismic data set. According to the time-invariant convolution model the forward system should be strictly linear, but neither the P-P and P-S Zoeppritz equations, nor the Bortfeld equation, nor even Equation (3.2.2) or the P-S Aki and Richards equation are linear in this regard. The proposed Equations (3.2.4) or (3.2.8), and its P-S counterpart, are not strictly linear either. But, within the range of applicability set by the physics of the problem, they serve the purpose of allowing quantitative interpretation of long offset seismic amplitudes.

The key to a true linearisation of forward modelling of seismic data is the introduction of a background velocity model in which all wave propagation takes place. This one simple concept solves a host of nasty issues that have dogged quantitative seismic interpreters ever since quantitative interpretation was invented, notably: non-linearity in the linearized Zoeppritz equations (scale dependency), the angle-of-incidence versus ray-parameter dilemma, the forward modelling of stretch and the handling of induced anisotropy in linear forward modelling. As a result the maximum angle of incidence (or ray-parameter or offset) allowable in linear forward modelling is pushed much further out than would have been possible with conventional two-term, or even three-term reflectivity approximations.

Reduced vertical resolution in imaging with waves with oblique angles of incidence is an inescapable fact. Ever since NMO was invented this effect has been called stretch. For forward modelling and inversion of long offset seismic, stretch is an important factor that needs to be taken into account. When attempting to describe stretch at the input log scale, it would constitute a strongly non-linear component of the forward modelling process. In our linearised approach it comes out naturally that stretch should be described at the scale at which the propagation of waves is observed (i.e. in the background medium).

Layering induced velocity anisotropy can and should be taken into account in long offset linear forward modelling, especially when considering a P-S converted wave situation. This can be achieved by defining seismic scale ϵ_0 and δ_0 Thomsen parameters in the background medium. There are several different approaches to obtaining

these parameters from the log data. The most rigorous one is apply the statistical method outlined by Shapiro et al. [1994] and Shapiro and Hubral [1995] Alternatively, one could estimate ϵ_0 and δ_0 in the long wavelength limit from sequential Backus averaging of the elastic parameters of the individual $0.1524m$ thick isotropic layers represented by the log samples. Yet another approach would be running a full elastic forward model at the $0.1524m$ log sampling scale and deriving ϵ_0 and δ_0 via the Hilterman [2001] approach.

4

Sparse pre-stack waveform inversion

4.1 Introduction

An immediate demand on quantitative seismic amplitude analysis technology is to
deliver a more detailed areal understanding of the reservoir. A particularly pressing
need is a quantitative map of the hydrocarbon saturation in the reservoir. Seismi-
cally estimating the reservoir density is the most direct way to address this need.
Traditionally, seismic density estimates have been considered inaccurate and un-
reliable due to various shortcomings in acquisition, processing, and quantitative
interpretation. Recent advances in acquisition and imaging have created a technol-
ogy push in characterization to explore density estimation by exploiting both the
compressional-to-compressional (P-P) mode and the compressional-to-shear (P-S)
mode amplitudes. Parameter estimation from pre-stack seismic amplitude data is
addressed in de Nicolao et al. [1993] via an eigenstructure analysis of a single inter-
face model. Veire and Landro [2001] demonstrate the ability to seismically estimate
density via the inversion of multi-component seismic data. A simulated annealing
(i.e. nonlinear) approach to the joint inversion problem is demonstrated by Dariu et
al. [2003], using small offset amplitude attributes (intercept and gradient) as input.
Mahmoudian and Margrave [2004] and Hampson et al. [2005] also put forth methods
to potentially estimate density from small offset seismic.

Chapter 4 extends these previous efforts to seismically estimate density and creates
a framework which furthers the use of seismic data in quantitative hydrocarbon
reservoir characterization and management. Within the paradigm of inverse theory,
the estimation of high-resolution reservoir rock properties from compressional wave
and converted wave data is cast as a linear-in-the-parameters optimization problem.
Through the formal separation of wave propagation and reflection effects, in addition

to the inclusion of the seismic source wavelet's ray-parameter dependency, all the first order information carried in the pre-critical P-P and P-S seismic amplitudes can be exploited through the forward models. Furthermore, the forward models are combined for a simultaneous consideration of compressional and converted wave pre-stack seismic amplitudes. The established inverse theory tools of least squares, iteration, regularization, and singular value decomposition are employed to overcome the ill-conditioning of the problem. In addition, these tools are used to handle the noise corruption and band-limitation of seismic data. Numerical analysis shows this inverse problem to have an optimal solution that is an accurate broadband reservoir rock properties estimate. In turn, these broadband reservoir properties can be used in quantitative seismic fluid detection.

Starting with the linear layered-earth P-P and P-S reflectivity equations developed in Chapter 3, forward model operators are constructed for compressional-to-compressional mode and compressional-to-shear mode data. Then a simultaneous forward operator is formed. Following this, a data driven approach to creating these operators is reviewed. After presenting the forward problem, least-squares seismic amplitude inversion is considered. Here, the concept of sparse regularization plays a key role. It enables a better seismic characterization of the reservoir by moving away from traditional band-limited parameter estimates and towards obtaining high-resolution rock properties. Singular value decomposition (SVD) is employed to gain a full understanding of the forward operators and the estimates they provide from the seismic. In particular, the SVD clearly establishes the effect of parameterization, how various parameterizations relate to different data, and shows the specific role of sparse regularization. Various aspects of the discussion will be illustrated with the use of the simple model shown in Figure (4.1) that consisting of an oil saturated clastic reservoir embedded in a shale background.

4.2   Data prediction kernels

Analyzing any physical system begins by identifying a minimum set of parameters that describe the system (i.e. the principle of parsimony), measurements of the system, and a relationship that links the parameters to the measurements. As such, parameter estimation begins by describing the observed data and means obtaining a mathematical abstraction by which to predict the data given the parameters of interest. This abstraction is a mathematical model that concisely captures the physics of interest contained in the data and is called a data kernel, forward operator or model. A model that captures all the physics can be claimed to be exact, but bear in mind that even exact models are imprecise as the physics itself is an idealized description of the observed natural phenomenon.
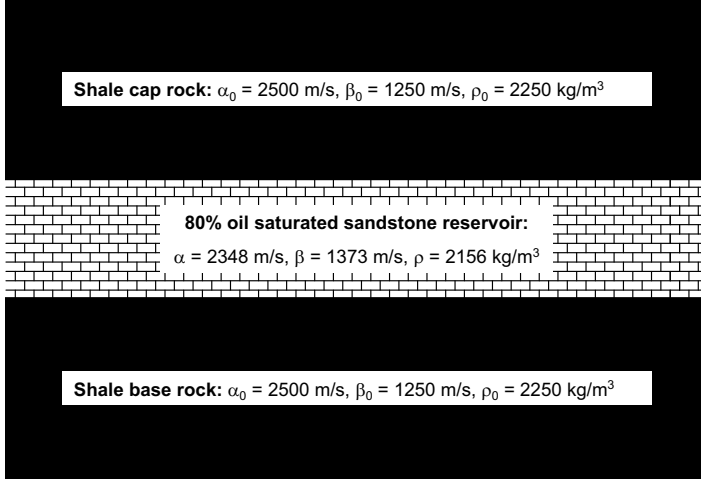
Figure 4.1: *The elastic properties of an ideal 80% saturated oil bearing sandstone reservoir with shale cap and base rocks.*

■ 4.2.1   The P-P case

Dey and Gisolf [2007] present the linear layered-earth P-P reflectivity equation that is fully developed in Chapter 3. Being stable and accurate throughout the entire pre-critical range for a horizontally layered earth, as well as incorporating 1st-order layering effects, Equation (3.2.8) will be the base of the mathematical model for P-P seismic data. Re-parameterizing from velocity and density reflectivities to acoustic impedance reflectivity ($\delta \mathbf{I_P}$), shear impedance reflectivity ($\delta \mathbf{I_S}$), and density reflectivity ($\delta \boldsymbol{\rho}$), the matrix representation of Equation (3.2.8) for a single ray-parameter becomes

$$\mathbf{r}^{\mathrm{PP}} = \left[\begin{array}{ccc} \mathbf{A} & \mathbf{B} & \mathbf{C} \end{array} \right] \left[\begin{array}{c} \delta \mathbf{I_P} \\[1em] \delta \mathbf{I_S} \\[1em] \delta \boldsymbol{\rho} \end{array} \right] \qquad (4.2.1)$$

where $\mathbf{A}$, $\mathbf{B}$, $\mathbf{C}$ are diagonal matrices with $A_{ii} = 1/\left(1 - \alpha_{0_i}^2 p^2\right)$, $B_{ii} = -8\beta_{0_i}^2 p^2$, $C_{ii} = 1 + 4\beta_{0_i}^2 p^2 - 1/\left(1 - \alpha_{0_i}^2 p^2\right)$, $\delta \mathbf{I_P} = \left[\frac{1}{2}\Delta \ln \alpha_1 \rho_1 \ldots \frac{1}{2}\Delta \ln \alpha_{nt} \rho_{nt}\right]^{\mathrm{T}}$, $\delta \mathbf{I_S} = \left[\frac{1}{2}\Delta \ln \beta_1 \rho_1 \ldots \frac{1}{2}\Delta \ln \beta_{nt} \rho_{nt}\right]^{\mathrm{T}}$, $\delta \boldsymbol{\rho} = \left[\frac{1}{2}\Delta \ln \rho_1 \ldots \frac{1}{2}\Delta \ln \rho_{nt}\right]^{\mathrm{T}}$, α_i = compressional-wave velocity, β_i = shear-wave velocity, ρ_i = density, α_{0_i} = background compressional-wave velocity, β_{0_i} = background shear-wave velocity, p = ray-parameter, and $i \in [1, n_t]$ is the ith pseudo-time sample τ [Dey and Gisolf, 2007]. Debski and Taran-

tola [1995] show that the chosen parameters $(\boldsymbol{\delta I_P}, \boldsymbol{\delta I_S}, \boldsymbol{\delta \rho})$ are optimal for seismic reservoir characterization, since it is this parameter set that can be reliably resolved from seismic data. In addition, impedance and density reflectivities are deviations in actual rock properties that can be directly related to reservoir hydrocarbon saturation S_h and reservoir effective stress σ_{eff}. This is critical in quantitative integrated hydrocarbon reservoir management.

Extending Equation (4.2.1) to the situation of many ray-parameters $p_i \in [p_1, p_{n_p}]$ gives

$$
\mathbf{R}^{PP} = \begin{bmatrix} \mathbf{r}_1^{PP} \\ \vdots \\ \mathbf{r}_{n_p}^{PP} \end{bmatrix} = \begin{bmatrix} \mathbf{A}_1 & \mathbf{B}_1 & \mathbf{C}_1 \\ \vdots & \vdots & \vdots \\ \mathbf{A}_{n_p} & \mathbf{B}_{n_p} & \mathbf{C}_{n_p} \end{bmatrix} \begin{bmatrix} \boldsymbol{\delta I_P} \\ \boldsymbol{\delta I_S} \\ \boldsymbol{\delta \rho} \end{bmatrix} . \tag{4.2.2}
$$

Accounting for the band-limitation of seismic data and the ray-parameter dependence of this band-limitation, means Equation (4.2.2) is multiplied by a block diagonal matrix $\mathbf{W}^{PP}$. This block diagonal matrix has Toeplitz convolution matrices along the diagonal containing the ray-parameter dependent imaged source wavelets. As is reported in Dey and Gisolf [2007], these wavelets have the functional form

$$
w(t, p) = w \left[t \left(\sqrt{1 - \alpha_0 p^2} \right) \right]
$$

and Figure (4.2) illustrates the *stretching* effect of the p-dependence. Equation (4.2.2) now becomes

$$
\begin{aligned}
\mathbf{d}^{PP} = \mathbf{G}^{PP}\mathbf{x} &= \mathbf{W}^{PP}\mathbf{R}^{PP} \\
&= \begin{bmatrix} \mathbf{W}_1^{PP} & \dots & 0 \\ \vdots & \ddots & \vdots \\ 0 & \dots & \mathbf{W}_{n_p}^{PP} \end{bmatrix} \begin{bmatrix} \mathbf{r}_1^{PP} \\ \vdots \\ \mathbf{r}_{n_p}^{PP} \end{bmatrix} \\
&= \begin{bmatrix} \mathbf{W}_1^{PP} & \dots & 0 \\ \vdots & \ddots & \vdots \\ 0 & \dots & \mathbf{W}_{n_p}^{PP} \end{bmatrix} \begin{bmatrix} \mathbf{A}_1 & \mathbf{B}_1 & \mathbf{C}_1 \\ \vdots & \vdots & \vdots \\ \mathbf{A}_{n_p} & \mathbf{B}_{n_p} & \mathbf{C}_{n_p} \end{bmatrix} \begin{bmatrix} \boldsymbol{\delta I_P} \\ \boldsymbol{\delta I_S} \\ \boldsymbol{\delta \rho} \end{bmatrix}
\end{aligned} \tag{4.2.3}
$$
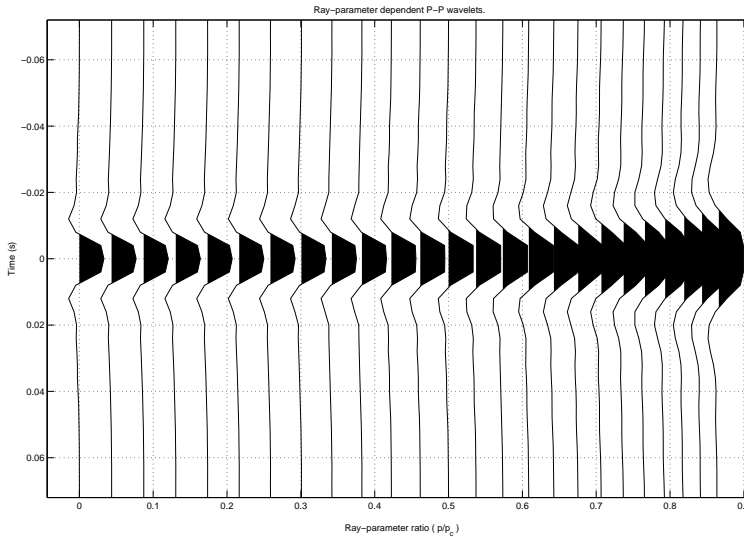
Figure 4.2: *The ray-parameter dependent P-P seismic source wavelets.*

and the P-P data kernel is

$$
\mathbf{G}^{\mathrm{PP}} = \begin{bmatrix} \mathbf{W}_1^{\mathrm{PP}}\mathbf{A}_1 & \mathbf{W}_1^{\mathrm{PP}}\mathbf{B}_1 & \mathbf{W}_1^{\mathrm{PP}}\mathbf{C}_1 \\ \vdots & \vdots & \vdots \\ \mathbf{W}_{n_p}^{\mathrm{PP}} & \mathbf{W}_{n_p}^{\mathrm{PP}}\mathbf{B}_{n_p} & \mathbf{W}_{n_p}^{\mathrm{PP}}\mathbf{C}_{n_p} \end{bmatrix}. \tag{4.2.4}
$$

■ **4.2.2   The P-S case**

Aki and Richards [2002] derive a linear P-S reflectivity equation for a single horizontal interface. Chapter 3 extends their equation to be linear in a horizontally layered earth by explicitly separating the macro-velocity field and the detailed-velocity field. The single ray-parameter matrix-vector form of Equation (3.3.19), parametrized in

terms of shear impedance reflectivity and density reflectivity, is

$$\mathbf{r}^{\mathrm{PS}} = \begin{bmatrix} \mathbf{D} & \mathbf{E} \end{bmatrix} \begin{bmatrix} \delta\mathbf{I_s} \\[2ex] \delta\boldsymbol{\rho} \end{bmatrix} \tag{4.2.5}$$

where $\mathbf{D}$ and $\mathbf{E}$ are diagonal matrices with

$$D_{ii} = \frac{\beta_{0_i}^3 p^3}{\left(1 - \beta_{0_i}^2 p^2\right)^{\frac{1}{2}}} - \frac{\beta_{0_i}^2 p}{\alpha_{0_i}} \left(1 - \alpha_{0_i}^2 p^2\right)^{\frac{1}{2}}$$

and

$$E_{ii} = \frac{-\beta_{0_i} p}{\left(1 - \beta_{0_i}^2 p^2\right)^{\frac{1}{2}}}.$$

Equation (4.2.5), extended to many ray-parameters $p_i \in [p_1, p_{n_p}]$ reads:

$$\mathbf{R}^{\mathrm{PS}} = \begin{bmatrix} \mathbf{r}_1^{\mathrm{PS}} \\ \vdots \\ \mathbf{r}_{n_p}^{\mathrm{PS}} \end{bmatrix} = \begin{bmatrix} 4\mathbf{D}_1 & \mathbf{E}_1 - 2\mathbf{D}_1 \\ \vdots & \vdots \\ 4\mathbf{D}_{n_p} & \mathbf{E}_{n_p} - 2\mathbf{D}_{n_p} \end{bmatrix} \begin{bmatrix} \delta\mathbf{I_s} \\[2ex] \delta\boldsymbol{\rho} \end{bmatrix}. \tag{4.2.6}$$

Equation (4.2.6) is multiplied by a block diagonal matrix, $\mathbf{W}^{\mathrm{PS}}$, to account for the ray-parameter dependent band-limitation of seismic data. As in the P-P case, this block diagonal matrix has Toeplitz convolution matrices containing the ray-parameter dependent P-S wavelets. These imaged wavelets have the functional form

$$w(t, p) = w\left[\frac{1}{2}t\left(\sqrt{1 - \alpha_0 p^2} + \frac{\alpha_0}{\beta_0}\sqrt{1 - \beta_0 p^2}\right)\right]$$

and Figure (4.3) illustrates the *stretching* effect of the p-dependence. The P-S
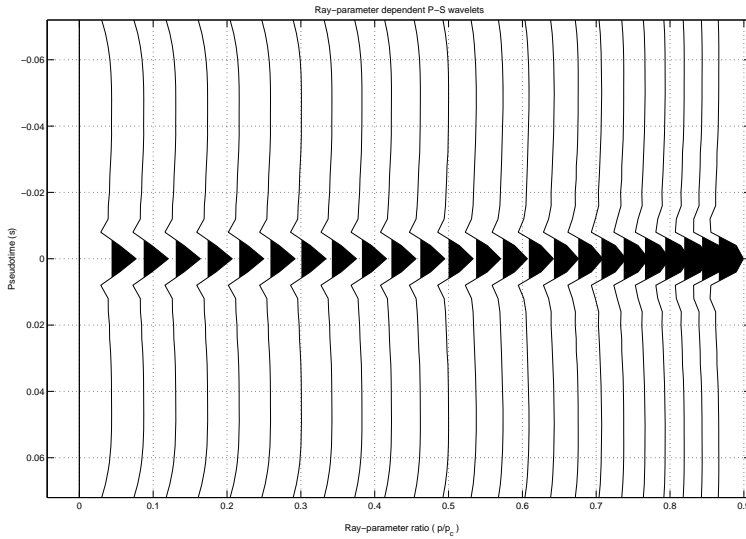
Figure 4.3: *The ray-parameter dependent P-S seismic source wavelets.*

seismic data relation is now written as

$$
\mathbf{d}^{\mathrm{PS}} = \mathbf{G}^{\mathrm{PS}}\mathbf{x}^{\mathrm{PS}} = \mathbf{W}^{\mathrm{PS}}\mathbf{R}^{\mathrm{PS}}
$$

$$
= \begin{bmatrix} \mathbf{W}_1^{\mathrm{PS}} & \cdots & 0 \\ \vdots & \ddots & \vdots \\ 0 & \cdots & \mathbf{W}_{n_p}^{\mathrm{PS}} \end{bmatrix} \begin{bmatrix} \mathbf{r}_1^{\mathrm{PS}} \\ \vdots \\ \mathbf{r}_{n_p}^{\mathrm{PS}} \end{bmatrix}
$$

$$
= \begin{bmatrix} \mathbf{W}_1^{\mathrm{PS}} & \cdots & 0 \\ \vdots & \ddots & \vdots \\ 0 & \cdots & \mathbf{W}_{n_p}^{\mathrm{PS}} \end{bmatrix} \begin{bmatrix} 4\mathbf{D}_1 & \mathbf{E}_1 - 2\mathbf{D}_1 \\ \vdots & \vdots \\ 4\mathbf{D}_{n_p} & \mathbf{E}_{n_p} - 2\mathbf{D}_{n_p} \end{bmatrix} \begin{bmatrix} \boldsymbol{\delta}\mathbf{I_s} \\ \boldsymbol{\delta\rho} \end{bmatrix}
\tag{4.2.7}
$$

and the data kernel is

$$\mathbf{G}^{\mathrm{PS}} = \begin{bmatrix} 4\mathbf{W}_1^{\mathrm{PS}}\mathbf{D}_1 & \mathbf{W}_1^{\mathrm{PS}}\mathbf{E}_1 - 2\mathbf{W}_1^{\mathrm{PS}}\mathbf{D}_1 \\ \vdots & \vdots \\ 4\mathbf{W}_{n_p}^{\mathrm{PS}}\mathbf{D}_{n_p} & \mathbf{W}_{n_p}^{\mathrm{PS}}\mathbf{E}_{n_p} - 2\mathbf{W}_{n_p}^{\mathrm{PS}}\mathbf{D}_{n_p} \end{bmatrix}. \tag{4.2.8}$$

■ 4.2.3   The joint P-P and P-S case

Combining the P-P and P-S forward operators and re-ordering along common ray-parameter instead of common wave propagation mode allows the multi-component (P-P,P-S) data equation to be written as:

$$\mathbf{d} = \mathbf{Gx} =$$

$$\begin{bmatrix} \mathbf{W}_1^{\mathrm{PP}} & \mathbf{0} & \ldots & \mathbf{0} & \mathbf{0} \\ \mathbf{0} & \mathbf{W}_1^{\mathrm{PS}} & \ldots & \mathbf{0} & \mathbf{0} \\ \vdots & \vdots & \ddots & \vdots & \vdots \\ \mathbf{0} & \mathbf{0} & \ldots & \mathbf{W}_{n_p}^{\mathrm{PP}} & \mathbf{0} \\ \mathbf{0} & \mathbf{0} & \ldots & \mathbf{0} & \mathbf{W}_{n_p}^{\mathrm{PS}} \end{bmatrix} \begin{bmatrix} \mathbf{A}_1 & \mathbf{B}_1 & \mathbf{C}_1 \\ \mathbf{0} & 4\mathbf{D}_1 & \mathbf{E}_1 - 2\mathbf{D}_1 \\ \vdots & \vdots & \vdots \\ \mathbf{A}_{n_p} & \mathbf{B}_{n_p} & \mathbf{C}_{n_p} \\ \mathbf{0} & 4\mathbf{D}_{n_p} & \mathbf{E}_{n_p} - 2\mathbf{D}_{n_p} \end{bmatrix} \begin{bmatrix} \delta\mathbf{I}_{\mathbf{P}} \\ \delta\mathbf{I}_{\mathbf{s}} \\ \delta\boldsymbol{\rho} \end{bmatrix} \tag{4.2.9}$$

and the (P-P,P-S) data kernel is

$$\mathbf{G} = \begin{bmatrix} \mathbf{W}_1^{\mathrm{PP}}\mathbf{A}_1 & \mathbf{W}_1^{\mathrm{PP}}\mathbf{B}_1 & \mathbf{W}_1^{\mathrm{PP}}\mathbf{C}_1 \\ \mathbf{0} & 4\mathbf{W}_1^{\mathrm{PS}}\mathbf{D}_1 & \mathbf{W}_1^{\mathrm{PS}}\mathbf{E}_{n_p} - 2\mathbf{W}_1^{\mathrm{PS}}\mathbf{D}_1 \\ \vdots & \vdots & \vdots \\ \mathbf{W}_{n_p}^{\mathrm{PP}}\mathbf{A}_{n_p} & \mathbf{W}_{n_p}^{\mathrm{PP}}\mathbf{B}_{n_p} & \mathbf{W}_{n_p}^{\mathrm{PP}}\mathbf{C}_{n_p} \\ \mathbf{0} & 4\mathbf{W}_{n_p}^{\mathrm{PS}}\mathbf{D}_{n_p} & \mathbf{W}_{n_p}^{\mathrm{PS}}\mathbf{E}_{n_p} - 2\mathbf{W}_{n_p}^{\mathrm{PS}}\mathbf{D}_{n_p} \end{bmatrix}. \tag{4.2.10}$$

Equation (4.2.9) is the fundamental system that needs to be solved using Equation (4.2.10) in order to estimate rock property reflectivities from band-limited multi-component seismic data.

■ **4.2.4   Data driven kernel estimation**

Before using Equation (4.2.4), Equation (4.2.8), or Equation (4.2.10), the data kernels must be calculated. Outputs from the imaging node of the Seismic Value Chain (i.e. the data processing stage) enable this. A necessary by-product of preparing the seismic data for amplitude analysis is a velocity model that explains the kinematics of the data. In addition to determining the location of subsurface reflectors, it is precisely this velocity model that plays the role of the background velocity field needed by the data kernel in an attempt to estimate reservoir lithology and pore-fill. Furthermore, ray-tracing in this macro-velocity field gives the kinematic-scale ray-parameters that are also required by the forward operator. Bjørke and Nilsen [2005] present a statistical method of trend/background determination, but the most common approach to estimating kinematic velocities is Migration Velocity Analysis (MVA). In this process, an initial velocity macro-model is created in some way and iteratively adjusted until the image gathers show flat horizontal events.

Thorbecke [1997] and Berkhout [1997a,b] present a fundamentally different approach to imaging based on Common Focal Point (CFP) technology. The method is a data driven approach that requires no a priori velocity model information. Building on the Berkhout [1980] **WRW**-model, CFP technology estimates re-focusing (back-propagation) operators [van de Rijzen, 2007] based on the principle of equal travel-time. These re-focusing operators are one-way Green's functions that are directly estimated from the seismic data itself and not computed from an a priori velocity model. In other words, the back-propagation operators represent the surface recorded responses from secondary sources (the so-called focal points) in the subsurface. Applying these operators to all subsurface points of the recorded wave-fields allows for the focusing of seismic data without the need of a velocity model. A very general summary of this focal transform approach to imaging is:

(a) estimate a focusing operator,

(b) generate a CFP gather,

(c) compute a Differential Time Shift (DTS) panel,

(d) if the zero-time event is not flat then pick the event,

(e) and use the picked event to update the focusing operator.

The process is illustrated in Figure (4.4). Final imaged/migrated data, and associated background velocity field, is created through via a wave-equation based tomographic inversion of the focal operators themselves [Cox, 2004]. Estimating the data kernels using the CFP approach allows reservoir characterization via linear model-based inversion of pre-stack seismic amplitude to be as *data-driven* as possible.

(a) Focusing operator

(b) CFP gather

(c) DTS panel

(d) Pick DTS panel

(e) Updated operator

(f) Final DTS panel
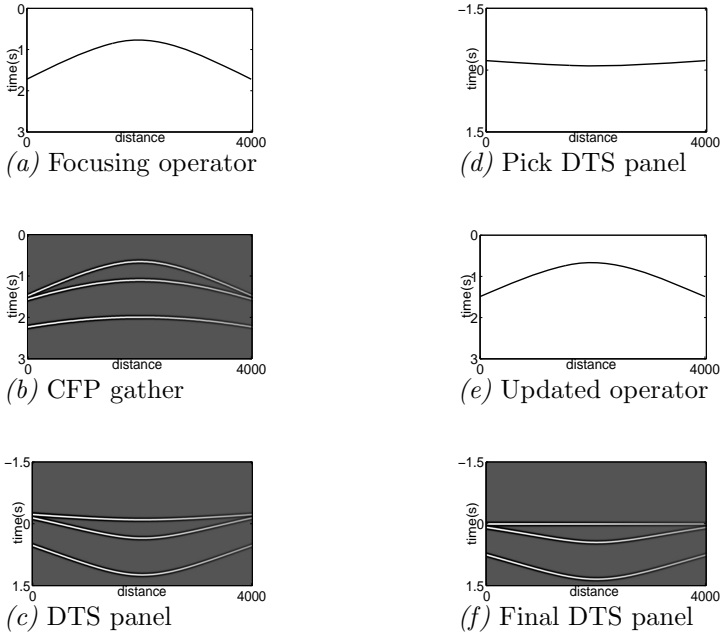
Figure 4.4: *The Common Focal Point approach to seismic imaging (images courtesy of doctordoctorandus Barbara Ellen Cox). Starting with an initial operator (a), compute the CFP gather (b) and DTS panel (c). Based on the deviation from $t = 0$ of the picked event (d), update the operator (e). Repeat steps (b) - (e) until the zero-time event in the DTS panel is flat (f) and the correct focusing operator is obtained.*

4.3 Least-squares AVP-waveform inversion

From data prediction, the analysis of a physical system proceeds to inversion. Depending on the particular area of study, inversion is synonymous with parameter estimation, regression, optimization and systems/parameter identification. Tarantola [2005] discusses that discovering the physics of a model and its minimal parameterization is inductive while inversion itself is, to a large extent, a deductive process. Inversion is defined as applying the methods of inverse theory [Menke, 1989; Tarantola, 2005] to make inferences about real world parameters given experimental measurements and a relationship to these measurements. Specifically, the response of the data kernels developed in the previous section are fitted to a finite set of pre-stack seismic amplitude data in order to estimate the impedance and density reflectivities of the earth. As all the forward data prediction relations (Equations 4.2.3, 4.2.7, and 4.2.9) are of the explicit linear form $f(\mathbf{d}, \mathbf{x}) = [\mathbf{I} - \mathbf{G}][\mathbf{d} \ \mathbf{x}]^{\mathrm{T}} = \mathbf{d} - \mathbf{G}\mathbf{x} = 0$, estimating the desired medium properties of the earth involves solving a linear inverse problem. The desired parameter vector $\mathbf{x}$ is approximated as the solution to the optimization problem

$$\underset{\mathbf{x} \in \mathbb{R}^n}{\text{minimize}} \left\{ J = \mathbf{e}^{\mathrm{T}}\mathbf{e} = \mathbf{e} \cdot \mathbf{e} = \|\mathbf{d} - \mathbf{G}\mathbf{x}\|_2^2 \right\} \qquad (4.3.11)$$

where J is the objective function, $\mathbf{d}$ is either P-P or P-S or joint (P-P,P-S) data, $\mathbf{G}$ is the corresponding data kernel, $\|\cdot\|_2^2$ is the square of the ℓ_2-norm, and $\mathbf{x} \in \mathbb{R}^n$ specifies that only real-valued parameter realizations are allowed. The solution $\mathbf{x}$ is such that $\nabla J(\mathbf{x}) = 0$. Equation (4.3.11) is a *least-squares* problem and its solution is

$$\mathbf{x} = \left(\mathbf{G}^{\mathrm{T}}\mathbf{G} \right)^{-1} \mathbf{G}^{\mathrm{T}}\mathbf{d}.$$

Lines and Treitel [1984] lucidly review the mathematical robustness of least-squares for parameter estimation from real seismic data, whose nature tends to be "inaccurate, insufficient, and inconsistent" [Jackson, 1972]. The data kernels Equation (4.2.4), Equation (4.2.8), and Equation (4.2.10) all capture the amplitude-versus-ray-parameter (AVP) nature of the data and also account for the ray-parameter dependence of the imaged source wavelet (i.e. source waveform/wavelet stretching effect). As such, Equation (4.3.11) is more correctly termed a linear least-squares AVP-waveform inverse problem.

■ 4.3.1 The data, the kernel, and the SVD

Given the fact that seismic data is non-ideal and the kernel is always (somewhat) deficient, difficulties are likely to arise while solving Equation (4.3.11). The singular value decomposition (SVD) is the most informative way of analyzing a linear

inversion. SVD is analogous to spectral decomposition in terms of sinusoidal basis functions [Lines and Treitel, 1984] and, following Gill et al. [1991], allows an arbitrary $m \times n$ matrix $\mathbf{G}$ to be factored into the product

$$\mathbf{G} = \mathbf{U}\boldsymbol{\Sigma}\mathbf{V}^{\mathrm{T}}$$

where $\mathbf{U}$ is an $m \times m$ orthogonal matrix, $\mathbf{V}$ is an $n \times n$ orthogonal matrix, and $\boldsymbol{\Sigma}$ is an $m \times n$ diagonal matrix with diagonal elements being the $s = \min(m, n)$ singular values σ (arranged in descending order). The number of non-zero σ's is the rank r of the matrix $\mathbf{G}$. If $r < s$, then $\mathbf{G}$ is said to be singular or rank deficient and $\sigma_{r+1} = \sigma_{r+2} = \cdots = \sigma_s = 0$. In this case, the singular value decomposition proceeds in a reduced form where only the non-zero σ's are considered and the size of the matrices $\mathbf{U}$ and $\mathbf{V}$ scale accordingly.

Estimating hydrocarbon reservoir rock properties from pre-stack seismic amplitudes using a linear data kernel generally results in $m \geq n$ and the singular value decomposition proceeds with the following steps:

- compute $\mathbf{G}^{\mathrm{T}}\mathbf{G}$,

- expand $\det\left(\mathbf{G}^{\mathrm{T}}\mathbf{G} - \sigma^2\mathbf{I}\right)$ into the characteristic polynomial,

- solve for the r non-zero eigenvalues and compute $\sigma_1 \ldots \sigma_r$,

- form $\boldsymbol{\Sigma}$ and compute $\boldsymbol{\Sigma}^{-1}$,

- find corresponding eigenvectors $\mathbf{v}_1 \ldots \mathbf{v}_r$,

- form $\mathbf{V} = [\mathbf{v}_1, \ldots, \mathbf{v}_r]$ and compute $\mathbf{V}^{\mathrm{T}}$,

- and, finally, compute $\mathbf{U} = \mathbf{G}\mathbf{V}\boldsymbol{\Sigma}^{-1} = [\mathbf{u}_1, \ldots, \mathbf{u}_r]$.

In the formal language of geophysical inverse theory, $\mathbf{U}$ is the rank r data space matrix while $\mathbf{V}$ is the rank r solution space matrix and the columns of both span their respective spaces [Menke, 1989]. This allows the AVP rock properties to be written as

$$\hat{\mathbf{x}} = \left(\mathbf{G}^{\mathrm{T}}\mathbf{G}\right)^{-1}\mathbf{G}^{\mathrm{T}}\mathbf{d} = \frac{1}{\sigma_1}\mathbf{v}_1\mathbf{u}_1^{\mathrm{T}}\mathbf{d} + \cdots + \frac{1}{\sigma_r}\mathbf{v}_r\mathbf{u}_r^{\mathrm{T}}\mathbf{d} = \frac{\gamma_1}{\sigma_1}\mathbf{v}_1 + \cdots + \frac{\gamma_r}{\sigma_r}\mathbf{v}_r. \quad (4.3.12)$$

Hence, the SVD shows the least-squares solution to be a weighted sum of the solution space eigenvectors. A very small weight γ_i/σ_i means that the contribution of the corresponding term $(\gamma_i/\sigma_i)\,\mathbf{v}_i$ to the solution will be negligible. Likewise, a large weight causes its corresponding term to have a dominant effect on the solution. Another diagnostic of the linear inverse problem that the SVD provides is through

the singular values themselves. The ratio of the largest singular value to the smallest singular value is called the condition number, or conditioning, of the problem. It is a measure of the data kernel's ability to recover the desired parameters. The smaller the condition number the better suited the data kernel is for parameter estimation. Very large, or infinite, condition numbers (corresponding to very small or zero singular values) indicate poor kernel structure. An alternative model parameterization may address this problem by leading to better conditioning. While the singular value decomposition can be simply and elegantly stated as a mechanical process, do not be fooled! The algebra quickly grows exponentially without bound and becomes intractable. For this reason, singular value decomposition is primarily employed as a numerical tool to obtain information about the inverse problem at hand. To illustrate how useful the SVD is, consider the ideal reservoir in Figure (4.1) and the waveforms shown in Figures (4.2) and (4.3). SVD is used to assess seismic rock property estimation as a function of data availability and model parameterization.

P-P data kernel conditioning

Figure (4.5) illustrates how various P-P amplitude inversion kernels behave as longer offset information is available. The parameterization from this chapter in terms of impedance and density (I_P, I_S, ρ) is compared to the parameterization from Chapter 3 in terms of velocities and density (α, β, ρ). A third comparison is made to a parameterization from Gisolf [2005] in terms of well as P-velocity, shear-modulus and density (α, μ, ρ). Notice that the choice of parameterization directly impacts the condition number behavior of the data kernel. Specifically, parameterizing in terms of impedance and density seems to be the best behaved. This is in accordance with reflectivity inversion analysis of Debski and Tarantola [1995]. As the available data range gets closer and closer to the critical angle, the various parameterizations converge to the same conditioning. For all the data kernels considered, the conditioning improves significantly as usable long-offset data becomes available. However, this improvement does not arise gradually. It is seen that the condition numbers are extremely high and then suddenly experience a rapid decrease. This indicates that before this transition, seismic parameter estimation from P-P data can be problematic. For the reservoir situation outlined in Figure (4.1), the available P-P data should span at least 60% of the pre-critical range if AVP-waveform is to be undertaken.

P-S data kernel conditioning

The situation for P-S data is markedly different, as is seen in Figure (4.6). The conditioning of the P-S inversion problem is two orders of magnitude lower than the P-P case, at less than 30% of the critical ray-parameter. Furthermore, the condition number curves possess the desirable property of smooth descent behavior so there
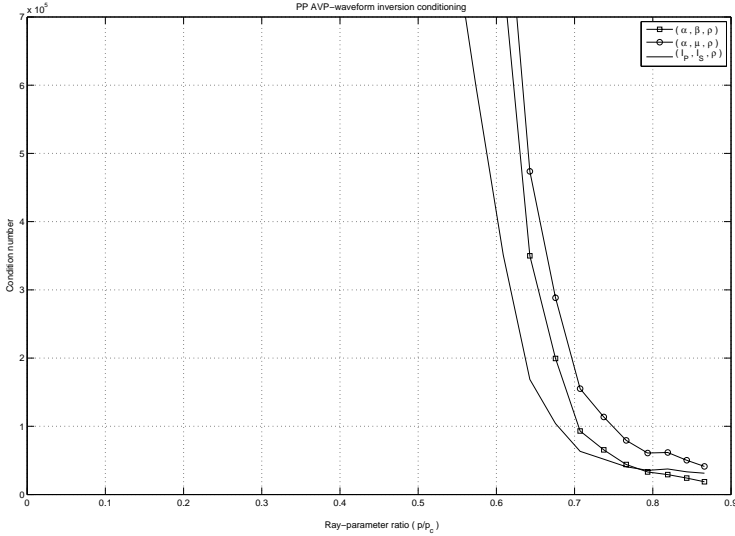
Figure 4.5: *The conditioning of various linear P-P AVP-waveform inversion kernels. These kernels are parametrized in terms of velocities and density (α, β, ρ), impedance and density $(\mathbf{I}_P, \mathbf{I}_S, \rho)$, as well as P-velocity, S-modulus and density (α, μ, ρ). As the ray-parameter ratio increase, there is longer and longer offset available for the inversion.*

is no extreme behavior in the kernel. As in the P-P case, parameterizing in terms of impedance and density facilitates the best problem conditioning. Contrary to the P-P case, the different parameterizations do not converge in the P-S case. The impedance-density formulation retains its advantage as the critical ray-parameter is approached. The multi-component scenario of simultaneous considering P-P and P-S data kernels has very desirable condition number behavior.

Joint (P-P,P-S) data kernel conditioning

For simultaneous multi-component inversion, Figure (4.7) shows that the conditioning comes under control at smaller offsets and has a strong but smooth descent. In particular, joint (P-P,P-S) inversion has its best conditioning at the minimum data range required to bring the conditioning of P-P inversion under control. The implication from Figures (4.5), (4.6), and (4.7) is that road mapping of a seismic project is essential. Should a project goal be seismically estimating reservoir rock properties in a quantitative manner, then the minimal long offset data range that needs to be acquired has to be assessed. Furthermore, the ability to properly pro-
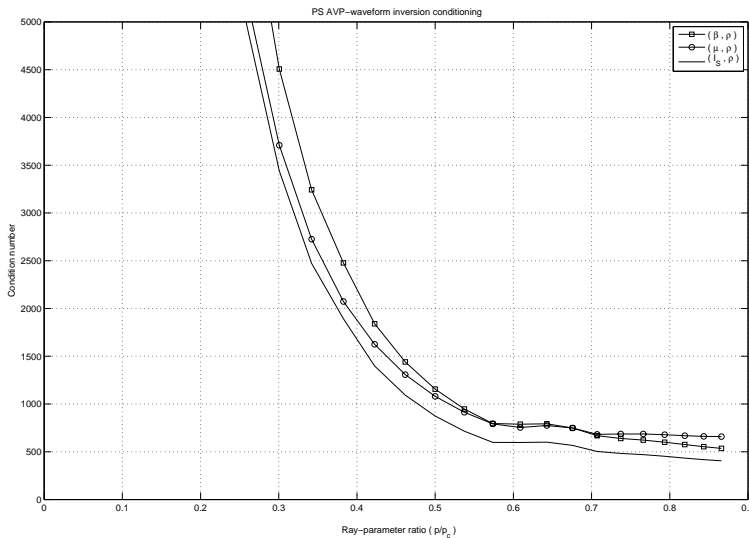
Figure 4.6: *The conditioning of various linear P-S AVP-waveform inversion kernels. As the ray-parameter ratio increase, there is longer and longer offset available for the inversion and the conditioning improves.*

cess this data in a true-relative-amplitude sense needs to be objectively considered. Cyclical interactions in this manner can greatly improve the seismic understanding of an area.

■ 4.3.2   Quadratic regularization

In addition to ill-conditioning due to very small or zero singular values, least-squares rock properties estimation can be ill-posed. Hadamard [1902] proposes that an ill-posed problem is one that has no solution or one of which the solution is not unique or is not a continuous function of the data. Hadamard himself believed these types of problems to be a purely mathematical concern with no actual consequence or physical significance. This proves to be incorrect as almost all industrially applied inverse problems turn out to be ill-posed. Addressing these issues of ill-conditioning and ill-posedness means regularizing the inverse problem.

Regularization is the inclusion in the inverse problem of additional, or constraining, information about the solution. Geophysical inverse problems are regularized, most commonly, by requiring the solution to be smooth. Levenberg [1944] introduces a
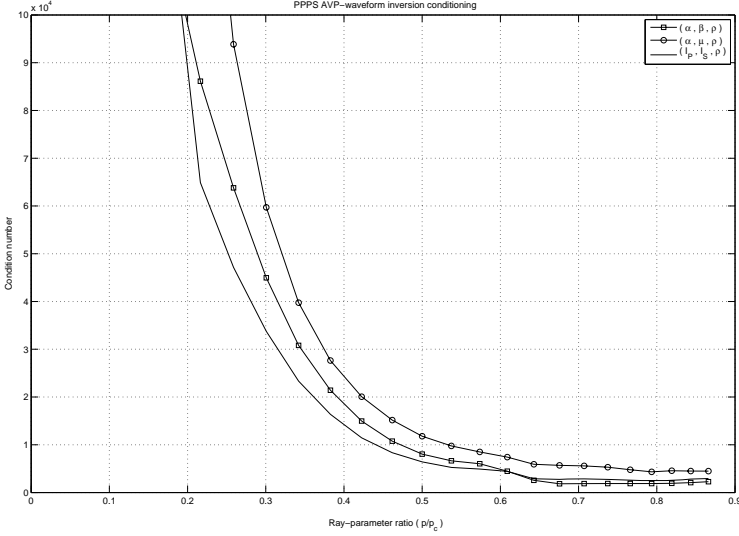
Figure 4.7: *The conditioning of various linear P-P-P-S AVP-waveform inversion kernels. As the ray-parameter ratio increase, there is longer and longer offset available for the inversion.*

regularization criterion that imposes smoothness on a least-squares solution. The details of the method using this technique are fully developed by Marquardt [1963]. This Levenberg-Marquardt approach forces the solution to be smooth by bounding the energy of the solution by some amount $\mathfrak{b}$. For this type of constraint, following Lines and Treitel [1984], Equation (4.3.11) becomes

$$\underset{\mathbf{x} \in \mathbb{R}^n}{\text{minimize}} \left\{ J = \mathbf{e}^{\mathrm{T}}\mathbf{e} + \zeta \left(\mathbf{x}^{\mathrm{T}}\mathbf{x} - \mathfrak{b} \right) = \|\mathbf{d} - \mathbf{Gx}\|_2^2 + \zeta \left(\|\mathbf{x}\|_2^2 - \mathfrak{b} \right) \right\}, \qquad (4.3.13)$$

where ζ is a damping parameter. Equation (4.3.13) is minimized when

$$\mathbf{x} = \left(\mathbf{G}^{\mathrm{T}}\mathbf{G} + \zeta \mathbf{I} \right)^{-1} \mathbf{G}^{\mathrm{T}}\mathbf{d}. \qquad (4.3.14)$$

The multiplier ζ is also called the regularization, or trade-off, parameter and it controls the amount of smoothness imposed on the solution. This is the classical damped least-squares, or minimum quadratic norm, solution. The factor ζ damps the non-smooth components of $\mathbf{x}$ and $\zeta \mathbf{I}$ can be viewed as a specific type of Tikhonov [1963] regularizer. To achieve even greater smoothness, iterative non-linear least-squares is used where Equation (4.3.14) is iterated and the damping factor ζ is multiplicatively adjusted with each iteration [Neumaier, 1998; Lines and Treitel, 1984].

■ 4.3.3 Nonquadratic regularization

Across many areas of physics, least-squares inverse problems arise where smooth solutions are not desired. These problems aim for solutions with desirable properties, other than smoothness, by introducing non-quadratic regularization. The concept comes from the field of robust statistics where the goal is to diminish the influence of data outliers by imposing non-quadratic norms on the data space. When the desire is to have a non-smooth parameter estimate, the goal is to minimize the effect of parameter outliers by applying non-quadratic norms to the model space. This approach is successfully applied to estimate sparse (i.e. non-smooth) solutions for a wide range of geophysical inverse problems. Sacchi and Ulrych [1995] use a Cauchy norm to reconstruct velocity gathers, while sparse inversion with a generalized Cauchy norm is used in the Fourier domain by Zwartjes [2005] to interpolate missing seismic data traces. Other geophysical applications of least-squares with non-quadratic regularization include the inversion approach to 3-D surface related multiple elimination [van Dedem and Verschuur, 2005], implementing the radon transform [Trad et al., 2003], and the wavelet deconvolution problem [Sacchi, 1999]. A simultaneous inversion approach to the AVO and NMO problems that explores the Cauchy regularizer is presented by Downton and Lines [2003] in a Bayesian framework.

In the same way, estimating broad-band differential rock properties through an iterative least-squares scheme with non-quadratic regularization is presented here. The Cauchy norm is the non-quadratic regularizer of choice. This results in sparse, broad-band, non-smooth, parameter estimates. Of course, the validity of imposing sparsity on the solution is only as good as the assumption that the input seismic data can be represented as the superposition of the earth's reflections. That is to say, the sparsity constraint on rock properties estimates is valid as long as the time-invariant convolutional data model of seismic processing holds true. Consequently, the following objective function is defined for high-resolution linear AVP-inversion:

$$\underset{\mathbf{x} \in \mathbb{R}^n}{\text{minimize}} \left\{ J = \mathbf{e}^{\mathrm{T}}\mathbf{e} + \mathfrak{R} = \|\mathbf{d} - \mathbf{G}\mathbf{x}\|_2^2 + \varsigma\xi\left(\mathbf{x}\right) \right\}, \qquad (4.3.15)$$

where $\xi(x_i) = \ln\left(1 + x_i^2/\nu_i^2\right)$ is the Cauchy norm, ς is the trade-off parameter, and ν_i is the Cauchy regularization parameter. This objective function is simply Equation (4.3.13) with the Cauchy norm, instead of $\left(\|\mathbf{x}\|_2^2 - \mathfrak{b}\right)$, for regularization. One drawback to this particular type of nonlinear regularization is that the Cauchy norm is not convex and, therefore, modern combinatorial optimization methods cannot be used. This does not pose a serious problem as the sparse solution can be sought by a classical method. Equation (4.3.15) is minimized using classical iterative re-weighted least squares (IRLS) on the normal equations. The minimum structure (or sparse) differential rock properties are determined via

$$\mathbf{x}^{(k)} = \left[\mathbf{G}^{\mathrm{T}}\mathbf{G} + \varsigma\mathbf{Q}^{(k-1)}\right]^{-1}\mathbf{G}^{\mathrm{T}}\mathbf{d} \qquad (4.3.16)$$

where $\mathbf{Q}^{(k-1)}$ is a diagonal matrix with

$$Q_{i,i}^{(k-1)} = \frac{2}{\nu^2 + \mathrm{x_i^{(k-1)}}},$$

and the iteration, starting at 1, terminates once a prescribed tolerance is met or the specified maximum number of iterations is exceeded. As three parameter vectors of differential rock properties are to be estimated from band-limited noise-corrupted seismic amplitude data, both hyper-parameters ς and ν must be dynamic in nature. That is to say, they are typically different for each property vector being estimated and must be adapted accordingly. This is termed dynamic diagonal regularization. The SVD form of this iteration is

$$\begin{aligned}
\mathbf{x}^{(k)} &= \frac{\sigma_1}{\sigma_1^2 + \varsigma_1 Q_{1,1}^{(k-1)}} \mathbf{v}_1 \mathbf{u}_1^{\mathrm{T}} \mathbf{d} + \cdots + \frac{\sigma_r}{\sigma_r^2 + \varsigma_r Q_{r,r}^{(k-1)}} \mathbf{v}_r \mathbf{u}_r^{\mathrm{T}} \mathbf{d} \\
&= \frac{\gamma_1 \sigma_1}{\sigma_1^2 + \varsigma_1 Q_{1,1}^{(k-1)}} \mathbf{v}_1 + \cdots + \frac{\gamma_r \sigma_r}{\sigma_r^2 + \varsigma_r Q_{r,r}^{(k-1)}} \mathbf{v}_r.
\end{aligned} \tag{4.3.17}$$

Equation (4.3.17) is an iterative weighted sum of the solution space eigenvectors. If the value of a particular weight is dominated by $Q_{i,i}^{(k-1)}$, then the contribution to the solution of the corresponding term comes primarily from the sparsity constraint. In both Equation (4.3.16) and Equation (4.3.17), the hyper-parameters play a key role in regularizing the estimation of parameters and in imposing desired properties on the parameter estimates themselves. Unfortunately, determining these parameters beforehand is not possible. Neumaier [1998] reviews the mathematical properties of regularization for estimates to be optimal, with attention paid to how the quantities such as ς and ν should be determined. Within the context of solving geophysical inverse problems, Farquharson and Oldenburg [2004] compare automated hyper-parameter determination by the generalized cross-validation approach to the L-curve approach.

Qualitatively, IRLS with nonlinear regularization yields results that are similar to post-stack sparse spike inversion but have very different interpretations. A post-stack sparse-spike inversion results from optimizing a solution to an ℓ_1-problem. Here, the objective/cost function is designed to minimise the effect of noise on the solution and, in doing so, a sparse solution is found. On the other hand, Equation (4.3.15) seeks to optimize an ℓ_2-problem with informative nonlinear a priori information. In this case, an assumption is made about the structure of the solution (i.e. it is sparse) and an earth model is sought with this structure that is a least-squares best-fit to the acquired data. That is, the problem at hand is one of making inferences about some desired parameters from imprecise observations and additional knowledge. Formal analysis in this manner should be carried out in a probabilistic/Bayesian framework. Tarantola [2005] uses probability theory and Bayes' Rule [Bayes, 1763] to show that

a regularized least-squares solution has the form

$$\mathbf{x} = \left(\mathbf{G}^{\mathrm{T}} \mathbf{C_d}^{-1} \mathbf{G} + \mathbf{C_x}^{-1} \right)^{-1} \left(\mathbf{G}^{\mathrm{T}} \mathbf{C_d}^{-1} \mathbf{d} + \mathbf{C_x}^{-1} \mathbf{x}_0 \right), \qquad (4.3.18)$$

where $\mathbf{C_d}^{-1}$ is the inverse data/noise covariance matrix, $\mathbf{C_x}^{-1}$ is the inverse covariance matrix of the a priori information, and $\mathbf{x}_0$ are the prior parameter estimates. The proposed iteration, Equation (4.3.16), with nonlinear regularization, results from assuming that the uncertainties follow a normal/Gaussian distribution and that the a priori probability follows a Cauchy distribution. By comparison to Equation (4.3.18), it is seen that Equation (4.3.16) has $\mathbf{C_d}^{-1} = \mathbf{I}$, $\mathbf{C_x}^{-1} = \varsigma \mathbf{Q}\left(\mathbf{x} \right)$, and $\mathbf{x}_0 = \mathbf{0}$. Mapping uncertainties in the data and the data kernel onto the parameter estimates is achieved via $\mathbf{C_d}^{-1}$. Constraining information, or a priori knowledge, maps onto the estimates through $\mathbf{C_x}^{-1}$. If the non-trivial construction of $\mathbf{C_d}^{-1}$ is possible, then Equation (4.3.18) delivers a least-squares solution with uncertainty estimates. Downton [2004] discusses how to form $\mathbf{C_x}^{-1}$ using local geological information and rock physics so that the problem incorporates as much geological knowledge as possible.

As an alternative to using the normal equations $\mathbf{G}^{\mathrm{T}} \mathbf{G} \mathbf{x} = \mathbf{G}^{\mathrm{T}} \mathbf{d}$ in solving a linear least-squares problem, Saunders [1996] suggests forming an augmented system and use a Cholesky matrix factorization based method. This factorization approach is preferred when the inverse problem is very large and horribly ill-conditioned. Gill et al. [1991] notes that decomposing into Cholesky factors instead of using the normal equations is also desirable because the conditioning will be better than when the normal equations are used and the process of forming the normal equations can potentially lead to numerical information loss.

4.4   Quantitative Seismic Fluid Detection

Integrated hydrocarbon reservoir management is proving to be ideal for optimal production and development of a field. An accurate and reliable seismically estimated map of hydrocarbon saturation S_{h}, or the change in hydrocarbon saturation ΔS_{h} (where Δ now means time-lapse change), is vital to this process. This is because seismic is the only measurement that commonly exists between wells that can guide the reservoir simulator. Given recent advances in the time-lapse seismic method, quantitatively estimating maps of ΔS_{h} with minimal reliance on a rock physics model looks feasible.

If the input to the previously discussed inverse problem is time-lapse multi-component seismic data, then the estimated time-lapse density reflectivity parameter $\Delta \mathbf{r}_\rho$ (where $\mathbf{r}_\rho \equiv \boldsymbol{\delta} \ln \boldsymbol{\rho}$) may be converted to a time-lapse interval density $\Delta \rho$. In turn, this $\Delta \rho$ can be used to estimate ΔS_{h}. So long as the time-lapse compressional wave reflection coefficients and time-lapse converted compressional wave reflection coefficients have an absolute magnitude that is less than about 0.3, the $\Delta \rho$ can be estimated from

$$\Delta\mathbf{r}_\rho(\tau) = \Delta d \left[\frac{1}{2}\ln\rho(\tau)\right]$$

by

$$\Delta\rho = \rho_0 \exp\left(2\sum_{u=0}^{u=\tau}\Delta\mathbf{r}_\rho(u)\right)$$

where ρ_0 is the background density, as is reported in Oldenburg et al. [1983].

Letting

$$\rho^{\mathrm{B}} = \phi\left[S_{\mathrm{h}}^{\mathrm{B}}\rho_{\mathrm{h}} + \left(1 - S_{\mathrm{h}}^{\mathrm{B}}\right)\rho_{\mathrm{w}}\right]$$

and

$$\rho^{\mathrm{M}} = \phi\left[S_{\mathrm{h}}^{\mathrm{M}}\rho_{\mathrm{h}} + \left(1 - S_{\mathrm{h}}^{\mathrm{M}}\right)\rho_{\mathrm{w}}\right]$$

represent the densities for the baseline (B) and monitor (M) surveys allows the $\Delta\rho$ to be defined as

$$\begin{aligned}\Delta\rho &= \rho^{\mathrm{B}} - \rho^{\mathrm{M}} \\ &= \phi\left(\rho_{\mathrm{h}} - \rho_{\mathrm{w}}\right)\left(S_{\mathrm{h}}^{\mathrm{B}} - S_{\mathrm{h}}^{\mathrm{M}}\right) \\ &= \phi\left(\rho_{\mathrm{h}} - \rho_{\mathrm{w}}\right)\Delta S_{\mathrm{h}},\end{aligned}$$

where ϕ is the reservoir porosity, ρ_{h} is the hydro-carbon density, ρ_{w} is the brine (water) density, ΔS_{h} is the hydro-carbon saturation change, and Δ is the time-lapse difference between the baseline and monitor surveys. Combining the two $\Delta\rho$ expressions allows ΔS_{h} to be estimated by the following:

$$\Delta S_{\mathrm{h}} = \frac{\rho_0 \exp\left(2\sum_{u=0}^{u=\tau}\Delta\left\{d\left[\frac{1}{2}\ln\rho(u)\right]\right\}\right)}{\phi\left(\rho_{\mathrm{h}} - \rho_{\mathrm{w}}\right)}.$$

4.5 P-P inversion example

Noise-corrupted P-P amplitude data is generated for the ideal reservoir illustrated in Figure (4.1). The data, shown in Figure (4.8), has a signal-to-noise ratio of 15 (SNR=15) and covers an angle of incidence range of $0° - 60°$ along the top of the reservoir, where the angles increase in steps of $2.5°$. The angle range is converted to ray-parameter p range using the shale background velocity of $\alpha_0 = 2500(m/s)$. As the critical ray-parameter is 4.0×10^{-4}, the p-range investigated spans from 0% to 86.6% of the critical ray-parameter. Although this is far beyond the standard range of AVP-analysis, current marine acquisition technologies now obtain usable angles up to $60°$ and it is reasonable to investigate using such long-offset data. Notice that the near offset traces (i.e. $0\% - 35\%$ of the critical ray-parameter) have
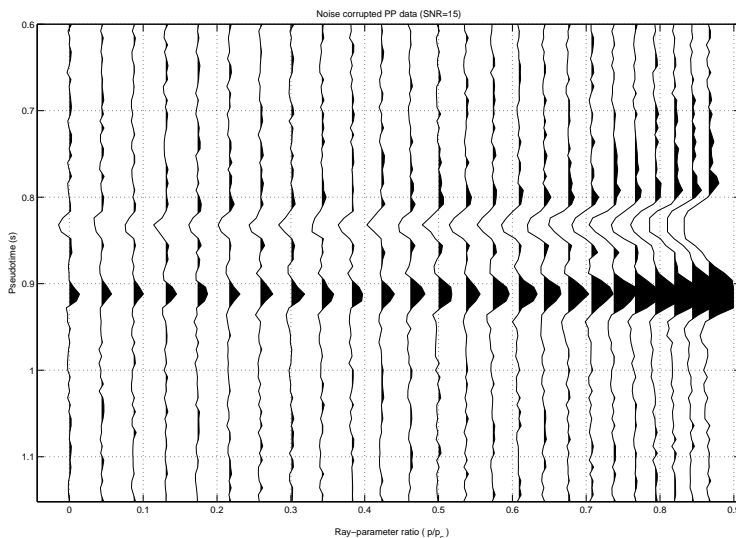
Figure 4.8: *Noise corrupted pre-stack P-P amplitude input data for inversion.*

very different waveform character than the middle and far offset ranges. Notice the pronounced and non-negligible variation in the waveforms as the critical ray-parameter is approached. These are exactly the kind of ray-parameter dependent stretching effects handled by the wavelet matrices in the P-P data kernel.

Figure (4.9) shows how the P-P objective function behaves under iteration. Specifically, it shows how Equation (4.3.15) behaves when Equation (4.3.16) is iterated

with input data $\mathbf{d}$ from Figure (4.8) and Equation (4.2.4) as the data kernel G. The objective function J rapidly decreases with the first 5 iterations of the non-
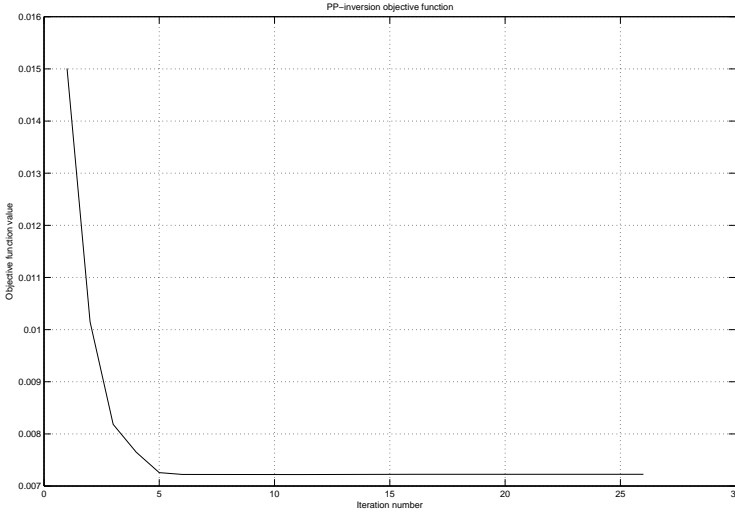
Figure 4.9: *The P-P residual misfit as a function of iteration number.*

quadratically regularized least-squares parameter estimate and then seems to level off. The IRLS solution developed in this chapter minimizes J to a final value of 7.2×10^{-3} while the damped least-squares solution (equivalent to Equation (4.3.16) after 1 iteration) minimizes J to 1.5×10^{-2}. In other words, non-quadratic regularization finds parameters $\mathbf{x}$ that minimize J better than quadratic minimization.

Figure (4.10) shows these estimates of acoustic impedance reflectivity, shear impedance reflectivity, and density reflectivity $(\boldsymbol{\delta I_P}, \boldsymbol{\delta I_S}, \boldsymbol{\delta \rho})$ against the actual rock property reflectivities. For the for the incomplete, imprecise, and noise-corrupted data shown in Figure (4.8), Equation (4.3.16) almost perfectly recovers the acoustic impedance reflectivity while the shear impedance reflectivity is underestimated and the density reflectivity is slightly underestimated. Integrating the reflectivities convert the estimates from interface rock properties to layer rock properties. The layer properties in Figure (4.11) show the underestimation, due to noise effects and a linear data kernel, more clearly. Also seen is that the subtle noise imprint on the parameter estimates, not visible when displayed as reflectivities, comes out after integration as the background shale values are slightly different above and below the reservoir unit. This is most evident on the density estimate.
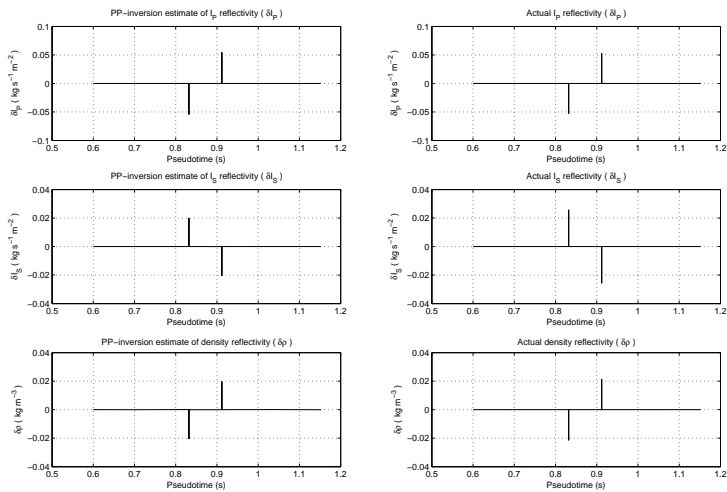
Figure 4.10: *Interface rock properties estimated from sparse pre-stack inversion of P-P data.*
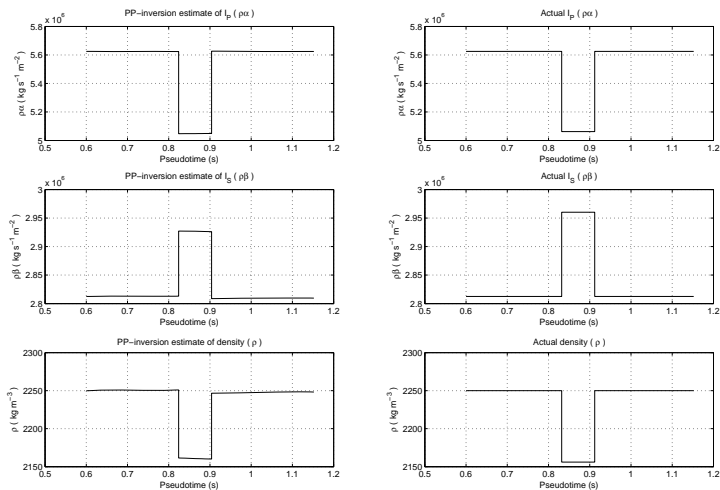

Figure 4.11: *Layer rock properties after integrating the P-P interface property estimates.*

4.6   P-S inversion example

The mode conversion situation of compressional-wave-to-shear-wave is now considered. As before, P-S amplitude data with a signal-to-noise ratio of 15 is created for the ideal Lego-block reservoir. The data, shown in Figure (4.12), covers the same angle of incidence range along the top of the reservoir and has the same $\Delta\theta$ of 2.5°. As such, the p-range investigated is identical and spans from 0% to 86.6% of the critical ray-parameter. The P-S data shows a gradual increase of amplitude with ray-
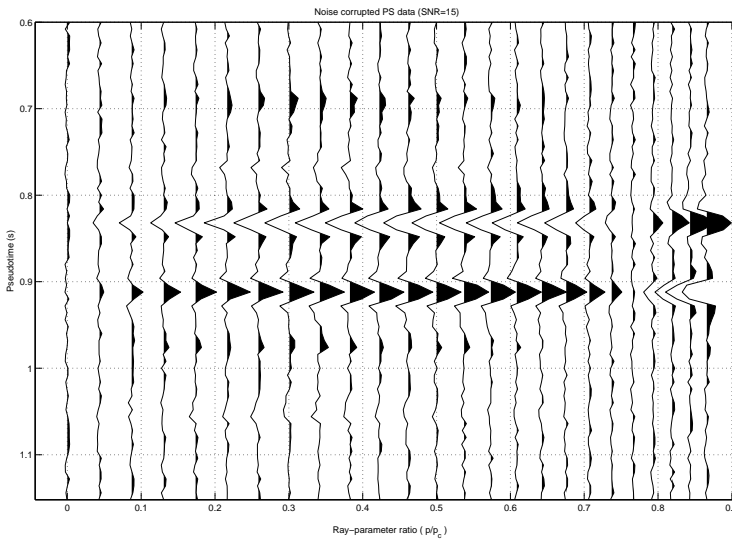
Figure 4.12: *Noise corrupted pre-stack P-S amplitude input data for inversion.*

parameter at the very near offsets (i.e. at $0\% - 15\%$ of the critical ray-parameter), followed by strong AVP-behavior out to about 65% of the critical angle, and then a polarity reversal with brightening at the ultra-far offsets (from 70% to over 80% of the critical ray-parameter). The amplitude behavior is quite complicated and the converted wave data suffers from reduced offset-dependent stretch effects. The implication is that imaging affects the multi-component waveform in a less severe manner.

For the P-S case, Figure (4.13) shows the evolution of the objective function Equation (4.3.15) as Equation (4.3.16) is iterated. The iteration of Equation (4.3.16) proceeds with input data from Figure (4.12) and Equation (4.2.8) as the data ker-

nel. The objective function's behavior is very different than in the P-P case. For the first 15 iterations there is marginal reduction in the misfit. Then there is a rapid descent to the minimum over the next 10 iterations before leveling out. The IRLS approach finds an optimum $\mathbf{x}$ that minimizes J to 2.7×10^{-4} while the damped least-squares solution delivers an optimal value for J as 5.96×10^{-4}. While non-quadratic regularization does reduce the residual by more than a factor of 2, it is not as dramatic as the order of magnitude reduction seen in the P-P situation.
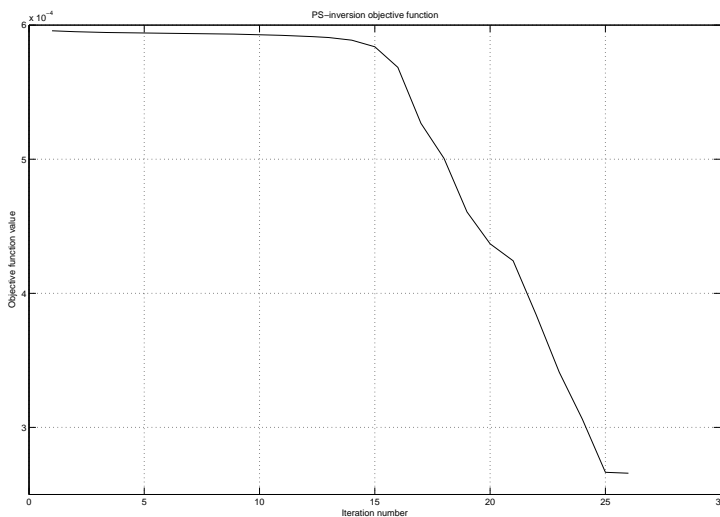
Figure 4.13: *The P-S residual misfit as a function of iteration number.*

As for parameter estimates, in this case, only two interface rock properties are estimated. This is because the P-S mode converted amplitudes only depend on shear impedance reflectivity and density reflectivity. Figure (4.14) shows these estimates of $(\boldsymbol{\delta \mathbf{I}_s}, \boldsymbol{\delta \rho})$ against the actual interface rock property values.

When estimating reservoir parameters from P-S data, Equation (4.3.16) almost perfectly recovers both the shear impedance reflectivity and the density reflectivity. However, as in the P-P case, converting to layer properties brings out subtleties not present when the estimates are analyzed as interface properties. Integrating the reflectivities to layer properties, Figure (4.15) shows the effects of noise and a linear data kernel more clearly in that it is now seen that the shear impedance is underestimated. Also seen is that both the shear impedance and density estimates predict slightly different reservoir thicknesses than are actually present.
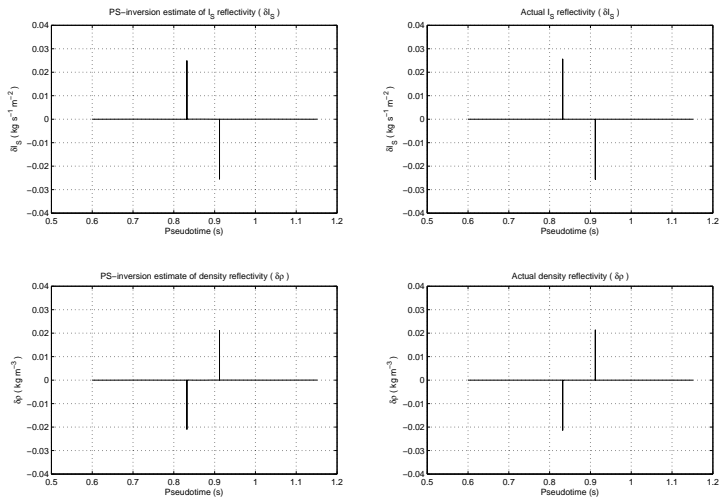
Figure 4.14: *Interface rock properties estimated from sparse pre-stack inversion of P-S data.*
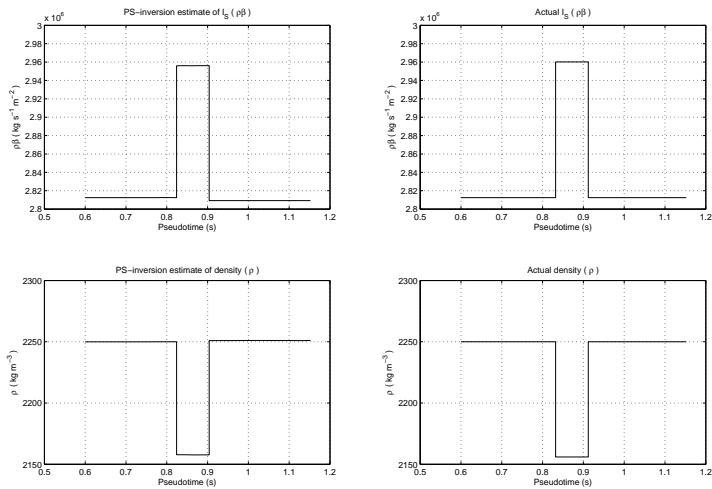

Figure 4.15: *Layer rock properties after integrating the P-S interface property estimates.*

4.7 Joint (P-P,P-S) inversion example

Finally, a situation where both the P-P and P-S datasets from Figures (4.8,4.12) are considered simultaneously. The objective function's behavior in Figure (4.16) now shows how Equation (4.3.15) evolves when Equation (4.3.16) is iterated with ordered multi-component input data as **d** and Equation (4.2.10) as the data kernel G. The pattern is similar to the P-P case in that there is a rapid decline at first and then the residual levels off. This implies that the P-P part of the optimization dominates. Notice, however, that the descent to a minimum is faster and the initial misfit is smaller than in the case of P-P data alone. This increase is due to simultaneously considering all the data. In this situation of joint inversion, damped least-squares gives the misfit J as 7.9×10^{-3} while the final residual value from IRLS is 3.8×10^{-3}. When compared to the inversion of P-P data alone, (P-P,P-S) inversion using Equation (4.3.16) minimizes the objective to the P-P level in one step and then continues the reduce the misfit function using the additional information from the P-S data.
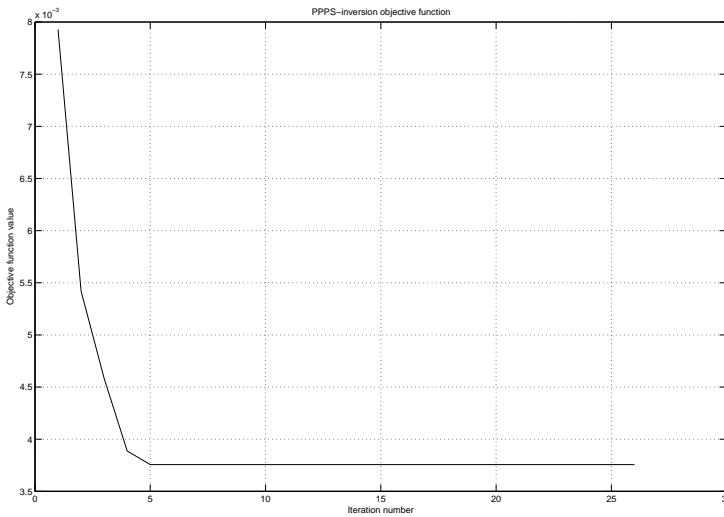
Figure 4.16: *The P-P-P-S residual misfit as a function of iteration number.*

Simultaneous (P-P,P-S) inversion aims for same three rock properties estimates as in the P-P case. Figure (4.17) and Figure (4.18) show these estimates of the interface and layer properties, respectively. Notice that both the shear impedance and density

estimates have improved from the P-P case. Also note that, since the acoustic impedance does not factor into the converted mode, there is no appreciable change in the acoustic impedance estimate.
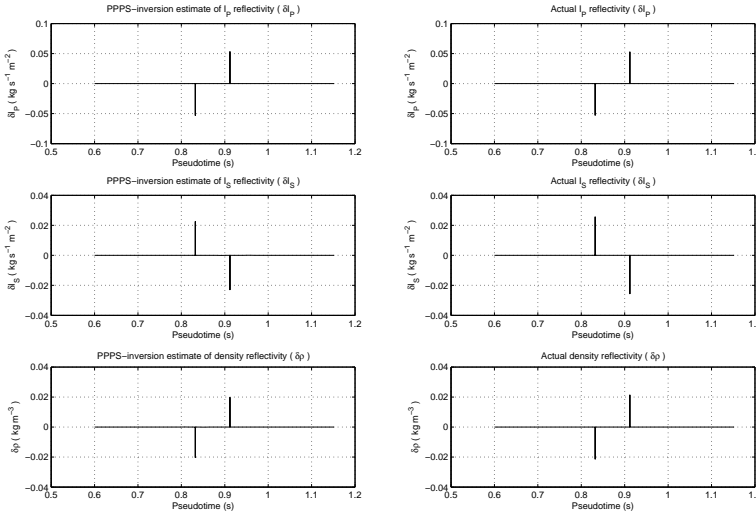
Figure 4.17: *Interface rock properties from sparse (P-P,P-S) pre-stack inversion.*

4.8   Conclusions

The application of stable and accurate linear, layered-earth, long-offset models, for estimation of three rock properties reveals some interesting things. Despite the notorious ill-conditioning and ill-posedness of AVP-waveform inversion, quantitative reservoir rock property estimates can be made. This chapter shows that data kernels built with the amplitude models developed in Chapter 3 and the imposition of non-quadratic regularization on the least-squares solution enables reliable broadband reservoir rock properties to be estimated from pre-stack seismic amplitudes. That is to say, IF the data is multi-component AND it has sufficiently long offsets AND there is an accurate background velocity field THEN linear target oriented high resolution inversion can deliver three broad-band rock properties .

This quantitative reservoir characterization results from several factors working together. Foremost among these is long offset, wide angle, or large ray-parameter
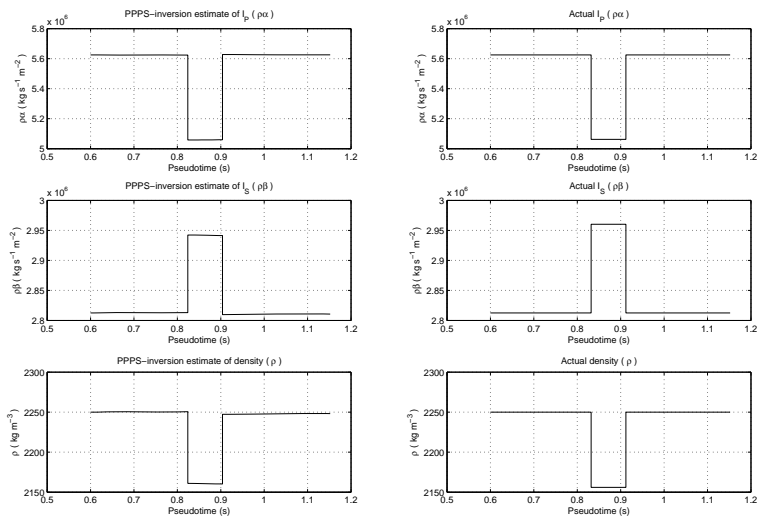
Figure 4.18: *Layer rock properties after integrating the (P-P,P-S) interface properties.*

data. There is no free lunch. Should more information be wanted from linear methods then more informative data must be acquired. For years, this was a problem as amplitude fidelity at the required offsets could not be guaranteed. Innovations in acquisition technologies can now deliver the data that is needed for quantitative characterization.

It is not enough to have this input data. The input seismic amplitude data itself can no longer be regarded as idealized delta functions from various layer interfaces in the subsurface. These data are actually wave-amplitudes with associated waveform effects that cannot be ignored at long offset. Accounting for these effects is crucial for the full exploitation of the available pre-critical information. Another requirement is that P-S converted wave amplitudes are needed. The examples show that P-S inversion delivers better estimates of parameters that suffer in P-P inversion alone. Furthermore, considering P-S data simultaneous with P-P data improves the conditioning and the parameter estimates.

Sparse, or non-smooth, rock properties that exploit the robustness of the ℓ_2-norm have been shown to be achievable through non-quadratic regularization. It should be noted, however, that low-frequency initial models will still need to be constructed to convert linear inversion results to absolute layer properties. Also shown is how to use the singular value decomposition to evaluate the parameterization of the

AVP-waveform inversion problem, how it can be used to assess the added value of long-offset data, and how the data and regularization contribute to the rock property estimates. Another aspect is that the non-quadratically regularized least-squares solution to the pre-stack amplitude inversion problem is shown to be an idealized version of a Bayesian solution. This means that if a proper probabilistic framework can be built, then high-resolution linear AVP-waveform inversion can deliver quantitative rock properties estimates with uncertainty measures.

5

Application to field data

5.1 Introduction

Inverse theory is a powerful, well developed, tool that enables the inference of model parameters given some set of observations. Solutions to problems of a practical interest that involve using inverse theory typically begin by establishing a linearised relationship, or model, or system, between the desired parameters and the available data. Aki and Richards [2002], Downton and Lines [2003], and Tarantola [2005] (among others) discuss the use of inverse theory to investigate geophysical problems in various contexts. Due to the fact that seismic amplitude data are incomplete, imprecise, and noise-corrupted, linear inverse theory cannot be applied in a straight forward way to infer a possible earth system. As such, constraint (or regularisation) is employed in seismic inversion to limit the family of feasible earth models admissible to the solution space. Previous applications of regularised inverse theory to problems in the oil and gas industry include, among others, the reconstruction of velocity gathers [Sacchi and Ulrych, 1995] and surface related multiple elimination in three dimensions [van Dedem and Verschuur, 2005].

There is a specific and immediate need for an efficient method to generate well-resolved rock property estimates of the subsurface, using pre-stack seismic amplitudes, in order to provide a more accurate picture of the hydro-carbon reservoir. This chapter addresses this need by taking aspects of linear inverse theory, developed in Chapter 4, and applying it to create a novel and practical method to infer sparse, high-resolution/well-resolved, rock properties from pre-stack compressional wave seismic amplitude data. This method evolves from current industry standard techniques for linear inversion and is a natural extension of the solution to the classical damped least-squares problem. The final deliverable is a pre-conditioned

conjugate gradient algorithm that performs minimum structure, broad-band, least-squares inversion of pre-stack seismic field data.

Following this theoretical development, the algorithm is applied to seismic data acquired over a glauconitic sandstone reservoir in Alberta, Canada. The seismic interpretation reveals three direct hydrocarbon indicators from the amplitude behavior. Though suffering from some lateral coherency and wavelet problems, the inversion confirms all of these indicators and identifies an additional one. Furthermore, the results of the inversion demonstrate that the proposed method successfully identifies the reservoir and its properties at a significantly higher resolution than is currently available with standard, commercially available techniques and that the results are more geologically plausible. The overall message from this case study is that sparse, broad-band/well-resolved, seismic reservoir characterization is possible from field acquired pre-stack seismic amplitude data. Generally, this case study endeavors to illustrate how linearised inverse theory can be used as a framework to further the use of seismic data in quantitative hydrocarbon reservoir characterization and management.

5.2   Practical implementation

Dey et al. [2006] shows that minimizing

$$J\left(\mathbf{y}\right) = \|\mathbf{d} - \mathbf{M}\mathbf{y}\|_2^2 + \lambda^2 \sum_{i=1}^{N} \ln\left(1 + \frac{y_i^2}{\sigma_i^2}\right) \tag{5.2.1}$$

leads to minimum structure (or sparse) estimates of the subsurface elastic parameters. In Equation (5.2.1), $\mathbf{d}$ is the pre-stack P-P seismic amplitude data, $\mathbf{M}$ is the robust model (or physical system matrix) described in Dey and Gisolf [2005], λ is the regularisation/trade-off parameter controlling the sparsity of the solution, $\Sigma_1^N \ln(1 + y_i^2/\sigma_i^2)$ is the regularisation term, y_i is the ith model parameter, σ_i is the the ith scale factor and N is the total number of model parameters. This objective function is simply the least-squares solution with a Cauchy norm, instead of a minimum quadratic norm, for regularisation. In same manner as in Sacchi and Ulrych [1995], Equation (5.2.1) is minimized using classical iterative re-weighted least squares to obtain

$$\mathbf{y}^{(k)} = \left\{\mathbf{M}^{\text{T}}\mathbf{M} + \lambda^2 \mathbf{Q}\left[\mathbf{y}^{(k-1)}\right]\right\}^{-1} \mathbf{M}^{\text{T}}\mathbf{d}, \tag{5.2.2}$$

where $\mathbf{Q}$ is a diagonal matrix which, for the kth iteration, has elements

$$Q_{jj} = \frac{1}{1 + \left[y_j^{(k-1)}/\sigma_j^{(k-1)}\right]^2}. \tag{5.2.3}$$

Direct implementation of Equation (5.2.2) and iterating until convergence is not advised when dealing with realistic data volumes. The two primary reasons to avoid this approach are that it does not exploit the fact that Equation (5.2.1) is a sparse linear system of normal equations (Figure (5.1)) and it does not recognize the fact that the convergence of the iteration can be quite slow (if it converges at all). Equation (5.2.2) can be used to understand and illustrate the effect of non-quadratic Cauchy norm regularisation in example situations but is not of practical use for inverting field seismic data.
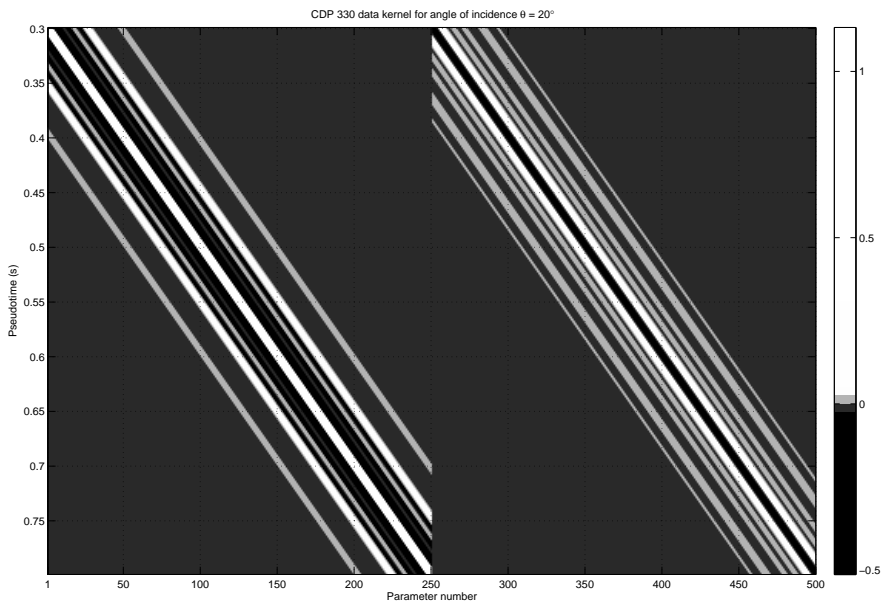
Figure 5.1: *A representative data kernel from CDP330 with angle of incidence* $\theta = 20°$. *Notice the sparsity of the system in that very few matrix elements are non-zero.*

Saad [2004] gives a rigorous overview of iterative methods for sparse linear systems, with special attention paid to efficient methods for solving a large system of normal equations. In particular, pre-conditioning the system before iteration and using the method of conjugated gradients is one way to rapidly obtain a solution. Successful

preconditioning strategies for seismic inverse problems have been reported by Trad et al. [2003] and their approach of finding an appropriate pre-conditioner is employed to solve inverse problem at hand.

Notice that, for a known $\mathbf{Q}$, a $\mathbf{y}$ that minimizes Equation (5.2.1) is similar to the solution of

$$J\left(\mathbf{y}\right) = \|\mathbf{d} - \mathbf{My}\|_2^2 + \lambda^2 \left\|\mathbf{Q}^{1/2}\mathbf{y}\right\|_2^2. \tag{5.2.4}$$

A change of variables where we let $\mathbf{z} = \mathbf{Q}^{1/2}\mathbf{y}$ transforms Equation (5.2.4) to

$$J\left(\mathbf{z}\right) = \|\mathbf{d} - \mathbf{MPz}\|_2^2 + \lambda^2 \|\mathbf{z}\|_2^2, \tag{5.2.5}$$

where $\mathbf{P} = \mathbf{Q}^{-1/2}$ is a diagonal matrix pre-conditioner which, for the kth iteration, has elements

$$P_{jj} = Q_{jj}^{-1/2} = \sqrt{1 + \left[y_j^{(k-1)}/\sigma_j^{(k-1)}\right]^2}. \tag{5.2.6}$$

Minimizing this new objective function is a Tikhonov-type problem [Hansen, 1998] and Equation (5.2.5) is re-written as

$$J\left(\mathbf{z}\right) = \left\| \begin{pmatrix} \mathbf{d} \\ \mathbf{0} \end{pmatrix} - \begin{pmatrix} \mathbf{MP} \\ \lambda^2 \mathbf{I} \end{pmatrix} \mathbf{z} \right\|_2^2. \tag{5.2.7}$$

Setting $\begin{pmatrix} \mathbf{d} \\ \mathbf{0} \end{pmatrix} = \mathbf{b}$, $\begin{pmatrix} \mathbf{MP} \\ \mu\mathbf{I} \end{pmatrix} = \mathbf{A}$, and $\mathbf{x} = \mathbf{z}$ transforms the original problem in Equation (5.2.1) into standard form

$$J\left(\mathbf{z}\right) = \|\mathbf{b} - \mathbf{Ax}\|_2^2. \tag{5.2.8}$$

In same manner as Sacchi and Liu [2005], Hansen [1998], and Wang [2005], the following pre-conditioned conjugate gradient procedure for the efficient estimation of sparse/blocky rock properties from acquired pre-stack seismic amplitudes is proposed.

$\mathbf{d} \Leftarrow \text{data}; \text{M} \Leftarrow \text{model}; \varepsilon \Leftarrow \text{tolerance}; \mathbf{z}_0 \Leftarrow \text{initial guess};$

$\mathbf{P}_0 = \mathbf{Q}^{-1/2}\left(\mathbf{z}_0\right)$

FOR ALL $u \in [0, 1, \dots, u_{max}]$ (start update loop)

        $\mathbf{s}_0 = \mathbf{d} - \mathbf{MP}_u\mathbf{z}_0$

        $\mathbf{r}_0 = \mathbf{P}_u^{\mathrm{T}}\mathbf{M}^{\mathrm{T}}\mathbf{s}_0$

        $\mathbf{p}_0 = \mathbf{r}_0$

        $\mathbf{q}_0 = \mathbf{MP}_u\mathbf{p}_0$

        FOR ALL $i \in [0, 1, \dots, i_{max}]$ (start iteration loop)

            $\alpha_{i+1} = \left(\mathbf{r}_i^{\mathrm{T}}\mathbf{r}_i\right) / \left(\mathbf{q}_i^{\mathrm{T}}\mathbf{q}_i\right)$

            $\mathbf{z}_{i+1} = \mathbf{z}_i + \alpha_{i+1}\mathbf{p}_i$

            $\mathbf{s}_{i+1} = \mathbf{s}_i - \alpha_{i+1}\mathbf{q}_i$

            $\mathbf{r}_{i+1} = \mathbf{P}_u^{\mathrm{T}}\mathbf{M}^{\mathrm{T}}\mathbf{s}_{i+1}$

            if $\mathbf{r}_{i+1}^{\mathrm{T}}\mathbf{r}_{i+1} \leq \varepsilon$ then BREAK

            $\beta_{i+1} = \left(\mathbf{r}_{i+1}^{\mathrm{T}}\mathbf{r}_{i+1}\right) / \left(\mathbf{r}_i^{\mathrm{T}}\mathbf{r}_i\right)$

            $\mathbf{p}_{i+1} = \mathbf{r}_{i+1} + \beta_{i+1}\mathbf{p}_i$

            $\mathbf{q}_{i+1} = \mathbf{MP}_u\mathbf{p}_{i+1}$ END   (end iteration loop)

      $\mathbf{P}_{u+1} = \mathbf{Q}^{-1/2}\left(\mathbf{z}_i\right)$ END   (end update loop)

Figure 5.2: *A pre-conditioned conjugate gradient algorithm with restarts.*

5.3   Land data case study

The theory and algorithm of the preceding section is now considered within the framework of a quantitative interpretation case study where the goal is to assess the method with respect to an observed reservoir amplitude anomaly. Under consideration is a mature sand trend in Alberta, Canada, where seismic data has been acquired and the inversion methodology is applied to generate minimum structure rock properties estimates. The validity of such sparse rock property estimates from seismic can be seen following a consideration of geological scaling phenomena (or $1/f$ geology). Pilkington and Todoeschuck [1990], working from the results of Walden and Hosken [1985], show that the geophysical expression of many geological properties have power spectra of the form $1/f$ (i.e. they are scaling phenomena). They conclude that the upper sedimentary part of the Earth's crust exhibits a degree of self-organisation. The macroscopic observations related to this so-called scaling geology are quasi-cyclic and blocky layering of the rock strata. Shtatland [1991] goes on to theoretically justify these (multi)fractal spectra from a consideration of entropy rate and shows blockiness to be a limiting case of quasi-cyclicity. In doing so, the blocky/sparse/minimum structure assumption used in seismic inversion for rock properties is given theoretical justification and meaningfulness in terms of geology. Furthermore, this means that should the fractal nature of crustal rock layering be uncovered, then a *natural/fractal* interpolation scheme could be derived that correctly goes from pore-to-seismic scale. Currently, this remains a challenging and open problem.

■ 5.3.1   Geological description

The reservoir zone of interest in this investigation is the Colony sand member of east-central Alberta, Canada. This member is comprised primarily of shales, siltstones, coals and sands. It trends north/north-west and is the uppermost unit of the informal subdivision of the Manville Group [Royle, 2002]. Putnam and Oliver [1980] note that the Colony member is commonly associated with thick shoestring channel sandstones and define the depositional environment as channel sandstones encased within siltstones, shales, coals, and thin-sheet sandstones. Three facies units are associated with the Colony sand: the channel facies, the crevasse splay facies, and the inter-channel wetland facies. This upper Manville sub-group is overlain by the marine shales of the Joli Fou formation and Wrightman et al. [1981] show that the reservoir sands are comprised of stacked paleochannels. While the stacked paleo-sand-channels are known to be gas and oil bearing, in this particular area the reservoir is gas charged. Figure (5.3) illustrates the depositional model for the Colony sand member.
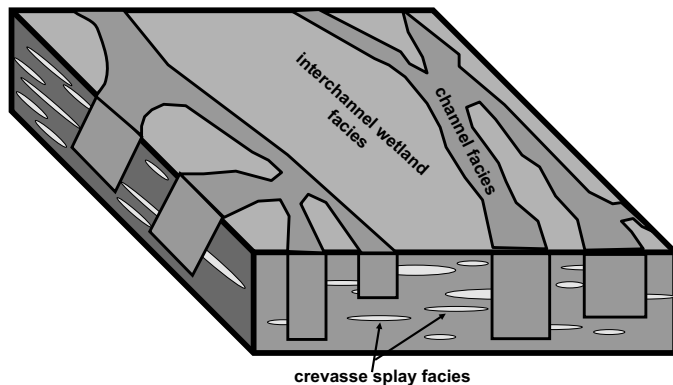
Figure 5.3: *The depositional model of the Colony sandstone and its three associated facies units.*

■ 5.3.2   Minimum structure inversion

A 2-D seismic survey was acquired in this area and a single line was made available for this study. From this line, every 10th common-depth-point (CDP) gather, with each gather comprised of 8 traces, was extracted. In addition, 3 more gathers near the start, middle, and end of the line are also used. Figure (5.4) shows the 23 gathers to be used as input for the inversion. Note the brightening of seismic amplitudes between $0.6s$ and $0.7s$ in the middle of the line.

After stacking these gathers, (Figure (5.5)) several hydrocarbon indicators are noticed. Hilterman [2001] illustrates that a Class 3 gas sand amplitude anomaly [Rutherford and Williams, 1989] appears as a bright spot on the stack section, the amplitudes are fairly constant over the extent of the anomaly, a phase change can occur off-structure at the reservoir edges, and the wavelet character is a trough-peak pair under the North American polarity standard. All of these characteristics are observed on the stack within the $0.60s$-$0.65s$ time window, between CDP numbers 10 and 15. The presence of multiple hydrocarbon indicators on the stack, combined with regional analogue knowledge, leads to the interpretation of an inter-channel wetland facies (the peaks at approximately $0.625s$) terminating against a gas charged paleo-sand-channel facies.

Following this analysis of the stack section amplitude, the gathers are inverted using the minimum structure method presented in Figure (5.2). That is to say, the least informative earth model that can adequately reproduce the data is sought. An angle range of $5°$ to $23°$ is available for the inversion. This limited angle range implies that the estimation of only 2 rock properties, at most, should be attempted and is an example of data acquisition that fails to exploit the full reservoir char-
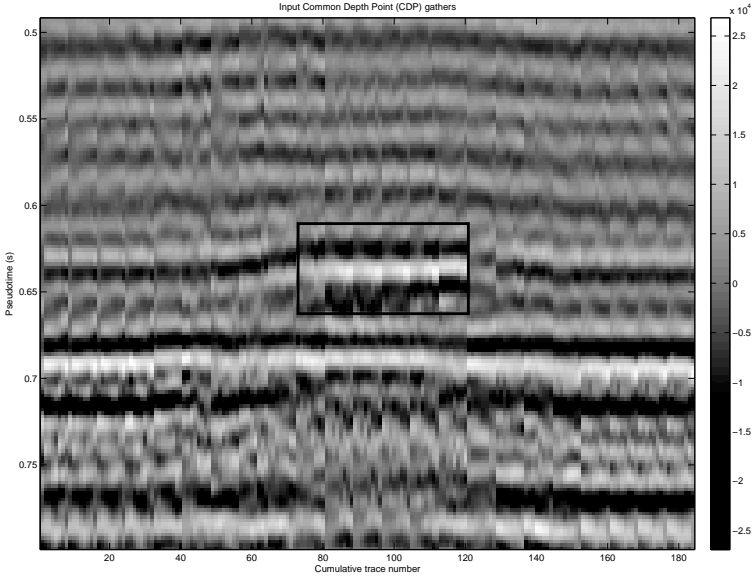
Figure 5.4: *The 23 common-depth-point (CDP) gathers, displayed in time, that are input data for the pre-stack inversion. Cumulative trace number annotates the x-axis.*

acterization potential of seismic amplitudes. In other words, the ultimate goal of reservoir characterization was not road-mapped back through the data processing to the acquisition survey design stage.
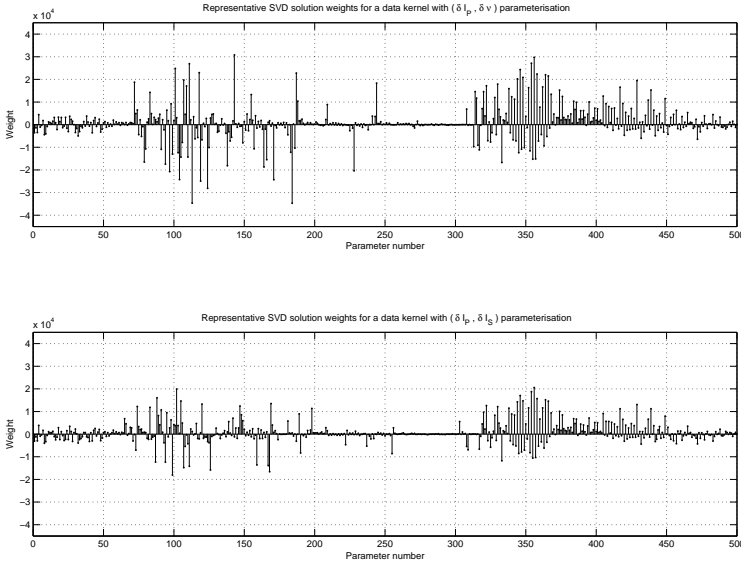

Parameterisation analysis

Since this is a bright spot anomaly, the gathers are used to estimate different rock properties via various two-term parameterisations of Equation (5.2.1). The popular intercept-gradient formulation $(\delta \mathbf{I_P}, \mathbf{G})$ of Shuey [1985] is not considered. This is because, traditionally, intercept and gradient have been extracted attributes obtained by model fitting, rather than data inversion. Furthermore, the gradient is the rate of change with which the intercept (or zero-offset reflectivity) response changes, not a direct rock property. Instead, the acoustic-shear impedances $(\delta \mathbf{I_P}, \delta \mathbf{I_S})$ of Gidlow et al. [1992], and the acoustic-Poisson impedances $(\delta \mathbf{I_P}, \delta \boldsymbol{\nu})$ of Hilterman [2001] are considered due to their direct link to lithology and fluids (as they are directly estimated rock properties). These have all been modified to explicitly separate the
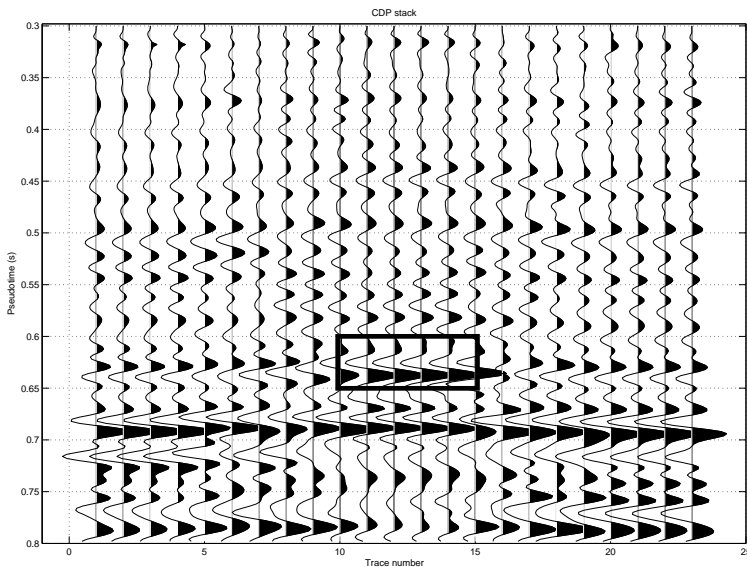
Figure 5.5: *The common-depth-point (CDP) stack. Notice the amplitudes, between traces* $10 - 15$ *within the time gate* $0.60s - 0.65s$ *(inside the rectangle), displaying features of a traditional Class 3 anomaly.*

kinematic and dynamic aspects of the reflection amplitudes as outlined in Chapter 3. All of the parameterisations estimate the acoustic impedance reflectivity, or intercept. This is the zero-offset response and should emphasize a bright spot. A benefit of our limited angle range means that the CDP stack can be used as a reasonable proxy for comparison to the filtered $\boldsymbol{\delta I_P}$ estimates. The shear impedance reflectivity and Poisson's ratio reflectivity are both lithological properties which are a measure of the integrity of the rock matrix. Ideally, both, Gidlow et al. [1992] and Hilterman [2001] estimate one fluid related rock property and one lithology related rock property. It remains up to the experimental design (i.e. the seismic survey) and the kinematic background to determine which pair of rock properties are best estimated from the data. That is to say, the kernels developed in Chapter 4 can aid in evaluating an inversion's quality. The singular value decomposition, or SVD, is the tool to exploit in this respect.

Figure (5.6) shows, SVD computed, representative solution weights for the various parameterisations. Recalling that the final earth model delivered by the inversion is a weighted sum, Equations (4.3.12) and (4.3.17), allows one to see that both

Figure 5.6: *The, SVD computed, estimation weights for various inversion parameterisations. Parameters with relatively larger weights will dominate the inversion solution.*

parameterisations will give solutions that are dominated by a relatively small number of parameters (an empirical justification of the sparsity assumption). Furthermore, the weights for the Hilterman [2001] parameterisation are seen to be about 1.5-2 times as large as those for the Gidlow et al. [1992] parameterisation. Hence, it is expected that the sparsity of the former to be stronger than that of the latter.

Independent of the weighted sum interpretation of a linearised inverse problem, the singular values are a diagnostic tool for parameter estimation. The ratio of the largest singular value to the smallest singular value, or condition number, is a measure of how well suited the experimental design is for estimating the parameters of interest. In other words, the condition number is a measure of reliability that the desired rock properties (or geology) can be recovered from the seismic data. This condition number can be computed *a priori* with a general knowledge of the background geology and, as such, can be used to evaluate various survey acquisition designs with respect to the final reservoir characterization goals. It is a tool for road mapping back through the double feed-back loop of the Seismic Value Chain.

Representative data kernel conditioning, Figure (5.7), illustrates how the P-P am-
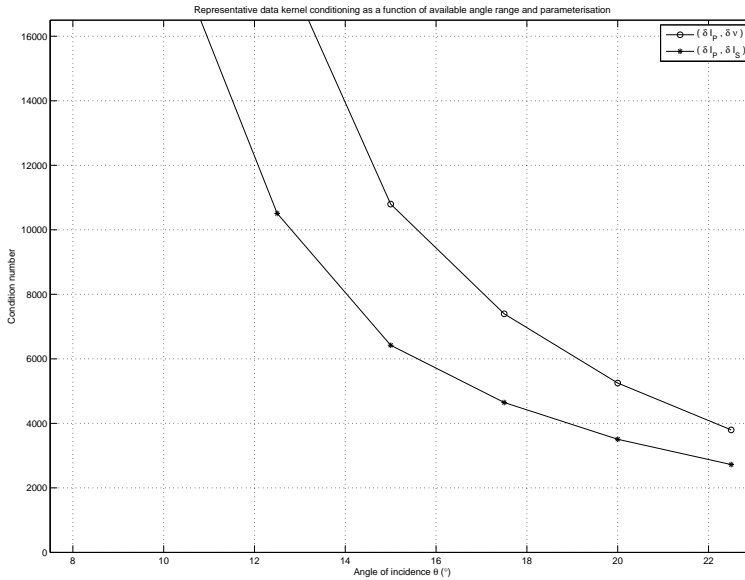
Figure 5.7: *The conditioning of various linear P-P amplitude inversion kernels. These kernels are parameterised in terms of the rock property reflectivites for acoustic impedance and Poisson's ratio $(\delta I_P, \delta \nu)$, as well as acoustic impedance and shear impedance $(\delta I_P, \delta I_S)$.*

plitude inversion behaves as a function of parameterisation and the available angles of incidence. Notice that the choice of parameterisation directly impacts the condition number behaviour of the data kernel. This implies that the desired rock properties to be estimated must be considered not only during the reservoir characterisation stage but also during the acquisition survey design stage. Overall, for this case study's data, parameterising in terms of impedance reflectivity seems to be the best behaved and would be most reliably estimated. However, as the available data range gets closer and closer to the maximum usable angle of incidence, the various parameterisations converge to conditioning that is of the same order. This convergence does not arise gradually, nor at the same rate. Note that the condition numbers are extremely high and then, suddenly, experience a rapid decrease, with the $(\boldsymbol{\delta I_P}, \boldsymbol{\delta I_S})$ parameterisation having a faster rate of conditioning improvement. For this particular survey design, the conditioning behaviour implies that seismic rock properties estimation from P-P amplitudes will be problematic for the angles of incidence smaller than $12°$.

The interface parameter estimates, made by the two inversion formulations, are shown in Figures (5.8) and (5.9). From the gathers, Figure (5.4), and the stack, Figure (5.5), the rock properties response of the reservoir is expected between CDPs $10 - 15$ and times $0.60s - 0.65s$. Notice the very sharp definition at the top and base of the reservoir in the property estimates from both parameterisations. Also note the preservation of the phase change at the reservoir edges. One problematic issue with the results of the estimated acoustic impedance contrasts in Figure (5.8) is that the trough delineating the top of the reservoir disappears along the structure while the base reservoir peak remains stable. This is an indication that the regularisation parameters may not be optimal and need to be adjusted using some prior geological knowledge of the area.
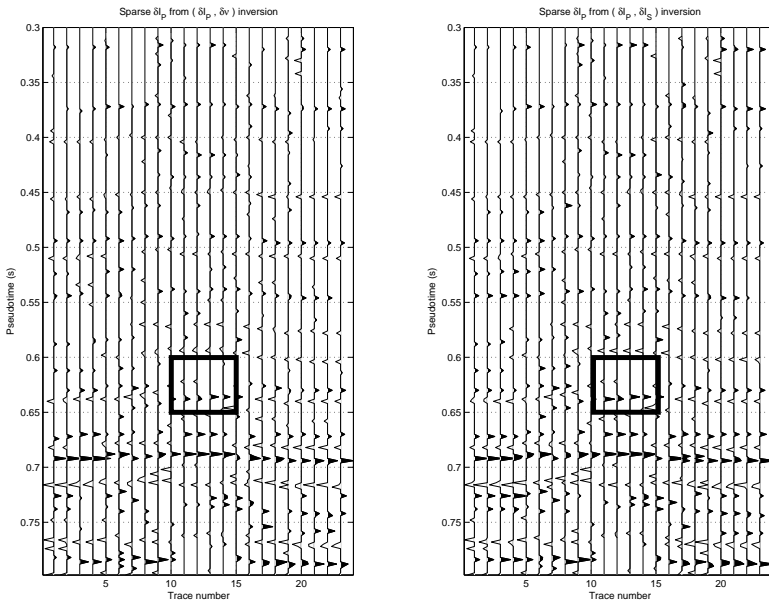
Figure 5.8: *A comparison of the acoustic impedance reflectivity (δI_P), estimated using the ($\delta I_P, \delta \nu$) and ($\delta I_P, \delta I_S$) inversion parameterisations.*

In contrast, Figure (5.9) shows the second estimated rock property reflectivity ($\delta \nu$ and δI_S, respectively) to clearly define the top and base of the reservoir. This provides another possible explanation as to why the trough delineating the reservoir top disappears. Since each of $\delta \nu$ and δI_S are so-called *lithology* indicators and δI_P

is comparatively sensitive to fluids (i.e. it is a *fluid* indicator), it could very well be that the measured amplitudes are dominated by the response to rock type. As such, the inversion focuses on estimating the rock property that forms the majority of the amplitude response. That is to say, the inversion estimates best the property which directs the physics of the geology's seismic response. It can be speculated that if a three-term pre-stack inversion were attempted with this data, an improvement would be seen in the δI_P estimate but there would be no uplift in the δI_S or $\delta \nu$ estimates, with the $\delta \rho$ estimate containing no information at all. Essentially, a three-term inversion would serve only to improve the δI_P estimate.
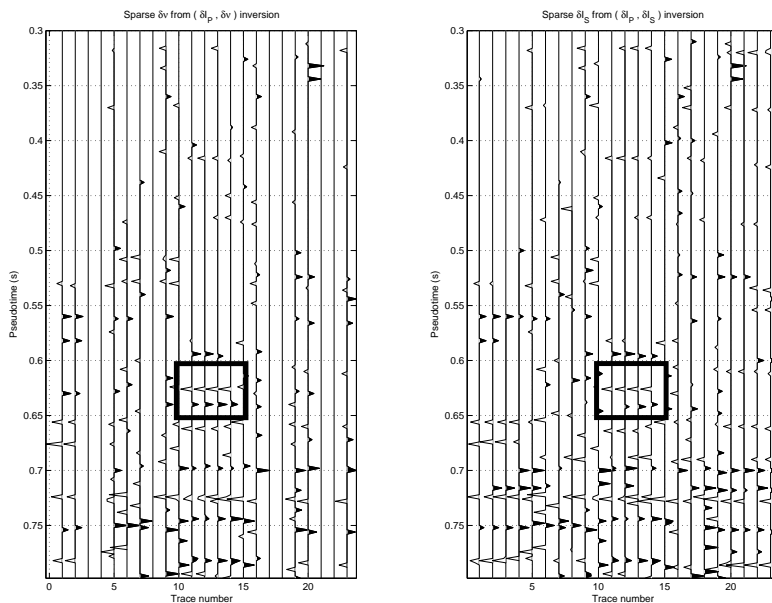
Figure 5.9: *A comparison of Poisson's reflectivity ($\delta \nu$) and shear impedance reflectivity (δI_S), estimated using the ($\delta I_P, \delta \nu$) and ($\delta I_P, \delta I_S$) inversion parameterisations.*

Also, note that the estimate of $\delta \nu$ is superior to that of δI_S. This may be somewhat surprising since the condition number analysis indicates that the ($\delta I_P, \delta I_S$) formulation to be the most reliable and, thus, expected to give the best results. However, looking at the estimated earth model in terms of a weighted sum (Figure (5.6)) indicates that the Hilterman [2001] formulation has stronger sparsity than that of the Gidlow et al. [1992] parameterisation. In this case, it seems as if sparseness (i.e. the

SVD weights) are a stronger factor in driving the inversion results than conditioning. Rather than undertaking many costly inversions, an SVD analysis should be carried out and inversion decisions be based on a balance of sparseness and conditioning. Alternatively, the approach of Downton [2004] can be used where a single inversion for the preferred rock properties is undertaken and the result transformed to any other desired set of rock properties.

Before further analysis of the inversion results, recall that the depositional model states that the overlying unit of the regional gas-charged sand is a marine shale. The expected behaviour of a gas bearing sand overlain by a shale that displays a seismic bright spot response is to have a fluid indicator (i.e. δI_P) and a lithology indicator (i.e. $\delta \nu$ or δI_S) at the top of the reservoir that is less than that for the overlying shale cap rock. That is to say, the fluid and lithology indicators at the top of the Colony sand should be expected to deflect to the left from the background Joli Fou shale (assuming gas-charging and North American polarity standard). This is precisely what is seen in both inversion results (albeit, before the trough definition is lost in the δI_P estimates) and represents another direct hydrocarbon indicator that holds true for this prospect.

Similar behaviour is expected when the interface properties are integrated to relative layer properties. Figure (5.10) and Figure (5.11) show this mapping and the preservation of the expected behaviour. Notice that the relative acoustic impedance estimates lose fidelity half-way across the reservoir in that the inversion estimates stop deflecting to the left of the background shale. These figures also highlight, in a real-world practical sense, the legitimacy of the sparseness assumption. When mapped from interfaces to layers, the final rock properties result in geologically plausible (local) horizontal layered earth models with abrupt/blocky transitions, rather than the more common smoothly varying geophysical earth models.

Figures (5.12)–(5.16) enable further analysis of the inversion results. Standard residual analysis (Figure (5.12) and Figure (5.13)) shows the input gathers, the final predicted gathers for the two parameterisations being considered, and their respective residuals. The residuals for both seem to show a faint hint at some coherent information remaining. These differences are, however, less noticeable when the predicted gathers are stacked and the residual computed with respect to the actual CDP stack (see Figure (5.14) and Figure (5.15)).

One possible explanation for the remaining coherent energy in the residual is due to the sparse nature of the inversion. The adopted approach seeks an earth model with the least information required to adequately explain the acquired data. That being the case, non-dominant reflectivities are rejected to preserve sparsity. This would lead to weak coherent energy remaining in the residual. Another, equally probable, explanation is that this possible remaining coherent energy indicates that using offset/ray-parameter/incidence-angle dependant wavelets estimated from the data does not adequately reflect the situation. While not pursued further in this study, it is expected that using a wavelet that results from a seismic-to-well matching
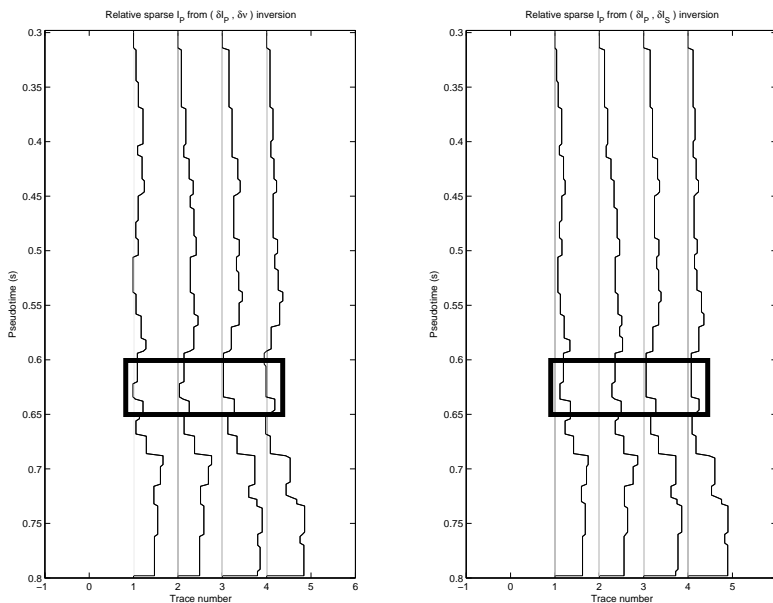
Figure 5.10: *A comparison of the relative acoustic impedance (I_P), estimated using the $(\delta I_P, \delta \nu)$ and $(\delta I_P, \delta I_S)$ inversion parameterisations.*

exercise and then imposing the physics of normal moveout, will improve the inversion results.

The engine of the inversion developed and applied in this chapter is Equation (5.2.1). Its ability to estimate rock properties that explain the input data is measured by the magnitude of the misfit between the real data and the forward modeled (or predicted) data. This misfit would, ideally, be zero, but, because of practical issues (such as noise and experimental design inadequacies), is usually some user determined tolerance ϵ that is deemed *close enough* to the acquired data being used to obtain parameter estimates. Quite often this tolerance, itself, cannot be achieved and a result with an undesirable misfit is accepted because the maximum number of iterations has been exceeded (see Figure (5.2)).

The final misfit for the two parameterisations of the inversion objective function considered in this chapter is shown in Figure (5.16). Supporting the previous observation that the $(\delta I_P, \delta \nu)$ formulation delivers superior results, the final misfit over the reservoir region (spanned by the 10$^{\text{th}}$–15$^{\text{th}}$ CDP gather) is smallest for the
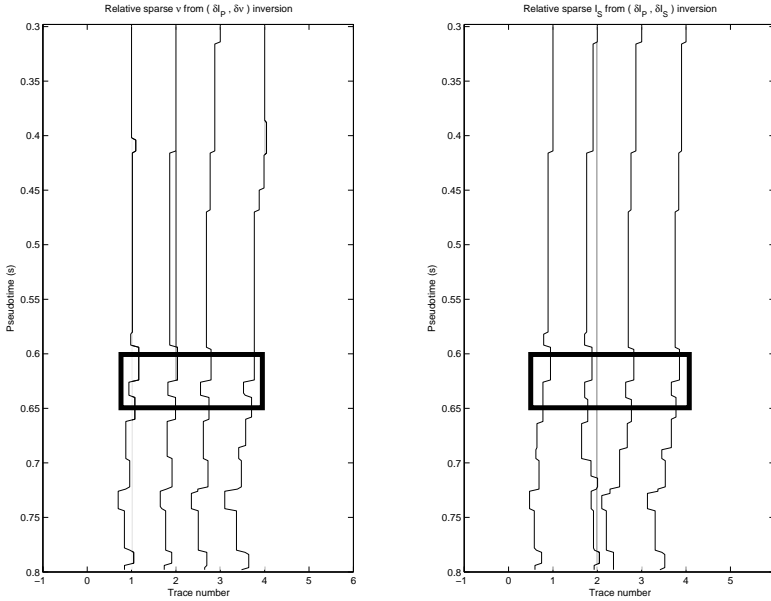
Figure 5.11: *A comparison of relative Poisson's ratio (ν) and relative shear impedance (I_S), estimated using the $(\delta I_P, \delta \nu)$ and $(\delta I_P, \delta I_S)$ inversion parameterisations.*

Hilterman [2001] set of parameters. Not only does the $(\delta I_P, \delta \nu)$ combination have strong sparsity/blockiness, it also forward models the reservoir seismic more accurately. This on top of the fact that these rock properties can be directly linked to pore-fill and lithology. All of this combines to support a strong case for $(\delta I_P, \delta \nu)$ being an ideal set of seismic rock properties for this data.
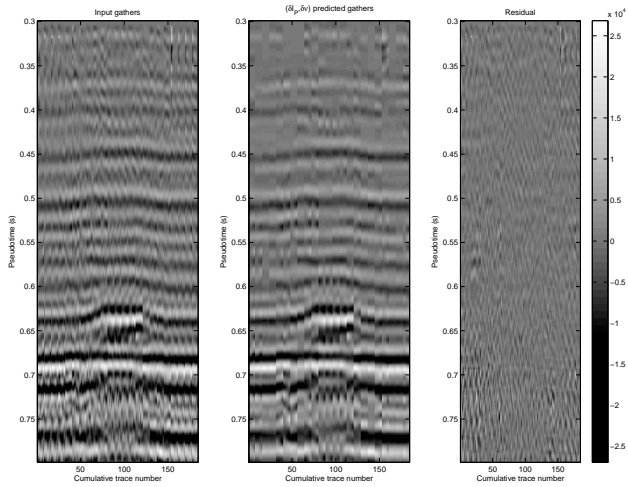
Figure 5.12: *The actual gathers compared to the $(\delta I_P, \delta \nu)$ predicted gathers.*
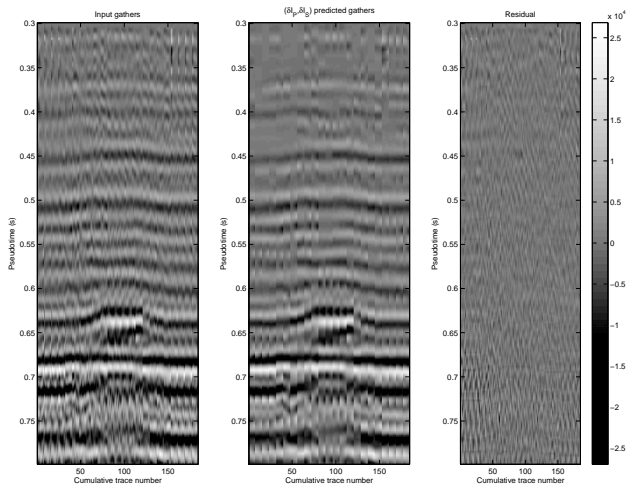
Figure 5.13: *The actual gathers compared to the $(\delta I_P, \delta I_S)$ predicted gathers.*
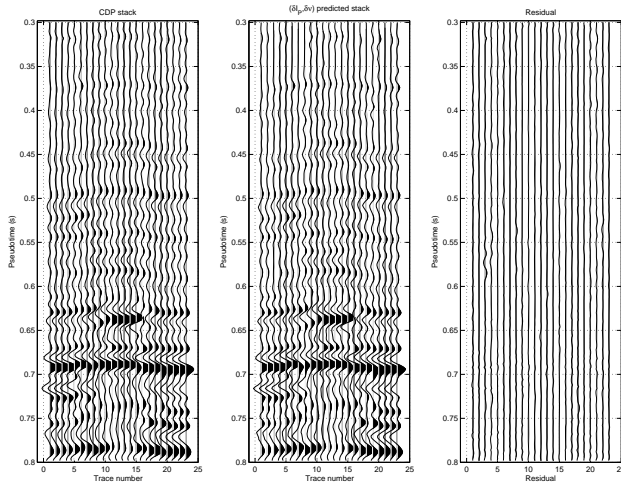
Figure 5.14: *A comparison of the actual stack and the $(\delta I_P, \delta \nu)$ predicted stack.*
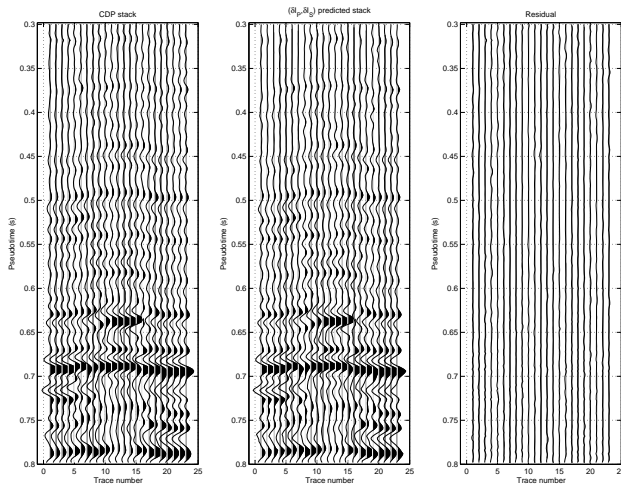
Figure 5.15: *A comparison of the actual stack and the $(\delta I_P, \delta I_S)$ predicted stack.*
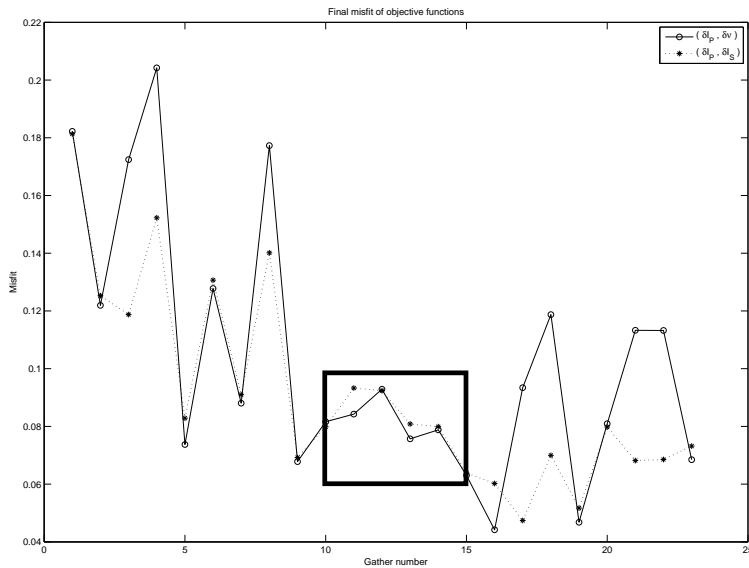
Figure 5.16: *A comparison of the final objective function misfit for the* $(\delta I_P, \delta \nu)$ *and* $(\delta I_P, \delta I_S)$ *parameterisations of the inverse problem. The points within the rectangle show the misfit for the gathers which span the reservoir.*

Resolution analysis

Another aspect of sparse inversion is that of *resolution*. In the Berkhout [1984] sense, resolution goes beyond thin-beds and is more about *focus*. Very generally, high-resolution is an issue of better/sharper focus. With respect to this case study, the Berkhout [1984] interpretation of resolution views the minimum-structure rock property estimates as ones that have high-resolution (high frequencies) but do not, necessarily, detect thin-beds. Figure (5.17) shows that over the zone of interest, the most noticeable difference between the sparse and standard acoustic impedance reflectivity results is in bandwidth. Though not full-band, the sparse result shown in Figure (5.17) represents a broad-band result that is much higher resolution than the output from standard least-squares inversion.
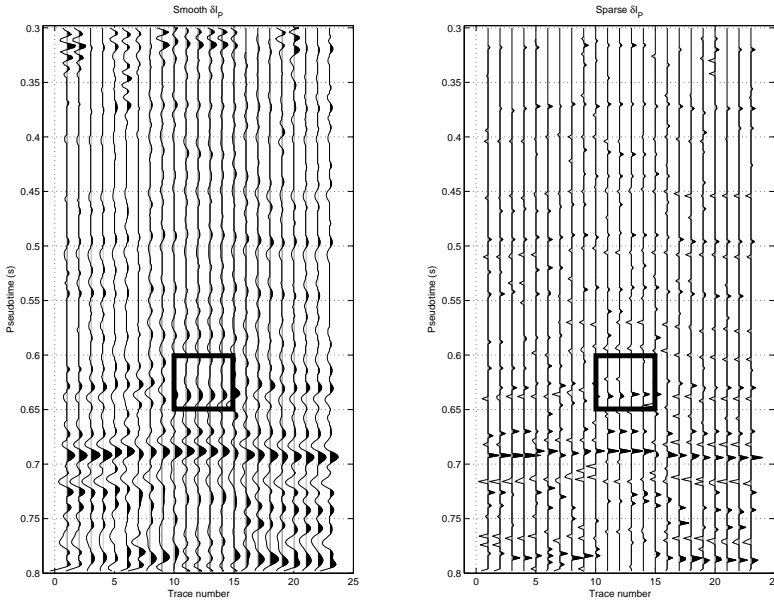
Figure 5.17: *A comparison of the smooth and sparse acoustic impedance reflectivity (δI_P), estimated using the $(\delta I_P, \delta\nu)$ parameterisation.*

Similarly, the smooth and sparse Poisson's ratio reflectivity are compared in Figure (5.18). In addition to the sharper focussing, the two estimates show quite a lot of difference in their respective information content. The smooth result has more
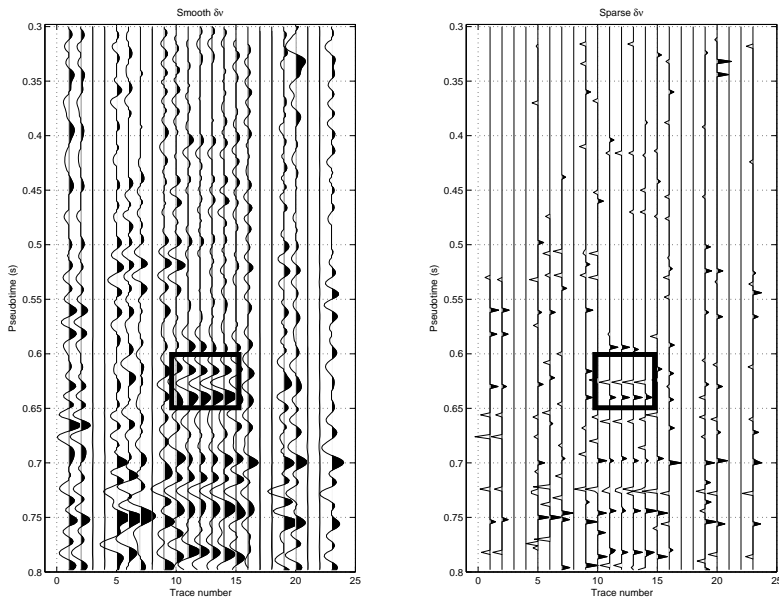
Figure 5.18: *A comparison of the smooth and sparse Poisson's reflectivity (δν), estimated using the (δI_P, δν) parameterisation.*

detail, but also appears noisier. At the same time, the sparse/high-resolution esti-
mate has fewer events (i.e. less information) but they are clear and sharp. When
transformed to relative layer properties, Figures (5.19) and (5.20), and compared to
the typical output from a commercial package, the added value of sparse estimation
becomes even clearer. Traditional methods deliver smooth models that geologists
are uncomfortable with, because they know geology is anything but smooth, well-
behaved, and continuous. The minimum-structure approach, developed in this and
in the previous chapter, delivers geologically plausible blocky earth models with
sharp boundaries that are readily interpretable by geologists.

On the other hand, from a pure statistical parameter estimation point of view,
least-squares parameter estimation with quadratic regularisation has appeal. Apart
from being the maximum a-postori estimator for Gaussian distributed parameters
that are uncorrelated, standard least-squares solutions provide the most smoothly-
varying detailed property estimates that *best-fit* the data. Non-quadratic regularised
least-squares deliver the least informative parameter estimates that fit the data
and tend to be more robust in the presence of noise. Typically, this difference in
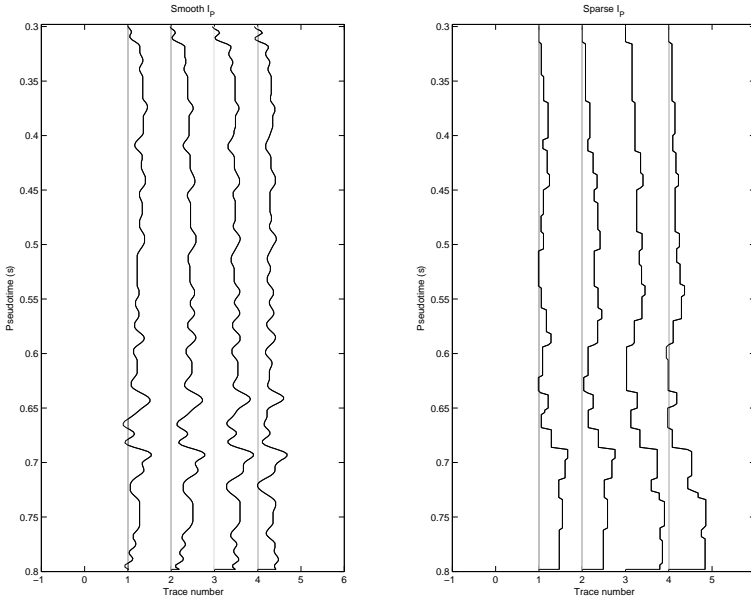
Figure 5.19: *A comparison of the smooth and sparse relative acoustic impedance (I_P).*

regularisation results in smooth objective functions having lower misfit values than sparse objective functions. Figure (5.21) illustrates this. Notice that the misfit curve for the quadratically regularised objective function tracks that of the sparse objective function but has a lower overall misfit.

A final consideration is the spectra of the smooth and sparse rock properties that have, to this point, been exclusively analysed in the spatial domain. When considered spectrally, the differences between smooth and sparse parameter estimates become even more pronounced. These estimates are presented in pseudo-time, which is defined to be the vertical two-way travel time mapping. This domain is chosen so that the spectral mapping can be represented using Hertz when, in fact, the proper spectral domain represents vertical wave-number.

The spectra shown in Figure (5.22) and Figure (5.23) are for the estimates of rock property reflectivities. On the left in both of these figures is the frequency domain response for the estimated interface rock properties based on a blocky earth assumption. Both have a fairly flat, broad-band, response. By comparison, on the right of these images, are the spectral representations of parameters estimated assuming a
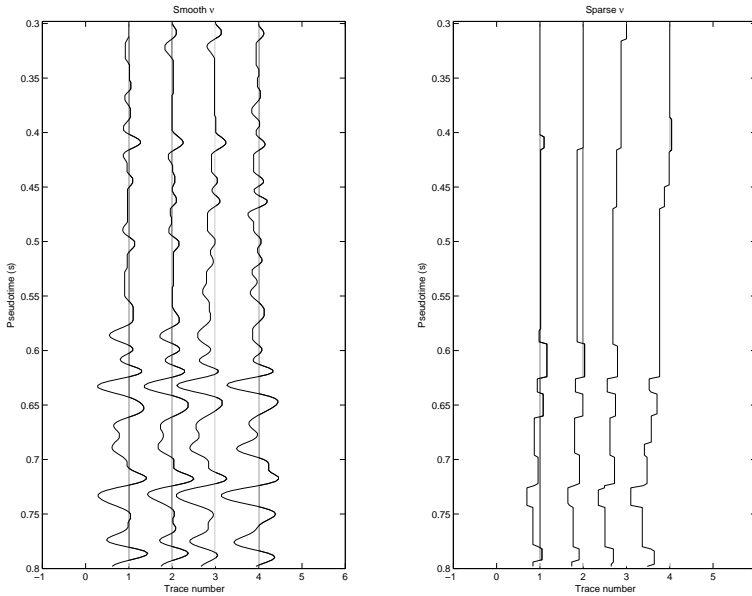
Figure 5.20: *A comparison of the smooth and sparse relative Poisson's ratio estimates.*

smoothly varying earth. This assumption of smoothness gives rise to interface properties with spectra that are partitioned. In particular, the damped least-squares estimates have a high magnitude spectral region between about 20–$80Hz$, with the remainder of the spectra being in a $30dB$-down region.

When the spectra of the relative layer properties are considered, Figure (5.24) and Figure (5.25), the geologic meaningfulness of the sparseness assumption also stands out. The spectra behave more like those for rock properties that have been measured in-situ by wire-line logs in the borehole. Compare the spectra of the sparse inversion estimates to those of the measured rock properties shown in Figure (3.5) and it is seen that both have the same decreasing manner from d.c. to greater than $30dB$-down. However, the smooth relative layer properties display spectra that deviate significantly from this. In fact, they also appear to be partitioned into a region of higher magnitude between about 20–$65Hz$ with a critical drop-off point around $70Hz$. It cannot be said that these spectral observations were wholly unexpected. As blocky layering is the macroscopic observable of the limit of $1/f$, scaling, geology, it stands to reason that estimates of geology made with such an assumption would be more realistic.
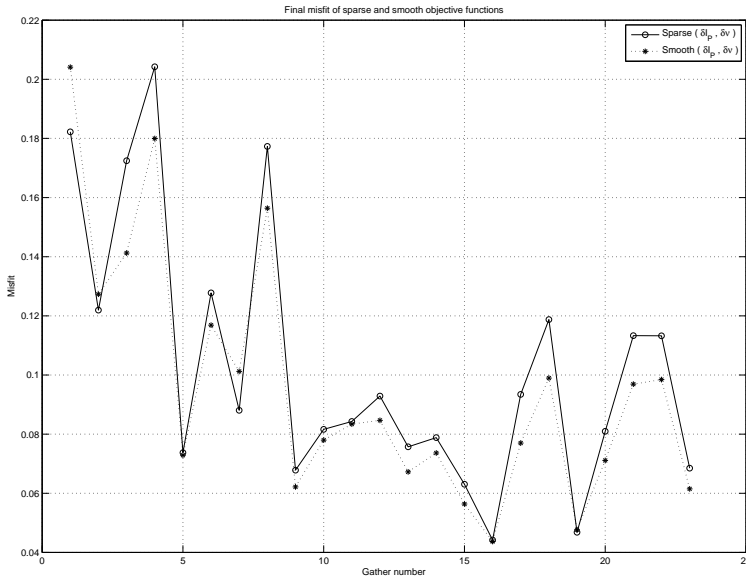
Figure 5.21: *The final objective function misfit for the smooth and sparse inversions.*

While the method put forth generates inversion results with much greater resolution, in the Berkhout [1984] sense, than the standard damped least-squares approach, some difficulties remain. The largest issue plaguing the results of minimum structure inversion is the apparent lateral discontinuity/disappearance of some reflectors. One way to address this is to impose some type of structure preservation on the inversion results. Wang et al. [2006] present a method to accomplish this by applying a frequency-space, f-x, filter to the inversion results after each iteration. This has appeal in that f-x filtering has established itself as an industry standard method for mitigating noise while preserving signal, but the drawback that it is essentially introducing a processing step into the inversion. An alternative approach is through the use of an objective function that is sparsely regularised in the time/depth/vertical direction and smoothly regularised in the offset/angle/ray-parameter/lateral direction, as outlined in Wang [2005]. This approach has the added elegance that the structure preservation is anticipated by the inversion itself and not imposed as a processing step within an inversion algorithm. Further appeal comes from the fact that geology is generally considered to be laterally locally flat, smooth, and continuous. Including a geologically explicit term into an objective function that is traditionally dominated by physics and statistics makes the inversion process more accessible to
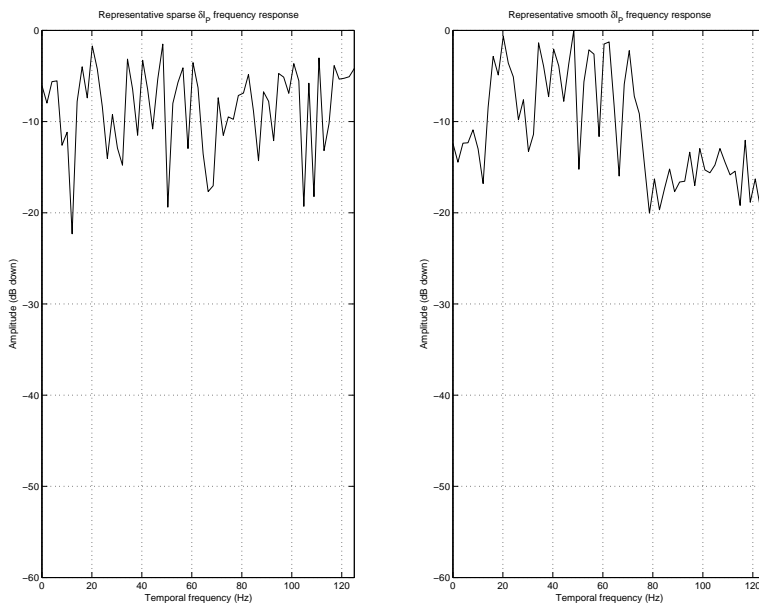
Figure 5.22: *The frequency response, after mapping vertical wave-number to pseudo-time, of a representative smooth and sparse acoustic impedance reflectivity (δI_P), estimated using the ($\delta I_P, \delta\nu$) parameterisation and the 13th CDP gather as input data.*

non-specialists. As we are concerned with an amplitude inversion problem, where locally plane reflectors are assumed, it is anticipated that including a local smoothing constraint will not adversely affect the physics which the method outlined in this work exploits. The new twice regularised objective function, for the kth iteration, has the form

$$J\left(\mathbf{z}_k\right) = \|\mathbf{d} - \mathbf{MP}\mathbf{z}_k\|_2^2 + \mu \left\| \sqrt{\mathbf{Q}_{k-1}}\mathbf{D}_{1h_x}\mathbf{z}_k \right\|_2^2,$$

where $\mathbf{D}_{1h_x}$ is a first-order derivative operator that imposes local structure preservation in the lateral direction. In other words, it laterally imposes geological reasonability.
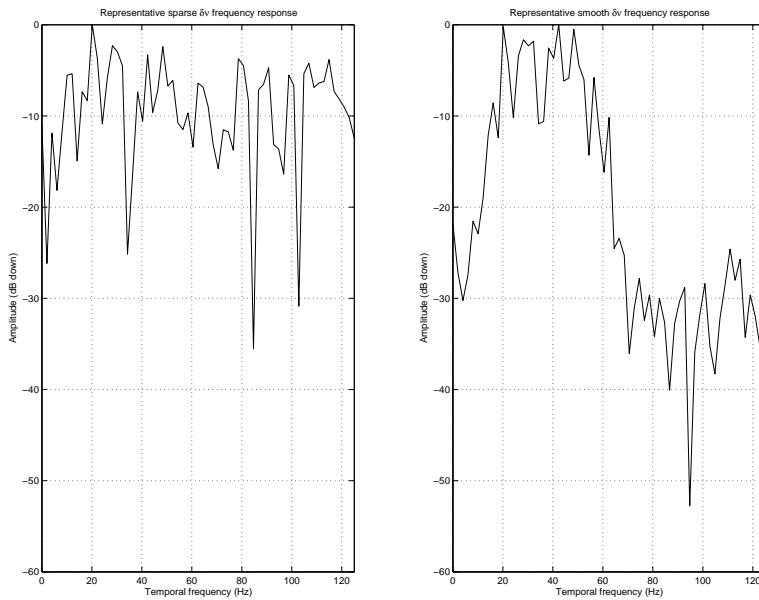
Figure 5.23: *The frequency response of a representative smooth and sparse Poisson's ra-tio reflectivity ($\delta\nu$), estimated using the ($\delta I_P, \delta\nu$) parameterisation and a gather over the reservoir (the 13$^{\text{th}}$ CDP gather).*
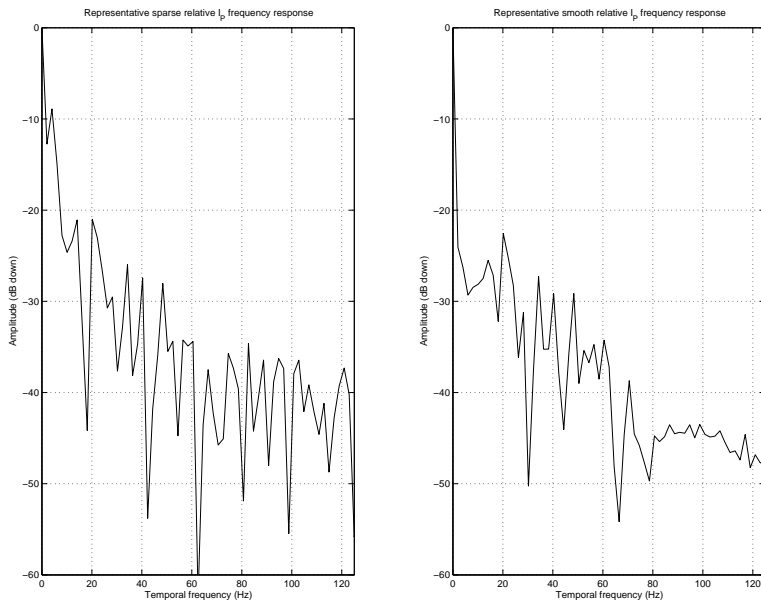
Figure 5.24: *The frequency response of a representative smooth and sparse relative acoustic impedance (I_P), estimated using the ($\delta I_P, \delta \nu$) parameterisation and a gather over the reservoir (the 13th CDP gather).*
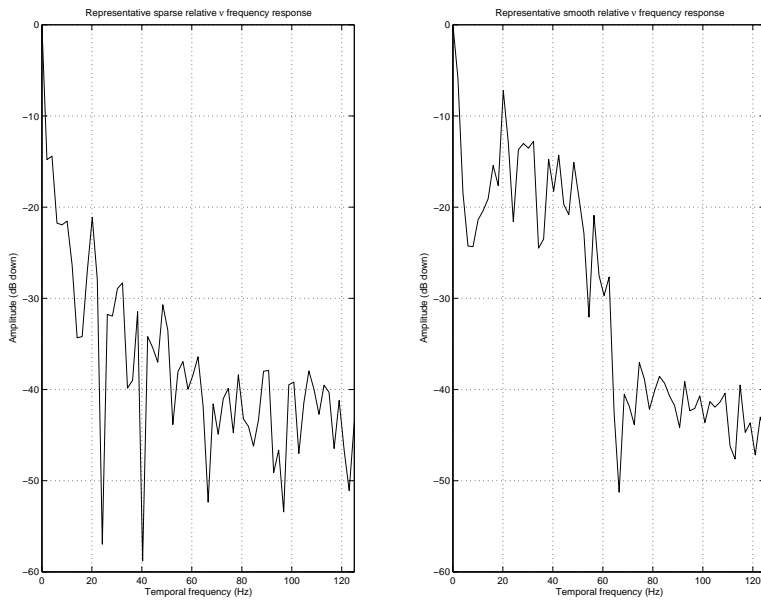
Figure 5.25: *The frequency response of a representative smooth and sparse relative Poisson's ratio ($\delta\nu$), estimated using the ($\delta I_P, \delta\nu$) parameterisation and a gather over the reservoir (the 13th CDP gather).*

5.4 Conclusions

From the outset, the goal was to develop a practical high-resolution attribute estimation method using pre-stack seismic amplitude gathers at input. This has been achieved though using insights from linear inverse theory. By casting the desired goal as the solution of a linearised inverse problem and applying the accumulated knowledge of inverse theory, a method is developed that successfully infers high-resolution rock properties. Rock property estimates beyond the seismic band-width are achieved by imposing a sparseness constraint on the inversion in the 'vertical' direction via the use of a Cauchy norm as the regularisation term in the objective function. Furthermore, the method is made efficient for real data situations by recasting the regularised inverse problem as a pre-conditioned inverse problem. Further efficiency is obtained by Tikhonov reformulation of the new problem to standard form and then using the very rapid method of conjugate gradients. The combination of all these aspects was successfully demonstrated by generating geologically meaningful, high-resolution, rock property responses for a gas bearing sandstone reservoir from band-limited pre-stack seismic amplitude gathers. Overall, it is seen that regularised linear inverse theory provides a means through which high-resolution reservoir characterization can be achieved from noise-corrupted, incomplete, and inaccurate seismic amplitude data.

6

Conclusions, recommendations, and the road ahead

6.1 Overall conclusions

Advances in seismic acquisition recreated a need for innovation in seismic imaging and characterisation. The fact that very long offset data maintains amplitude fidelity, and its acquisition has now become routine, demands new methods to analyse these long offset amplitudes. This thesis develops an accurate method to simulate long offset amplitudes that is in agreement with the assumed convolutional model of seismic data.

The philosophy behind the approach applied has been to achieve consistency between the assumptions underlying the seismic signal processing and imaging on the one hand, and the reflectivity model to be used for forward modelling and inversion, on the other. Recall that the time-invariant convolution model for seismic data demands that the forward system (survey design, acquisition itself, and some data processing) be strictly linear, but neither the P-P and P-S Zoeppritz equations, nor the Bortfeld equation, nor even Equation (3.2.2) or the P-S Aki and Richards equation meet this linearity requirement. The proposed Equations (3.2.4) or (3.2.8), and their P-S counterparts, also violate the linear data model. However, the physics of the problem defines a range of practical applicability and these proposed models serve the purpose of allowing quantitative interpretation of long offset seismic amplitudes. This is of critical importance if the seismic amplitude data is to be exploited to extract information about reservoir fluid saturation. It is in the long offset domain that the existing methods to calculate the reflectivity response violate the linear convolution data model that underlies seismic data processing. Scale dependency in

the modelling of the synthetic seismic response is introduced when applying a non-linear method to calculate reflectivities to match seismic data processed on the basis of a linear data model. The research pursued in this thesis resolves the inconsistency by introducing a forward modelling operator that is linearised in the earth input as far as physically meaningful.

Chapter 3 shows that the key to a true linearisation of forward modelling of seismic amplitude data is the realisation that the kinematics (wave-field propagation) and the dynamics (wavefield scattering) are separate phenomena at vastly different scales. Explicitly recognising this and introducing a background velocity model in which all wave propagation takes place is an elegantly simple concept that solves a host of nasty issues that have dogged quantitative seismic interpreters. Notably, these are: non-linearity in the linearised Zoeppritz equations (scale dependency), the angle-of-incidence versus ray-parameter dilemma, the forward modelling of stretch and the handling of induced anisotropy in linear forward modelling. As a result the maximum usable angle of incidence (or ray-parameter or offset) is pushed much further out than would have been possible with conventional two-term, or even three-term reflectivity approximations. Furthermore, in the proposed linearised approach it comes out naturally that wavelet stretch associated with normal move-out is described at the scale at which the wave propagation is observed (i.e. in the background medium). The reduced vertical resolution in imaging with waves with oblique angles of incidence cannot be avoided. For forward modelling and inversion of long offset seismic, stretch is an important factor that needs to be taken into account. Attempting to account for this effect at the input log scale, would introduce a strong non-linearity into the forward modelling process. Another advantage of the layered earth models developed in this thesis is that layering induced velocity anisotropy, a kinematic effect, can be handled at the scale of wave propagation (i.e. the scale at which it occurs). This is achieved by defining seismic scale ϵ_0 and δ_0 Thomsen parameters in the background medium.

Applying these stable and accurate linearised, layered-earth, long-offset models to estimating three rock properties reveals that, despite the notorious ill-conditioning and ill-posedness of AVP-waveform inversion, quantitative reservoir rock property estimates can be made. Within the framework of linear seismic inversion, this thesis goes on to show that data kernels built from the previously developed amplitude models combined with non-quadratic regularization deliver reliable broadband reservoir rock properties from long-offset pre-stack seismic amplitudes. That is to say, once more, IF the data is multi-component AND it has sufficiently long offsets AND there is an accurate background velocity field THEN linear target oriented high resolution inversion can deliver three broad-band rock properties .

This quantitative reservoir characterization is an innovation that requires modern acquisition and imaging results to be projected onto the characterisation capability axis, as illustrated in Figure (1.6). Foremost among these is long offset, wide angle, or large ray-parameter data. Increased acquisition and imaging costs are the burden

to bear should more information be wanted from linear methods. Nothing comes for free and if quantitative amplitude analysis is desired then more informative data must be acquired. But, this modern data is not enough. There must also be a conceptual paradigm shift where the input seismic amplitude data itself is no longer thought of as idealized delta functions from various layer interfaces but, instead, must be thought of as actual wave-amplitudes that have associated waveform effects which cannot be ignored at long offset. Accounting for these effects is a crucial aspect for the full exploitation of the available pre-critical information. Furthermore, it is clear that P-S converted wave amplitudes are needed as P-S inversion delivers better estimates of parameters that suffer in P-P inversion alone.

Chapters 4 and 5 show that sparse rock properties are reliably estimated by exploiting the ℓ_2-norm with non-quadratic regularization but that full-band low-frequency models still need to be constructed to map the relative inversion results to absolute layer properties. In addition, the added-value of singular value decomposition to evaluate the parameterization of the AVP-waveform inversion problem, how it can be used to assess long-offset data, and how the data and the regularization contribute to the rock property estimates is developed. Furthermore, the non-quadratically regularized least-squares pre-stack amplitude inversion problem is shown to be an idealized version of a full Bayesian solution. The implication being that if a proper probabilistic framework can be built, then high-resolution linear AVP-waveform inversion can deliver quantitative rock properties estimates with uncertainty measures. Projecting this research into an application meant building a practical high-resolution attribute estimation method using pre-stack seismic amplitude gathers as input. Delivering this algorithm required insights from casting the desired goal as the solution of a linearised inverse problem and applying the accumulated knowledge of inverse theory. As a result, rock property estimates beyond the seismic band-width are achieved by imposing a sparseness constraint on the inversion in the vertical direction via the use of a Cauchy norm in the objective function. Keep in mind, however, that the bandwidth/resolution enhancement is driven by the Cauchy statistics. Whether or not these statistics have an underlying physical interpretation is still an open problem. As research continues into aspects of the multi-scale earth, there are indications that a minimum-structure (or sparse) earth may represent the macroscopic/seismic-scale limit of the pseudofractal earth. Adapting the methodology so that it is made efficient for real data situations meant recasting the regularised inverse problem as a pre-conditioned inverse problem. The efficiency is further improved by Tikhonov reformulation into standard form and then, finally, using a modified conjugate gradient algorithm. The sum total of all these aspects are successfully demonstrated by generating geologically meaningful, high-resolution, rock property responses for a gas bearing sandstone reservoir from band-limited pre-stack seismic amplitude gathers. The overall take-away is that regularised linear inverse theory provides a means through which high-resolution reservoir characterization can be achieved from noise-corrupted, incomplete, and inaccurate seismic amplitude data.

6.2   Overall recommendations

- Introduce a background medium in which all wave propagation phenomena take place.

- Linearise long offset reflectivity operators in terms of contrasts of material properties, at any depth, to this background medium.

- Analyse long offset data for induced anisotropic effects and account for these effects in the background medium.

- Include wavelet stretch effects when simulating long offset seismic data.

- Always attempt amplitude analysis in a true time domain.

- Acquire long offset compressional-to-compressional mode and compressional-to-shear mode seismic data.

- Form data kernels that have linearised rock properties in terms of contrasts, at any depth, to a background.

- Include relevant waveform effects in the data kernel.

- Estimate the kernel in a data-driven manner.

- Regularize ℓ_2-inversion with a Cauchy norm.

- Ultimately, take an Bayesian ℓ_2-approach.

- Leverage the feed-back nature of the Seismic Value Chain and road-map seismic reservoir characterisation goals back to acquisition survey design parameters through forward modelling the desired rock properties response .

- Analyse seismic data kernels using singular value decomposition to determine sparseness promoting parameterisations.

- Estimate seismic rock properties with the strongest sparseness and transform to others of interest.

- Do not estimate wavelets on the fly, undertake a seismic-to-well matching exercise and then impose normal moveout stretch effects.

- Assume sparseness in the vertical direction and smoothness in the horizontal direction.

6.3   The road ahead

This thesis develops how existing quantitative amplitude analysis techniques need to be extended so that their full potential can be exploited. The extended methodologies, however, remain within the current seismic imaging paradigm. Daring to gaze into a crystal-ball, this thesis concludes with a few words about what lies ahead for seismic reservoir characterisation. Through an analysis of a simple synthetic example, the critical influence of *non-linearity* on the stability and quality of the inversion result is demonstrated. It highlights fundamental limits caused by assuming a linear relationship between surface recorded wave-field data and subsurface earth properties (i.e. the current imaging and analysis paradigm).

Gisolf and Verschuur [2010], Chapter 13, sketches a path for full non-linear inversion in the acoustic approximation from the inverse scattering perspective. The modelling analysis is a review of their synthetic experiment to illustrate a fundamental limitation of the linear approach. In the same manner, consider a set of well-logs (as in Figure (6.1)) where the true well-log properties have had the variability in the medium property contrasts reduced to one hundredth (0.01) of the true variability (relative to respective mean of the property being considered). This data is unrealistically linear in the contrasts but is expected to fully obey the assumptions that drive a standard linear least-squares inversion approach.

In addition to the mass density (ρ), compressional-wave velocity (α), and shear-wave velocity (β), Figure (6.1) shows very smooth overlying curves representing the background medium properties (as developed in Chapter 3). These background properties are extracted as outlined earlier and this simulates the kinematic velocity information that can be extracted directly from the seismic data by the Common Focal Point technique described in Chapter 4. In terms of practical applications, the mass density background that can only be inferred from the velocity background properties through a locally calibrated rock physics transform (i.e. via the use of a local, macro-scale, velocity-density relationship).

These log properties are used to simulate the exact plane wave full-waveform response (Figure (6.2)), as a function of the horizontal slowness (ray-parameter). The maximum ray-parameter corresponds to a maximum angle-of-incidence, (θ_{max}), of $50°$. This is where the background medium has maximum compressional-wave velocity . The seismic source is simulated using a $6 - 12 - 50 - 75 Hz$ zero-phase wavelet. Finally, 5% random white noise is added to the synthetic data. Notice that, due to the artificially imposed very low contrasts, a coda of internal reverberations is absent.

Figure (6.3) compares the damped linear least-squares estimates to the actual medium properties. This is the same approach from Chapter 5 that yields the standard, smooth/damped, relative rock properties estimates. The estimated relative rock properties are integrated and transformed to absolute property values. Note that
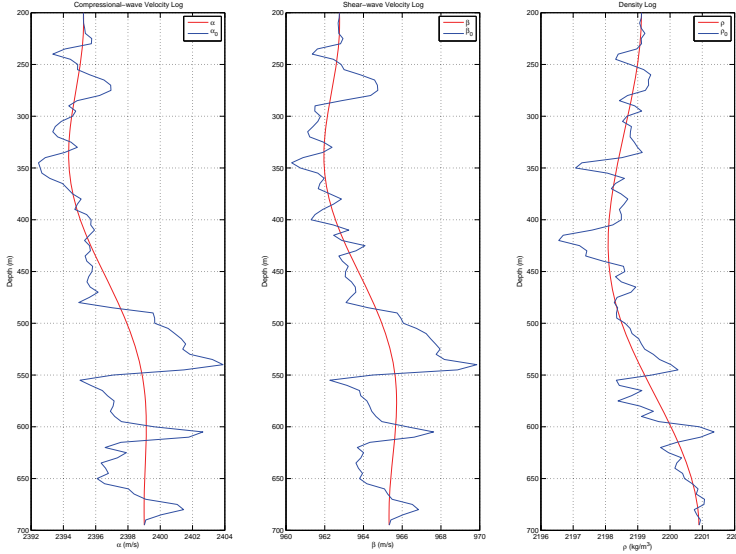
Figure 6.1: *The input α, β, and ρ well logs that have had their contrasts artificially reduced by 0.01, relative to their mean values. Overlying these logs are the kinematic/macro scale α_0 , β_0, and ρ_0 background properties.*

these estimates are an accurate realisation of the actual earth model in the sense that the input data is faithfully reproduced. All that remains in the data residual is the 5% additive noise. However, several things need to be considered. As the logs have very low property contrasts and there is relatively low noise corruption, one expects that an almost perfect estimate would result since this experiment uses as linear as possible synthetic data without actually committing an inversion crime. In addition, the diagonal damping (i.e. the velocities and density have different damping factors) had to be tuned before this result was obtained and, in fact, the damping relating to the mass density had to be 25 times stronger than the damping for the compressional and shear velocities. In spite of all the idealised conditioning, linear inversion is not able to produce ideal predictions of the absolute property values. This is because a spectral gap remains in the linear inversion estimates. Partitioning of the wavefield velocities enables accurate layered earth forward modelling but there is a gap between the top-end of the kinematic bandwidth and low-end of the dynamic bandwidth (i.e. the wavelet band). This spectral gap will remain in the medium property estimates from true one-step damped linear least-squares inversion. That being said, it appears as if the mass density predictions suffer less from the spectral
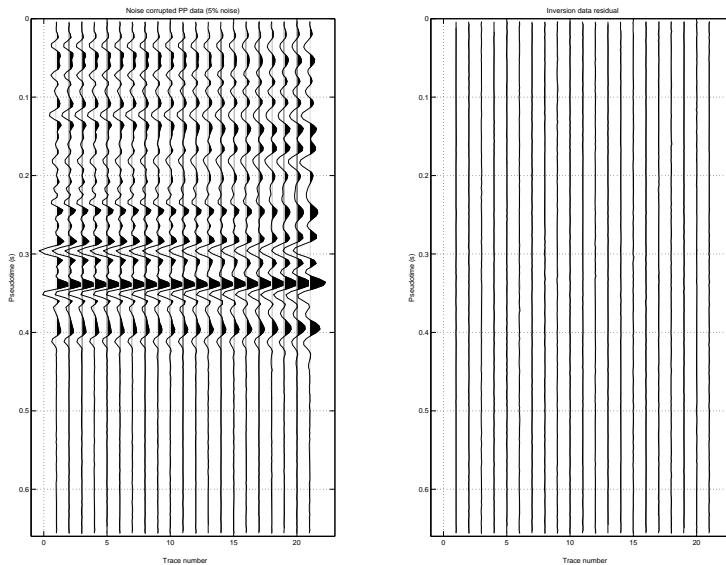
Figure 6.2: *The total elastic P-P reflectivity response imaged to $t = 0s$, from the logs shown in Figure (6.1), with 5% noise corruption and the data residual after standard damped linear least-squares inversion. Note that the background properties are not used to generate this response, except for establishing $\theta_{\max} = 50°$.*

gap than the velocity predictions do.

Now consider a more realistic synthetic experiment using the true logged properties in Figure (6.4) to generate full-waveform synthetic data (Figure (6.5)), under exactly the same conditions as for the low contrast experiment. An immediate difference is the coda of internal multiple scattering trailing the primary reflections, particularly on the traces with the larger horizontal slownesses. The multiple contamination exists above the noise corruption level and indicates that the wavefield is significantly non-linear in the property contrasts across the interfaces. This synthetic represents the ideal data that could be expected from standard production processing in that all free surface effects have been perfectly handled, in addition to random noise being reduced to 5%. What remains unaccounted for are the transmission losses, losses due to mode conversions, and internal reverberations. These effects are left in the data as it is standard processing practices to turn a blind-eye to these realities.

Figure (6.6) shows an inversion result that is extremely sensitive to the damping applied and even these less-than-optimal results could not have been achieved without
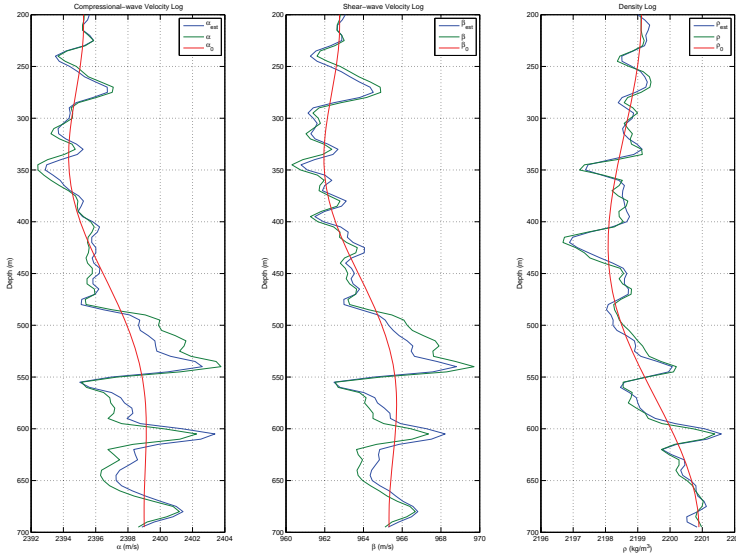
Figure 6.3: *Actual medium properties* (α, β, ρ), *shown in Figure (6.1), and estimates of those properties* $(\alpha_{\mathrm{est}}, \beta_{\mathrm{est}}, \rho_{\mathrm{est}})$ *from the damped linear least-squares inversion of the data shown in Figure (6.2).*

knowing what the target result is. Furthermore, the estimates worsen with depth, indicating that the non-linearity is a depth dependant phenomenon. Further observational evidence of this is seen by considering the inversion data residual. Over the time window of the primary reflections, as shown in Figure (6.2), the residual is mainly noise. However, rigorously linear inversion can never match the coda below the primary reflections and it is in this depth region where the residual amplitudes are the highest. The existence of a significant coda confirms that there is non-negligible multiple internal scattering, yet all the primary data is explained by the linear inversion. Damped linear least-squares inversion misinterprets the internal multiples deeper in the time window, as primaries, leading to incorrect property predictions deeper in the depth domain.

All seismic data suffers from the fundamental issues illustrated through the two simple toy examples above. Furthermore, there can never be any resolution of these problems with a pure linear approach. Presently, two basic ways to address filling the spectral gap and handling the higher order data effects that exist. One is by exploiting the true, intrinsic, non-linearity within the system. The other is by maintaining a linearity assumption about the data and imposing an iterative non-linear
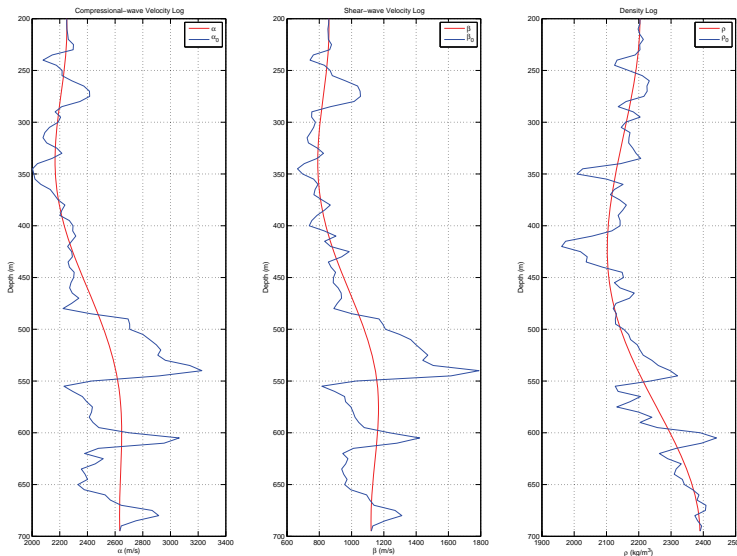
Figure 6.4: *The original, unaltered, input α, β, and ρ well logs. Note the overlying (i.e. kinematic/macro scale) α_0 , β_0, and ρ_0 backgrounds.*

constraint on the medium properties estimates. Ideally, this constraint is based on some *a priori* knowledge of the geology. The latter can be considered a weakly non-linear approach while the former is a full non-linear approach. A significant portion of this thesis, Chapter 4 and Chapter 5, concerns itself with the latter approach. This was a pragmatic choice as almost all seismic imaging workflows try to identify the part of the wave-field that is non-linear in the earth property contrasts and re-move it to yield a seismic data-set that better fits the linearity assumption (as in the first example, above).

The road ahead, both immediately and longer-term, lies in the strong non-linear approach. It is reasonable to expect target oriented non-linear inversion to mature in the near future, while general full-waveform inversion – where all the raw seismic is directly inverted for detailed subsurface properties – will be further down the road. In either case, the critical point involves building a forward model that honours, to some extent, the intrinsic data non-linearity and use this in an iterative non-linear inversion scheme. It represents the only direct data-driven way to fill the spectral gap that will always remain in the medium properties estimated using a linear data relationship and, also, ensures that real earth effects (like internal scattering) are properly accounted for.
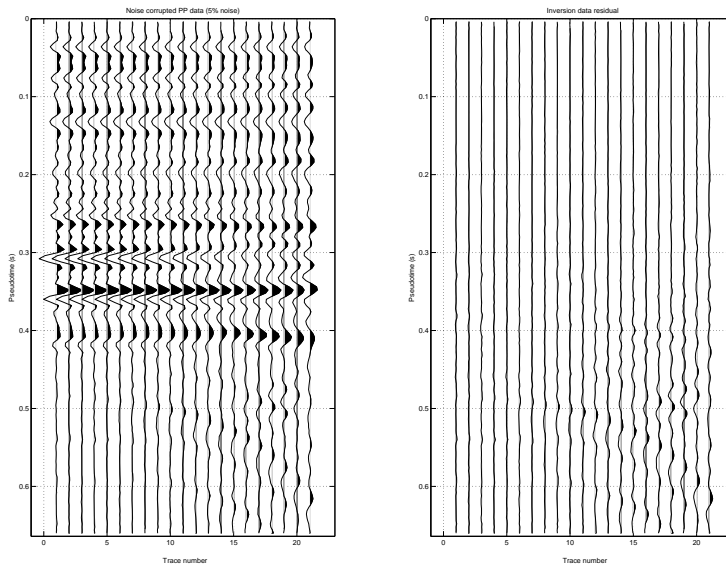
Figure 6.5: *The full-waveform P-P synthetic seismogram, as calculated by the reflectivity method, of the well logs shown in Figure (6.4) with 5% noise corruption and the data residual remaining after standard damped linear least-squares inversion. Again, the background properties are not used to generate this response, except for establishing $\theta_{\max} = 50°$.*

The above experiments, and these few brief paragraphs, are meant to illustrate and introduce the concept that a non-linear data-model is the ultimate solution to the seismic rock properties estimation problem. There is no doubt that the future of quantitative amplitude analysis belongs to the non-linear data model and Gisolf and Verschuur [2010], Chapter 13, provides a doorway to this journey. To those who travel down this path, I wish you faith and Godspeed.
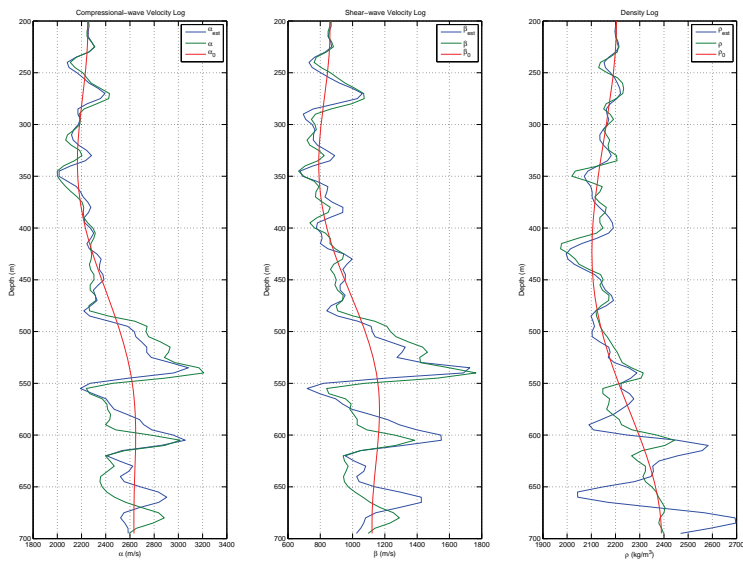
Figure 6.6: *A comparison of the actual medium properties* (α, β, ρ), *shown in Figure (6.4), and the estimates of those properties* $(\alpha_{\mathrm{est}}, \beta_{\mathrm{est}}, \rho_{\mathrm{est}})$, *from the damped linear least-squares inversion of the data shown in Figure (6.5).*

Bibliography

Aki, K., and Richards, P. G., 2002, Quantitative Seismology, Second Edition: University Science Books.

Alkhalifah, T., Tsvankin, I., Larner, K., and Toldi, J., 1996, Velocity analysis and imaging in transversely isotropic media: Methodology and a case study: The Leading Edge, **15**, no. 05, 371–378.

Asveth, P., Mukerji, T., and Mavko, G., 2005, Quantitative Seismic Interprettion: applying rock physics tools to reduce interpretation risk: Cambridge University Press.

Backus, G. E., 1962, Long-wave elastic anisotropy produced by horizontal layering: J. Geophys. Res., **67**, 4427–4440.

Bayes, T., 1763, Essay towards solving a problem in the doctrine of chances: republished in Biometrika (1958), , no. 45, 293–315.

Berkhout, A. J., 1980, Seismic migration, imaging of acoustic energy by wave field extrapolation: Elsevier.

Berkhout, A. J., 1984, Seismic resolution, a quantitative analysis of resolving power of acoustical echo techniques: Geophysical Press.

Berkhout, A. J., 1997a, Pushing the limits of seismic imaging, Part I: Prestack migration in terms of double dynamic focusing: Geophysics, **62**, no. 3, 937–953.

—— 1997b, Pushing the limits of seismic imaging, Part II: Integration of prestack migration, velocity estimation, and avo analysis: Geophysics, **62**, no. 3, 954–969.

Berkhout, A. J., 2005, The Seismic Value Chain - providing a new business concept for the seismic industry: The Leading Edge, **24**, no. 02, 146–149.

Berkhout, A. J., 2007, The DELPHI Consortium, creating value with science: DELPHI Reservoir Characterization and Management Volume V, Chapter 1, pages 1 – 8.

Berryman, J. G., Grechka, V. Y., and Berge, P. A., 1999, Analysis of Thomsen parameters for finely layered VTI media: Analysis of Thomsen parameters for finely layered VTI media:, Eur. Assn. Geosci. Eng., Geophys. Prosp., 959–978.

Bjørke, J. T., and Nilsen, S., 2005, Trend extraction using average interpolating subdivision: Trend extraction using average interpolating subdivision:, Springer, Mathematical Geology, 615–634.

Bortfeld, R., 1961, Approximations to the reflection and transmission coefficients of plane longitudinal and transverse waves: Geophys. Prosp., **09**, no. 04, 485–502.

Chapman, C. H., 2004, Fundamentals of Seismic Wave Propagation: Cambridge University Press.

Cox, B. E., 2004, Tomographic Inversion of Focusing Operators: Ph.D. thesis, Delft University of Technology.

Dariu, H., Garotta, R., and Granger, P. Y., 2003, Simultaneous inversion of PP and PS wave AVO/AVA data using simulated annealing: SEG Technical Program Expanded Abstracts, **22**, no. 1, 120–123.

de Nicolao, A., Drufuca, G., and Rocca, F., 1993, Eigenvalues and eigenvectors of linearized elastic inversion: Geophysics, **58**, no. 5, 670–679.

Debski, W., and Tarantola, A., 1995, Information on elastic parameters obtained from the amplitudes of reflected waves: Geophysics, **60**, no. 5, 1954–1966.

Dey, A. K., and Gisolf, A., 2005, Forward modelling seismic amplitudes with multi-scale velocity functions: DELPHI, Reservoir Characterization and Flow Simulation Project, Volume III, Chapter 6, pages 51 – 70.

Dey, A., and Gisolf, A., 2007, Wide-angle linear foward modelling of synthetic seismograms: Wide-angle linear foward modelling of synthetic seismograms:, EAGE, Geophysical Prospecting, 707–718.

Dey, A. K., Sacchi, M. D., and Gisolf, A., 2006, High-resolution reservoir rock properties via joint pre-stack seismic amplitude inversion: DELPHI, Reservoir Characterization and Flow Simulation Project, Volume IV, Chapter 4, pages 43 – 60.

Downton, J., and Lines, L., 2003, High-resolution AVO analysis before NMO:, *in* 73rd Ann. Internat. Mtg. Soc. of Expl. Geophys., 219–222.

Downton, J. E., 2004, AVO inversion: Ph.D. thesis, University of Calgary.

Farquharson, C. G., and Oldenburg, D. W., 2004, A comparison of automatic techniques for estimating the regularization parameter in non-linear inverse problems: Geophys. J. Int., , no. 156, 411–425.

Gassman, F., 1951, Uber die elastizitat poroser medien: Uber die elastizitat poroser medien:, Vierteljahrsschr. Der Naturforsch. Gesellschaft Zurich, 1–21.

Gidlow, P. M., Smith, G. C., and Vail, P. J., 1992, Hyderocarbon detection using fluid factor traces, a case study: How useful is AVO analysis?: Technical Program and Abstracts, Joint SEG/EAGE Summer Research Workshop, pages 78–89.

Gill, P. E., Murray, W., and Wright, M. H., 1991, Numerical Linear Algebra and Optimization, Volume 1: Addison-Wesley, *The Advanced Book Program.*

Gisolf, D., and Verschuur, E., 2010, The Principles of Quantitative Acoustical Imaging: EAGE Publications BV.

Gisolf, A., 2005, Time-Lapse Seismic Inversion: DELPHI Reservoir Characterization and Management Volume III, Chapter 3, pages 15 – 28.

Hadamard, J., 1902, Sur les problmes aux drives partielles et leur signification physique: Princeton University Bulletin, **13**, 49–52.

Hampson, D. P., Russell, B. H., and Bankhead, B., 2005, Simultaneous inversion of pre-stack seismic data: SEG Technical Program Expanded Abstracts, **24**, no. 1, 1633–1637.

Hansen, P. C., 1998, Rank-Deficient and Discrete Ill-Posed Problems: Numerical Aspects of Linear Inversion (SIAM Monographs on Mathematical Modeling and Computation 4): SIAM.

Hilterman, F. J., 2001, Seismic amplitude interpretation:, *in* Distinguished Instructor Series Soc. of Expl. Geophys.

Hubbert, M. K., 1950, A discussion on the United Nations Scientific Conference: Geophysics, **15**, no. 10, 110–111.

Jack, I. G., 1997, Time-lapse seismic in reservoir management:, *in* Time-lapse seismic in reservoir management Soc. of Expl. Geophys., 282.

Jackson, D. D., 1972, Interpretation of inaccurate, insufficient and inconsistent data: Geophysical Journal of the Royal Astronomical Society, **28**, 97–109.

Knott, C., 1899, Reflection and refraction of elastic waves with seismological applications: Phil. Mag., **48**, 64–97.

Koefoed, O., 1955, On the effect of Poisson's ratios of rock strata on the, reflection coefficients of plane waves: On the effect of Poisson's ratios of rock strata on the, reflection coefficients of plane waves:.

Levenberg, K., 1944, A method for the solution of certain nonlinear problems in least squares: Quarterly of Applied Mathematics, , no. 2, 164–168.

Lines, L. R., and Treitel, S., 1984, A review of least-squares inversion and its application to geophysical problems: A review of least-squares inversion and its application to geophysical problems:, EAGE, Geophysical Prospecting, 159–186.

Mahmoudian, F., and Margrave, G. F., 2004, Three parameter AVO inversion with PP and PS data using offset binning: SEG Technical Program Expanded Abstracts, **23**, no. 1, 240–243.

Marquardt, D. W., 1963, An algorithm for the least squares estimation of non-linear paramters: Journal of the Society of Industrial and Applied Mathematics, , no. 11, 431–441.

Mavko, M., Mukerji, T., and Dvorkin, J., 1998, The Rock Physics Handbook: Tools for Seismic Analysis in Porous Media: Cambridge University Press.

Menke, W., 1989, Geophysical Data Analysis: Discrete Inverse Theory, Revised Edition: Academic Press.

Neumaier, A., 1998, Solving Ill-Conditioned and Singular Linear Systems: A Tutorial on Regularization: SIAM Review, **40**, no. 3, 636–666.

O'Doherty, R. F., and Anstey, N. A., 1971, Reflections on amplitudes: Geophys. Prosp., **19**, no. 03, 430–458.

Oldenburg, D. W., Scheuer, T., and Levy, S., 1983, Recovery of the acoustic impedance from reflection seismograms: Geophysics, **48**, no. 10, 1318–1337.

Ostrander, W. J., 1982, Plane wave reflection coefficients for gas sands at non-normal angles of incidence: SEG Technical Program Expanded Abstracts, pages 216–218.

Ostrander, W. J., 1984, Plane wave reflection coefficients for gas sands at non-normal angles of incidence: Geophysics, **49**, 1637–1648.

Paige, D. S., 1973, The dark side of the bright spot: GSH Lithology and direct detection of hydrocarbons using geophysical methods symposium.

Pilkington, M., and Todoeschuck, J. P., 1990, Stochastic inversion for scaling geology: Geophys. J. Int., **102**, 205–217.

Putnam, P. E., and Oliver, T. A., 1980, Stratigraphic traps in channel sandstones in the Upper Mannville (Albian) and east-central Alberta: Bulletin of Canadian Petroleum Geology, Volume 28, pages 489–508.

Royle, A. J., 2002, Exploitation of an oil field using AVO and post-stack rock prop-
   erty analysis methods:, *in* 72nd Ann. Internat. Mtg. Soc. of Expl. Geophys., 289–
   292.

Rüger, A., 1996, Reflection coefficients and azimuthal AVO analysis in anisotropic
   media: Ph.D. thesis, Colorado School of Mines.

Rutherford, S. R., and Williams, R. H., 1989, Amplitude-versus-offset variations in
   gas sands: Geophysics, Soc. of Expl. Geophys., Volume 54, pages 680–688.

Saad, Y., 2004, Iterative methods for sparse linear systems (2nd ed.): SIAM.

Sacchi, M. D., and Liu, B., 2005, Minimum weighted norm wavefield reconstruction
   for AVA imaging: Geophysical Prospecting, EAGE, Volume 53, pages 787–801.

Sacchi, M. D., and Ulrych, T. J., 1995, High-resolution velocity gathers and offset
   space reconstruction: High-resolution velocity gathers and offset space reconstruc-
   tion:, Soc. of Expl. Geophys., Geophysics, 1169–1177.

Sacchi, M. D., 1999, Statistical and Transform Methods for Seismic Signal Process-
   ing: Department of Physics, University of Alberta.

Saunders, M. A., 1996, Cholesky-based Methods for Sparse Least Squares: The
   Benefits of Regularization, *in* Adams, L., and Nazareth, J. L., Eds., Linear and
   Nonlinear Conjugate Gradient-Related Methods: SIAM.

Shapiro, S., and Hubral, P., 1995, Frequency-dependent shear-wave splitting and
   velocity anisotropy due to elastic multilayering: J. Seismic Explor., **04**, 151–168.

Shapiro, S., Hubral, P., and Zien, H., 1994, Frequency-dependent anisotropy of scalar
   waves in a multilayered medium: J. Seismic Explor., **03**, 37–52.

Shtatland, E. S., 1991, Fractal stochastic models for acoustic impedance: An ex-
   planation of scaling or $1/f$ geology and stochastic inversion: SEG, Expanded
   Abstracts, **10**, no. 1, 1598–1601.

Shuey, R. T., 1985, A simplification of the Zoeppritz-equations: Geophysics, **50**, no.
   04, 609–614.

Tarantola, A., 2005, Inverse Problem Theory and Methods for Model Parameter
   Estimation: SIAM.

Thomsen, L., 1986, Weak elastic anisotropy: Geophysics, **51**, no. 10, 1954–1966.

Thomsen, L., 1993, Weak anisotropic reflections, *in* Backus, M. M., Ed., Offset-
   dependent reflectivity - theory and practice of AVO analysis: Soc. of Expl. Geo-
   phys., 103–111.

Thorbecke, J. W., 1997, Common Focus Point Technology: Ph.D. thesis, Delft University of Technology.

Tikhonov, A. N., 1963, Solution of incorrectly formulated problems and the regularization method: Soviet Math Dokl, , no. 4, 1035–1038.

Trad, D., Ulrych, T., and Sacchi, M. D., 2003, Latest views of the sparse radon transform: Latest views of the sparse radon transform:, Soc. of Expl. Geophys., Geophysics, 386–399.

Tsvankin, I., 2001, Seismic signatures and analysis of reflection data in anisotropic media, *in* Helbig, K., and Treitel, S., Eds., Handbook of geophysical exploration, seismic exploration: Pergamon.

van de Rijzen, M. J., 2007, One-step Estimation of Focusing Operators for 3D Seismic Data: Ph.D. thesis, Delft University of Technology.

van Dedem, E. J., and Verschuur, D. J., 2005, 3D surface-related multiple prediction: A sparse inversion approach: 3D surface-related multiple prediction: A sparse inversion approach:, Soc. of Expl. Geophys., Geophysics, V31–V43.

Veire, H. H., and Landro, M., 2001, Joint inversion of PP- and PS-seismic data: SEG Technical Program Expanded Abstracts, **20**, no. 1, 861–864.

Verm, R., and Hilterman, F., 1995, Lithology color-coded seismic sections, the calibration of AVO crossplotting to rock properties: The Leading Edge, **14**, 847–853.

Walden, A. T., and Hosken, J. W. J., 1985, An investigation of the spectral properties of primary reflection coefficients: Geophys. Prosp., **33**, 400–435.

Wang, J., Wang, X., and Perz, M., 2006, Structure preserving regularization for sparse deconvolution:, *in* 76nd Ann. Internat. Mtg. Soc. of Expl. Geophys., 2072–2076.

Wang, J., 2005, 3-D least-squares Wave-Equation AVP/AVA Migration of Common-Azimuth Data: Ph.D. thesis, University of Alberta.

Wrightman, D. M., Tilley, B. J., and Last, W. M., 1981, Stratigraphic traps in channel sandstones in the Upper Mannville (Albian) and east-central Alberta: Discussion: Bulletin of Canadian Petroleum Geology, Volume 29, pages 622–629.

Zoeppritz, K., 1919, Erdbebenwellen VIIIB, On the reflection and propagation of seismic waves: Göttinger Nachrichten, **I**, 66–84.

Zwartjes, P. M., 2005, Fouier reconstruction with sparse inversion: Ph.D. thesis, Delft University of Technology.

Summary

Quantitative Seismic Amplitude Analysis

The Seismic Value Chain quantifies the cyclic interaction between seismic acquisition, imaging and reservoir characterization. Modern seismic innovation to address the global imbalance in hydrocarbon supply and demand requires such cyclic interaction of both feed-forward and feed-back processes. Currently, the seismic value chain paradigm is in a feed-forward mode. Modern seismic data now have the potential to yield the best images in terms of spatial resolution, amplitude accuracy, and increased illumination in terms of offset and azimuth. Today's challenge lies with reservoir characterisation. An immediate requirement is extracting quantitative rock properties information from these improved data-sets and images, to move from a, geophysically based, smooth elastic characterisation of reservoirs towards a, geologically accessible, blocky layer-based rock properties parameterisation. Currently reservoir characterization does not fully exploit the wide-angle information present in seismic data. This is primarily due to the fact that the current paradigm for analyzing reflectivities is at odds with the assumptions made for standard seismic data processing. The current practice of using single interface models to calculate reflectivities in a long-offset layered earth is inconsistent with the assumed time-invariant convolution data model for seismic. The interplay of the modelling and inversion enables a better seismic characterisation of the reservoir by moving away from traditional band-limited, smooth, elastic attributes and towards obtaining high-resolution, blocky, rock properties that correlate better to well measurements.

A new layered earth forward model is developed that preserves linearity at large ray-parameter and handles kinematic wave-field effects at their proper scale. This full linearization of the elastic property contrasts for successive layers means partitioning

the compressional wave and shear wave velocity fields into two fundamental scales: a kinematic scale that governs wave-field propagation effects and a dynamic scale that governs wave-field scattering effects. Introducing a background/kinematic velocity model in which all wave propagation phenomena takes place is a simple and elegant concept solves the problems of non-linearity in the linearised Zoeppritz equations (scale dependency), the angle-of-incidence versus ray-parameter dilemma, and the forward modelling of stretch and the handling of induced anisotropy. As a result, the maximum angle of incidence (or ray-parameter or offset) allowable in linear forward modelling is pushed much further out than is possible with conventional two-term, or even three- term single-interface reflectivity approximations. An explicit medium at the kinematic scale handles the inescapable fact of reduced vertical resolution when imaging waves with oblique angles of incidence. For exploiting the long offset seismic amplitude information, stretch is an important factor that needs to be taken into account. Attempting to describe stretch at the dynamic scale governing wave-field scattering would introduce a strongly non-linear component into the forward modelling process. In the linearised approach presented, it comes out naturally that stretch is described at the kinematic scale where the propagation of waves is observed (i.e. in the background medium). Another wave-field propagation phenomenon to be accounted for at the kinematic scale is layering induced velocity anisotropy. This is achieved by defining seismic scale Thomsen parameters, ϵ_0 and δ_0, in the background medium. The proposed layered-earth forward model recognizes the physics of seismic wave propagation, in addition to wave-field scattering, and allows for a more complete exploitation of the information available in the pre-critical seismic amplitudes.

Following the extension of linear amplitude analysis to the layered earth, in so far as to be physically meaningful, a second step in quantitative seismic amplitude analysis is taken. Leveraging the knowledge gained from the forward analysis, a methodology to extract quantitative layer properties from the acquired seismic data is developed. Particularly, there is a need for quantitative maps of reservoir (not elastic) properties. Seismically estimating the interval rock properties is the most direct way to deliver a detailed areal understanding of the reservoir. Quite often, seismic rock properties (especially density estimates) are considered inaccurate and unreliable due to various shortcomings in acquisition, processing, and interpretation. Recent advances in acquisition and imaging, however, have created a technology push in characterization to explore 3-term, high-resolution, reservoir properties estimation by exploiting both the compressional-to-compressional mode and the compressional-to-shear mode amplitudes. The current work extends previous efforts and creates a framework which furthers the use of seismic data in quantitative hydrocarbon reservoir characterization and management. Within the paradigm of linear inverse theory, the estimation of high- resolution reservoir rock properties from compressional wave and converted wave data is cast as a linear-in-the-parameters optimization problem. Through the previously developed linear layered earth forward models, all the first order information carried in the pre-critical compressional and converted-wave seis-

mic amplitudes can be exploited, despite the notorious ill-conditioning of Amplitude-Versus-ray-Parameter waveform- inversion, and quantitative reservoir rock property estimates can be made. Data kernels built with these new forward models combines with the imposition of non-quadratic regularisation (in the vertical direction) on the least-squares solution to deliver reliable broadband reservoir rock properties estimates from pre-stack seismic amplitudes. This quantitative characterization results from several factors working together. Foremost of which is long offset, wide angle, or large ray-parameter data. This is the cost of enhanced reservoir knowledge. Should more information be wanted from linear methods then more informative data must be acquired. It is not enough to have this data. There must also be a shift in how modern seismic data is viewed. No longer can the amplitudes be regarded as idealised delta functions from independent layer interfaces in the sub-surface. These data are actually wave-amplitudes with associated waveform effects that cannot be ignored at long offset. Accounting for these effects is crucial for the full exploitation of the available pre-critical information. Another requirement is that the compressional-to-shear converted wave amplitudes are needed. The analysis shows that this converted wave inversion delivers better estimates of parameters that suffer in the compressional wave inversion alone. Furthermore, considering both wave-modes simultaneously improves both the problem conditioning and the parameter estimates.

The final thrust of the inversion analysis takes the theoretical inversion development and applies it to create a novel and practical method to infer sparse, high-resolution/well- resolved, rock properties from pre-stack compressional wave seismic amplitude data. Evolving from current industry standard techniques for linear inversion, the method is an extension of the solution to the classical damped least-squares problem. The final deliverable is a pre-conditioned conjugate gradient algorithm that performs broad-band, minimum structure, least-squares inversion of pre-stack seismic field data. After mapping to a form that is computationally efficient, an algorithm is constructed and applied to seismic data acquired over a glauconitic sandstone reservoir. Though suffering from some lateral coherency and wavelet problems, the inversion confirms three direct hydrocarbon indicators and identifies an additional one. The outcome of the inversion demonstrates that the proposed method successfully identifies the reservoir and its properties at a significantly higher resolution than is currently available with most standard, commercial, techniques and that the results are more geologically plausible. The overall message from this case study is that sparse, well-resolved, seismic reservoir characterization is possible from field acquired pre-stack seismic amplitude data.

The essence of the approach taken in this thesis is to achieve consistency between the assumptions underlying the seismic signal processing and imaging on the one hand, and the reflectivity model to be used for forward modelling and inversion, on the other. This is particularly important if long offset seismic is to be exploited to extract reservoir information about saturation and stress. Because it is in the long offset domain that the customary ways to calculate reflectivity violate the lin-

ear convolution data model that underlies the methods of seismic data processing. From the outset, the goal was to develop a practical high-resolution attribute estimation method using long-offset pre- stack seismic amplitude gathers at input. This is achieved though using insights from forward modelling and linear inverse theory. By casting the desired goal as the solution of a linearised inverse problem and applying the accumulated knowledge of inverse theory, a method is developed that successfully infers high-resolution rock properties. Rock property estimates beyond the seismic band-width are achieved by imposing a sparseness constraint on the inversion in the 'vertical' direction via the use of a non- quadratic regularisation term in the objective function. Furthermore, the method is made efficient for real data situations by recasting the regularised inverse problem as a pre- conditioned inverse problem and then applying Tikhonov reformulation of the new problem to standard form. This makes the problem suitable for solution using the very rapid method of conjugate gradients. The combination of all these aspects is successfully demonstrated by generating geologically meaningful, high-resolution, rock property responses for a gas bearing sandstone reservoir from band-limited pre-stack seismic amplitude gathers. Overall, it is seen that regularised linear inverse theory provides a means through which high-resolution reservoir characterization can be achieved from noise-corrupted, incomplete, and inaccurate seismic amplitude data.

Unfortunately, all seismic data suffers from fundamental issues that can never be resolved with a pure linear approach. Presently, two basic ways to address handling the higher order physical effects that exist. One is by exploiting the true, intrinsic, non- linearity within the system. The other is by maintaining a linearity assumption about the data and imposing an iterative non-linear constraint on the properties estimates. Ideally, this constraint is based on some a priori knowledge of the geology. The latter can be considered a weakly non-linear approach while the former is a full non-linear approach. A significant portion of this thesis concerns itself with the latter approach. This is a pragmatic choice as almost all seismic imaging workflows try to identify the part of the wave-field that is non-linear in the earth property contrasts and remove it to yield a seismic data-set that better fits the linearity assumption. The road ahead, both immediately and in the longer-term, lies in the strong non-linear approach. It is reasonable to expect target oriented non-linear inversion to mature in the near future, while general full-waveform inversion – where all the raw seismic is directly inverted for detailed subsurface properties – is further down the road. In either case, the critical point involves honouring the intrinsic data non-linearity and uses this in a non-linear inversion scheme. It represents the only direct data-driven way to fully explain all the physics within the data and, also, ensures that all real earth effects are properly accounted for. There is no doubt that the future of quantitative amplitude analysis belongs to the non-linear data model and, to those who travel down this path, I wish you faith and Godspeed.

Ayon Kumar Dey

Samenvatting

Kwantitatieve Seismische Amplitude Analyse

De Seismische Waardeketen beschrijft de wederzijdse interactie tussen seismische acquisitie, afbeelding en reservoir karakterisering. Moderne seismische innovaties vereisen, om de wereldwijde onbalans tussen vraag naar en aanbod van olie en gas te bestrijden, dat deze drie processen zowel voorwaarts als terugwaarts wisselwerken. Echter, het huidige paradigma is dat van een voorwaartse seismische waardeketen. Modernde seismische data hebben de capaciteit om de best mogelijke afbeeldingen te verkrijgen in termen van spatile resolutie, amplitude nauwkeurigheid en bestralingsapertuur. De uitdaging ligt hedendaags in de reservoir karakterisering. Een sterke vereiste daartoe is het extraheren van kwantitatieve eigenschappen van de gesteentes uit deze superieure datasets en afbeeldingen. Er moet van een, op geofysica gebaseerde, langzaam varirende, elastische reservoir karakterisering richting de geologisch correctere blokkerige, gelaagde gesteente beschrijving gewerkt worden. Hedendaagse reservoir karakterisering benut de aanwezige informatie in wijde apertuur seismische data niet ten volle. Dit komt voornamelijk doordat de huidige denkwijze om reflectiviteiten te bepalen, conflicteert met de gemaakte aannamen in standaard seismische dataverwerking. De gewoonte om reflectiviteiten in wijde apertuur metingen van een gelaagde aarde te berekenen aan de hand van modellen van enkelvoudige laagovergangen, conflicteert met het seismische tijd-invariante convolutie model. De wisselwerking tussen modellering en inversie leidt tot betere overeenkomst tussen seismische karakterisatie en bron metingen, omdat de traditionele, band gelimiteerde, uitgestreken elastische eigenschappen vervangen worden door hoge resolutie, blokkerige gesteente beschrijvingen.

Een nieuw voorwaarts model om een gelaagde aarde te beschrijven is ontwikkeld,

waarin lineariteit gehandhaafd blijft voor grote hoek van inval en kinematische golfveld effecten op de juiste schaal behandeld worden. De volledige linearisatie van de contrasten in elastische eigenschappen vereist dat de druk- en afschuivingsgolfvelden op twee fundamenteel verschillende schalen behandeld worden: een kinematische schaal waarop de propagatie effecten een rol spelen en een dynamische schaal die de verstrooiingseffecten voor zijn rekening neemt. Door een achtergrond/kinematisch snelheidsmodel te introduceren, worden op elegante wijze de problemen ten gevolge van niet-lineariteit in de gelineariseerde Zoeppritz vergelijkingen (als gevolg van schaalafhankelijkheid), de discrepantie tussen de hoek van inval en de zogeheten straal parameter en de voorwaartse modellering van spanning en de daardoor veroorzaakte anisotropie aangepakt. Als gevolg hiervan kan de maximaal toegestane hoek van inval (of straal parameter of dislocatie) voor lineaire voorwaartse modellering ver opgerekt worden in vergelijking met modellering waarbij gebruik wordt gemaakt van conventionele twee- of drieterms enkelvoudige overgangs reflectiviteiten. Dankzij een expliciete mediumbeschrijving op de kinematische schaal is tevens de onvermijdelijke reductie in verticale resolutie bij scherende inval meegenomen. Spanning is een belangrijke factor die meegenomen dient te worden om de seismische amplitudeinformatie verkregen op grote dislocatie uit te kunnen buiten. Echter, pogingen om spanning te beschrijven op de dynamische schaal, welke verstrooiing beschrijft, introduceert sterke niet- lineariteiten in de voorwaartse modellering. In de gelineariseerde formulering is het vanzelfsprekend dat spanning op de kinematische schaal, waar de golfpropagatie plaats vindt, beschreven wordt. Een ander fenomeen in golfveld propagatie dat meegenomen dient te worden op kinematische schaal, is anisotropie ten gevolge van een gelaagd medium. Dit is bewerkstelligd door Thomsen parameters ϵ_0 and δ_0 in het achtergrond medium te definiren. Het geopperde voorwaartse gelaagde aarde-model omvat de fysica van zowel seismische golfpropagatie als verstrooiing, en faciliteert een betere benutting van de aanwezige informatie in seismische amplitudes verkregen met grote apertuur.

Om tot fysisch zinnige inzichten te komen, wordt na de lineaire amplitude analyse in de gelaagde aarde een tweede stap in kwantitatieve seismische amplitude analyse genomen. Gebruik makend van de kennis opgedaan tijdens de voorwaartse analyse is een methode ontwikkeld om kwantitatieve laageigenschappen uit de verkregen seismische data te extraheren. Er is in het bijzonder behoefte aan het kwantitatief in kaart brengen van reservoir (dus niet elastische) eigenschappen. Het seismisch afschatten van de eigenschappen van gesteentes is de meest directe manier om inzicht in het reservoir te verkrijgen. Seismische gesteenteparameters, en dichtheidsschattingen in het bijzonder, worden vaak als onnauwkeurig en onbetrouwbaar beschouwd door tekortkomingen in dataacquisitie, -verwerking en -interpretatie. Recente ontwikkelingen in acquisitie- en afbeeldingstechnieken hebben echter een technologische ontwikkeling in de richting van drie-terms, hoge resolutie reservoirparameterschatting bewerkstelligd waarbij gebruik wordt gemaakt van zowel druk-naar-druk als druk-naar-afschuif conversie modes. Dit werk bouwt voort op voorafgaand werk en schetst een methode om seismische data meer en beter te gebruiken bij kwan-

titatieve reservoir karakterisering en bij het beheren van een reservoir. Binnen de lineaire inversie theorie wordt het afschatten van hoge resolutie reservoir parameters uit data over drukgolven en golfconversie aangepakt als een optimalisatie van een probleem dat lineair is in deze parameters. Met behulp van de hierboven ontwikkelde voorwaartse gelaagde aarde modellen kan alle eerste orde informatie van druk- en conversiegolven, aanwezig in de seismische amplitudes, gebruikt worden, ondanks de instabiliteit in de golfvorm inversie als gevolg van de conversie van amplitude naar straal parameter. Hierdoor kunnen kwantitatieve schattingen van de reservoir parameters verkregen worden. Data kernels welke met deze nieuwe voorwaartse modellen opgezet worden leiden, tezamen met niet-kwadratische regularisatie (in de verticale richting) op de kleinste-kwadraten oplossing, tot betrouwbare, breedbandige reservoir parameter schattingen uit pre-stack seismische amplitudes. Deze kwantitatieve karakterisatie wordt bewerkstelligd door een combinatie van factoren. De belangrijkste hiervan is het verkrijgen van data onder grote dislocatie of apertuur. Dit is de prijs die men moet betalen voor verbeterd reservoirinzicht; als lineaire methoden meer informatie op moeten leveren dan zal meer informatie verzameld moeten worden. Echter, het is niet voldoende enkel over deze data te beschikken; er dient ook verandering plaats te vinden in hoe moderne seismische data beschouwd wordt. Amplitudes kunnen niet langer gezien worden als delta pieken welke onafhankelijk zijn van de aardlaagovergangen. Deze data zijn in werkelijkheid golfamplitudes met bijbehorende pulsvorm effecten welke op grote dislocaties niet verwaarloosd kunnen worden. Om alle aanwezige informatie in seismische data te kunnen benutten, is het van cruciaal belang dit soort effecten mee te nemen. Een andere vereiste is dat druk-naar-afschuiving conversiegolf amplitudes bekend zijn. Het blijkt dat inversie van deze conversiegolven betere schattingen van reservoir parameters oplevert welke onnauwkeurig afgeschat worden indien enkel drukgolven gebruikt worden. Bovendien verbeteren zowel de conditionering van het probleem en de parameter schattingen wanneer druk- en conversiegolven tegelijk beschouwd worden.

In het laatste deel van de inversie analyse worden theoretische inversieontwikkelingen toegepast om op praktische wijze schone, hoge-resolutie gesteente-eigenschappen uit pre-stack seismische drukgolf amplitude data te verkrijgen. Voortbouwend op standaard lineaire inversie technieken (in de huidige industrie), betreft de inversie een uitbreiding van de oplossing van een klassiek gedempt kleinste-kwadraten probleem. De laatste schakel is een gepreconditioneerd Conjugate Gradient algoritme dat de breedbandige, minimale structuur, kleinste kwadraten inversie van pre-stack seismische data uitvoert. Nadat dit algoritme is omgeschreven tot een computationeel efficiënte vorm, is het toegepast op seimische data gemeten aan een glauconitisch zandsteenreservoir. Afgezien van enkele pulsvorm- en fase-aberraties, worden drie koolwaterstofindicatoren bevestigd en een vierde indicator aangewezen. Het resultaat van deze inversie toont aan dat de voorgestelde methode succesvol het reservoir identificeert en de reservoirparameters met significant hogere resolutie dan met de meeste standaard commercile technieken afschat. Tevens zijn de resultaten aannemelijker vanuit een geologisch standpunt. Het blijkt hieruit dat het mogelijk is

om, uit pre- stack seismische data verkregen uit metingen in het veld, tot heldere reservoir karakterisering te komen.

De essentie van de aanpak in dit proefschrift is om de aannames gemaakt in seismische signaalverwerking en afbeeldingstechnieken samen te laten gaan met het reflectiviteitsmodel gebruikt in zowel voorwaartse modellering als inversie. Het samengaan van deze aspecten is vooral van belang als seismische metingen gedaan met grote apertuur gebruikt worden om reservoir informatie over spanning en verzadiging te verkrijgen, aangezien in het bijzonder voor grote dislocaties de gebruikelijke reflectiviteitsberekeningen niet voldoen aan de aannames in het lineaire dataconvolutiemodel. Van meet af aan was het doel de ontwikkeling van een praktische methode welke met hoge resolutie materiaal parameters af kan schatten uit wijde apertuur, pre-stack seismische amplitude metingen. Dit is verwezenlijkt met behulp van inzichten verkregen uit voorwaartse modellering en lineaire inversie theorie. Door het gewenste doel in de vorm van een gelineariseerd inversie probleem te gieten is, gebruik makend van de opgedane kennis van inversie theorie, een methode ontwikkeld welke met succes hoge resolutie gesteenteparameters voorspelt. De hoge resolutie kan voorbij gaan aan de bandbreedte in seismische metingen door, via een niet-kwadratische regularisatieterm in de te minimaliseren functie, een zogeheten sparseness eis op te leggen aan de inversie in de verticale richting. De methode is vervolgens in een voor echte data efficiënte vorm gegoten door het geregulariseerde inversieprobleem te schrijven als een gepreconditioneerd inversieprobleem, en daarbij het nieuwe probleem middels Tikhonov herformulering tot standaard vorm te herleiden. Hierdoor wordt het mogelijk het probleem op te lossen met de zeer snelle Conjugate Gradients methode. Het succes van de combinatie van deze aspecten is gedemonstreerd door geologisch zinnige, hoge resolutie gesteenteparameters voor een gashoudend zandsteenreservoir te bepalen uit bandbreedte beperkte pre-stack seismische amplitude metingen. Samenvattend kan gesteld worden dat men met geregulariseerde lineaire inversietheorie in staat is om hoge resolutie reservoir parameters te bepalen uit aan ruis onderhevige, incomplete en onnauwkeurige seismische amplitude data.

Helaas is alle seismische data onderhevig aan fundamentele beperkingen welke nooit weggenomen kunnen worden met een zuiver lineaire aanpak. Op dit moment bestaan er twee principes om met de hogere orde fysische effecten om te gaan. Het eerste is het uitbuiten van de ware, intrinsieke niet-lineariteit van het systeem. Het tweede berust op het vasthouden aan de aanname van lineariteit in de data terwijl een iteratieve niet-lineaire eis aan de parameterschattingen opgelegd wordt. In het ideale geval is deze eis gebaseerd op a priori kennis van de geologie. Dit tweede principe kan gezien worden als een zwak niet-lineaire aanpak, waar het eerste principe een volledig niet-lineaire aanpak is. Een significant gedeelte van dit proefschrift houdt zich bezig met dit tweede principe. Dit is een verstandige keuze, daar vrijwel alle seismische afbeeldingsschema's trachten dat deel van het golfveld dat niet-lineair in de materiaalparameters is, te identificeren en verwijderen. Dit om een seismische dataset te verkrijgen die beter voldoet aan de niet lineariteitsaanname. De toekomst,

zowel op korte als op lange termijn, is die van de volledige niet-lineaire aanpak. De rijping van doelgerichte niet-lineaire inversie is redelijkerwijs op korte termijn te verwachten, terwijl voor algemene inversie van het complete golfveld – waarbij alle ruwe seismische data direct genverteerd wordt voor gedetailleerde onderaardse eigenschappen – nog flink aan de weg getimmerd zal moeten worden. Hoe dan ook is het essentieel om de intrinsieke niet-lineariteit van de data te erkennen en deze te gebruiken in een niet-lineair inversieschema. Dit is de enige directe manier om op grond van de data alle fysica in de data te verklaren, en tevens garandeert de methode dat alle voorkomende aardeffecten correct meegemodelleerd worden. Het is onbetwist dat de toekomst van kwantitatieve amplitude analyse ligt bij het volledig niet-lineaire datamodel, en zij die dit pad bewandelen wens ik een goede en vruchtbare reis.

Ayon Kumar Dey

Curriculum vitae

Ayon Kumar Dey was born in St. John's, Newfoundland and Labrador, Canada on May 31st, 1974. He attended secondary school in St. John's at Gonzaga High School, where he received his diploma in 1992. Starting university studies in microbiology and immunology at Queen's University in Kingston, he continued at Memorial University of Newfoundland (in St. John's) and received his B.Sc. degree in applied mathematics during the spring of 1996. That fall, he began M.Sc. studies in applied geophysics at Memorial and completed in 1999 at University of Calgary, as his supervisor relocated to Calgary, Alberta, Canada, and extended an invitation to come along and join the Consortium for Research in Elastic Wave Exploration Seismology. While undertaking research leading to a thesis on seismic wavelet estimation, he spent one summer working on a marine seismic acquisition vessel off the east coast of Newfoundland for Husky (now HuskyEnergy) as well as spending another summer working for Amoco (now BP) at their research division in Tulsa. Following his M.Sc. graduation, an additional year was spent at the University of Calgary researching active seismic noise suppression. He then moved on to join Geo-X Systems in 2001 as a reservoir geophysics specialist. Returning to graduate school in 2003, he moved to Europe and pursued a Ph.D. within the DELPHI consortium of the Laboratory of Acoustical Imaging and Sound Control at Delft University of Technology in Delft, The Netherlands. The next four years were spent on quantitative seismic amplitude analysis with research leading to this Ph.D. thesis. During the course of this work, time was spent with the Signal Analysis and Imaging Group at the University of Alberta. Furthermore, six months were spent developing various aspects of his Ph.D. research with CGG-Veritas in Calgary and Chevron in San Ramon, California, USA. In 2007, he relocated to The Kingdom of Saudi Arabia and took up his current role as a reservoir geophysicist with the Saudi Arabian Oil Company (Saudi Aramco).

Acknowledgements

"All children must look after their own upbringing. Parents can only give good advice or put them on the right paths, but the final forming of a person's character lies in their own hands." – Anne Frank

First, and foremost, I must acknowledge my parents. It is only fitting that I am able to acknowledge my parents using a quote from one the most powerful symbols my adopted home of 5 years has given the world. Mom and Dad, you are both symbols of inspiration to me. Without your never ending support, insight, and advice, this dissertation would have never come into being. You both are my foundation and I'll forever cherish that. Simply put, thank you.

After my parents, there are three fundamental pillars that supported this work from beginning to end. Dries, you rolled the dice and signed on to supervise me. This is no simple task (just ask Larry Lines). Through it all, you taught me to never just accept things. To rigorously master the physics is to fully understand the observed phenomena. This is the approach I take with me. Then there is Eric, your never ending enthusiasm for all the DELPHI graduate projects is inspiring. You were always willing to discuss ideas and clarify points of confusion. Especially when trying to understand the subtleties of the physical systems approach to the beast called seismic wave-propagation. Your pragmatic approach of solving problems with the simplest physics that can explain the data is forever with me. Finally, there is Professor Berkhout. Always one to insure that I never lost sight of the big picture, you've taught me, more than anything else, that it is not enough to understand

the system but one also needs to understand the interconnectedness of the system. A heartfelt thanks and appreciation to you three for your guidance, support, and insight.

There is quite the supporting cast of characters who've all played a role in taming this beast of a thesis. Too many to name but none forgotten. That being said, some special thanks need to be extended or I'll be without. Ewoud, without that summer spent working with you at Amoco I'd have never made the trip across the pond. And to my DELPHI colleagues (Paul, Maurice, Sandra, Barbara, Edith, Mustafa, Dana, Gert-Jan, Justyna, Ahmad, and Mohammed), a heartfelt thanks to everybody. Each one of you have contributed to this work in your own way by helping me form my critical outlook. Paul and Barbara, you two are due so much more than the thanks given here. As, I'm sure, being my office-mate must have been quite challenging. Barbara, will you soon forget the "unhealthy" music? I think not. My last set of office-mates, Dana and Justyna, should never forget that just because I'm gone doesn't mean that I'll give up on getting you both to "say it with me one time". Sandra, your infinite patience in humouring my lunatic ravings on Germany (among other things) is well appreciated. A lesser person would have had me committed.

Fuelling thoughts outside of geoscience were the greatly valued daily lunchtime discussions. Crocodile Steve, Jasper, Lars, Anton and Margaret, the *gezellig* nature of lunch was a very Dutch experience that I'll always carry with me. A very special shout-out goes to Crocodile Steve and Margaret. Erwin were doing your B.Sc. as I showed up and you're doing your Ph.D. as I leave. Are you fast or am I slow? Don't answer that but know that this book would never have been published without your selfless act of Dutch translation. You, sir, are a gentleman and I am in your debt. And Margaret, such patience and helpfulness can never be properly acknowledged with just a few words. Tirelessly sorting my issues and always with a smile. You were truly a mom-away-from-mom.

Then there is The Joker. Or is he The Gangster of Love? He was then, as he is now, just Maurice. What can I say my man? From the shared hotel rooms to the elixir of life to Lowlands, you, more than anybody or anything, are my Dutch experience. You were always ready, and about, to rock. I salute you.